

Development of Multirate Filter - based Region Features for Iris Identification

Soubhagya Sankar Barpanda



Department of Computer Science and Engineering
National Institute of Technology Rourkela
Rourkela-769 008, Odisha, India

Development of Multirate Filter - based Region Features for Iris Identification

*Thesis submitted in partial fulfillment
of the requirements for the degree of*

Doctor of Philosophy

in

Computer Science and Engineering

by

Soubhagya Sankar Barpanda

(Roll: 512CS605)

under the guidance of

Dr. Banshidhar Majhi

&

Dr. Pankaj Kumar Sa



Department of Computer Science and Engineering
National Institute of Technology Rourkela
Rourkela-769 008, Odisha, India
January 2016



Department of Computer Science and Engineering
National Institute of Technology Rourkela
Rourkela-769 008, Odisha, India.

January 25, 2016

Certificate

This is to certify that the work in the thesis entitled **Development of Multirate Filter - based Region Features for Iris Identification** submitted by **Soubhagya Sankar Barpanda**, bearing roll number 512CS605, is a record of an original research work carried out by him under our supervision and guidance in partial fulfillment of the requirements for the award of the degree of **Doctor of Philosophy in Computer Science and Engineering**. Neither this thesis nor any part of it has been submitted for any degree or academic award elsewhere.

Pankaj Kumar Sa
Assistant Professor

Banshidhar Majhi
Professor

Dedicated To My Family

Acknowledgment

If God brings you to it, he will bring you through it. . .

Thank you God for showing me the path.

I take this opportunity to thank all those who have contributed in this journey.

Foremost, I would like to express sincere gratitude to my advisor, Prof. Banshidhar Majhi for providing motivation, enthusiasm, and critical atmosphere at the workplace. His profound insights and attention to details have been true inspirations to my research. Prof. Majhi has taught me to handle difficult situations with confidence and courage.

I would like to thank Prof. Pankaj Kumar Sa for his constructive criticism during the entire span of research. His insightful discussions have helped me a lot in improving this work.

My sincere thanks to Prof. S.K. Jena, Prof. S.K. Rath, Prof. B.K. Patra, Prof. A.K. Turuk, Prof. G.K. Panda, Prof. S. Meher, and Prof. K.B. Mohanty for their continuous encouragement and valuable advice.

I would like to thank my friends and colleagues at NIT Rourkela for the help they have offered during the entire period of my stay.

Soubhagya Sankar Barpanda

Abstract

The emergence of biometric system is seen as the next-generation technological solution in strengthening the social and national security. The evolution of biometrics has shifted the paradigm of authentication from classical token and knowledge-based systems to physiological and behavioral trait based systems. R & D on iris biometrics, in last one decade, has established it as one of the most promising traits. Even though, iris biometric takes high resolution near-infrared (NIR) images as input, its authentication accuracy is very commendable. Its performance is often influenced by the presence of noise, database size, and feature representation. This thesis focuses on the use of multi resolution analysis (MRA) in developing suitable features for non-ideal iris images.

Our investigation starts with the iris feature extraction technique using Cohen – Daubechies – Feauveau 9/7 (CDF 9/7) filter bank. In this work, a technique has been proposed to deal with issues like segmentation failure and occlusion. The experimental studies deal with the superiority of CDF 9/7 filter bank over the frequency based techniques. Since there is scope for improving the frequency selectivity of CDF 9/7 filter bank, a tunable filter bank is proposed to extract region based features from non-cooperative iris images. The proposed method is based on half band polynomial of 14th order. Since, regularity and frequency selectivity are in inverse relationship with each other, filter coefficients are derived by not imposing maximum number of zeros. Also, the half band polynomial is presented in x -domain, so as to apply semidefinite programming, which results in optimization of coefficients of analysis/synthesis filter.

The next contribution in this thesis deals with the development of another powerful MRA known as triplet half band filter bank (THFB). The advantage of THFB is the flexibility in choosing the frequency response that allows one to overcome the magnitude constraints. The proposed filter bank has improved frequency selectivity along with other desired properties, which is then used for iris feature extraction. The last contribution of the thesis describes a wavelet cepstral feature derived from CDF 9/7 filter bank to characterize iris texture. Wavelet cepstrum feature helps in reducing

the dimensionality of the detail coefficients; hence, a compact feature presentation is possible with improved accuracy against CDF 9/7.

The efficacy of the features suggested are validated for iris recognition on three publicly available databases namely, CASIAv3, UBIRISv1, and IITD. The features are compared with other transform domain features like FFT, Gabor filter and a comprehensive evaluation is done for all suggested features as well. It has been observed that the suggested features show superior performance with respect to accuracy. Among all suggested features, THFB has shown best performance.

Keywords: CDF 9/7, Tunable filter bank, THFB, Wavelet cepstrum, Energy feature.

Contents

Certificate	iii
Acknowledgement	v
Abstract	vi
List of Figures	xi
List of Tables	xiii
List of Acronyms	xiv
1 Introduction	1
1.1 Anatomy of Iris Image	5
1.2 Automated Iris Biometric System	9
1.3 Fusion in Biometrics	11
1.4 Iris Biometric Databases	13
1.5 Performance Measures	17
1.5.1 Recognition Performance	17
1.5.2 Identification Performance	18
1.6 Wavelet: A Suitable Candidate for Texture Analysis	19
1.7 Research Challenges	22
1.8 Research Objectives	22
1.9 Thesis Organization	23
2 Literature Review	25
2.1 Global Features	26
2.2 Region Based Features	30

2.3	Local Features	31
2.4	Observations	37
3	CDF 9/7 for Iris Feature Extraction	39
3.1	Related Work On Biorthogonal Filter Bank	40
3.2	Iris Texture Analysis with CDF 9/7 FB	42
3.2.1	Advantage of CDF 9/7 Filter Bank over FFT	44
3.2.2	Feature Extraction using CDF 9/7	45
3.3	Results and Discussion	48
3.3.1	Analysis of Results	53
3.4	Summary	53
4	Tunable Filter Bank for Iris Feature Extraction	54
4.1	Design Issues in Multirate Filters	55
4.2	Proposed Tunable Filter Bank	56
4.2.1	Iris Feature Extraction using Tunable Filter Bank	62
4.3	Results and Discussion	65
4.4	Summary	69
5	Iris Feature Extraction Using THFB	70
5.1	Related Work on THFB	71
5.2	Proposed Filter Bank	72
5.2.1	Iris Feature Extraction using THFB	75
5.3	Results and Discussion	78
5.3.1	Advantage of the Proposed Approach	83
5.4	Summary	84
6	WCF for Iris Recognition	85
6.1	Proposed WCF for Iris Recognition	87
6.2	Results and Discussion	89
6.2.1	Advantage of Wavelet Cepstrum Feature	93
6.3	Summary	93

7 Conclusions	94
Bibliography	97
Dissemination	112
Index	114

List of Figures

1.1	Illustration of the front pigmented fibrovascular tissue from eye images.	5
1.2	Different modes of operation of a generic biometric system.	7
1.3	Different modules of an automated iris recognition system.	10
1.4	Different modes of operation of a generic biometric system.	11
1.5	Categorisation of fusion approaches depending upon the nature of evidence.	13
1.6	Various levels of fusion in multimodal biometric.	14
1.7	A hypothetical curve demonstrating the performance measures.	18
1.8	Two level decomposition using DWT (a) original image (b) First level decomposition (c) Second level decomposition	21
2.1	Categorization of literature explored in iris biometrics into three domains.	26
2.2	Contributions of this thesis.	37
3.1	Generalized block diagram of iris-recognition system	40
3.2	Block diagram of two band filter bank	43
3.3	Normalized iris image divided into six equal regions	46
3.4	Iris localization with IDO	46
3.5	Iris localization failure with IDO	47
3.6	Two level decomposition using wavelet	48
3.7	Block diagram showing proposed approach for iris recognition system	49
3.8	Performance of CDF 9/7 filter bank technique on CASIAv3, UBIRISv1, and IITD databases	51

3.9	CMC curves on CDF 9/7 filter bank feature on CASIAv3, IITD, and UBIRISv1 databases	52
4.1	Performance of tunable filter bank technique on CASIAv3, UBIRISv1, and IITD databases	67
4.2	CMC curves on tunable filter bank feature for IITD, UBIRISv1, and CASIAv3 databases	68
5.1	Analysis filters of THFB	72
5.2	Proposed approach	76
5.3	Iris segmentation failure with IDO	77
5.4	Performance of THFB on CASIAv3, UBIRISv1, and IITD databases	81
5.5	CMC curves on THFB based features for CASIAv3, UBIRISv1, and IITD databases	82
6.1	Performance of wavelet cepstrum on CASIAv3, UBIRISv1, and IITD databases	91
6.2	CMC curve on wavelet cepstrum for CASIAv3, UBIRISv1, and IITD databases	92
7.1	Failure in image acquisition due to non-cooperative user	96

List of Tables

1.1	Comparison of different biometric modalities based on their characteristics.	6
1.2	Detail of some existing iris databases	16
2.1	Recognition through iris biometric	34
3.1	Comparative analysis of proposed feature on different databases . . .	50
4.1	Co-efficient vector \mathbf{a} of z -domain	62
4.2	Co-efficient vector \mathbf{b} of x -domain	62
4.3	Comparative analysis of proposed feature on different databases . . .	66
5.1	Comparative analysis of proposed feature on different databases . . .	80
6.1	Computational cost of different iris recognition algorithms (with respect to time)	89
6.2	Comparative analysis of proposed feature on different databases . . .	90

List of Acronyms

- CDF 9/7 Cohen-Daubechies-Feauveau 9/7, page 22
- CMC Cumulative Match Characteristic, page 18
- DCT Discrete Cosine Transform, page 39
- DFT Discrete Fourier Transform, page 85
- DWF discrete wavelet frame, page 32
- DWT Discrete Wavelet Transform, page 20
- FAR False Acceptance Rate, page 17
- FIR Finite-duration Impulse Response, page 70
- FMR False Match Rate, page 17
- FNMR False Non Match Rate, page 17
- FRR False Rejection Rate, page 17
- GAR Genuine Acceptance Rate, page 17
- MFCC Mel-Frequency Cepstrum Coefficients, page 87
- MLDF Multilobe Differential Filters, page 28
- POC Phase-Only Correlation, page 32
- ROC Receiver Operating Characteristic, page 17
- SDP Semidefinite Programming, page 56
- SIFT Scale Invariant Feature Transform, page 31
- SURF Speeded Up Robust Features, page 32
- THFB Triplet Half Band Filter Bank, page 70
- UAE United Arab Emirates, page 4
- WCF Wavelet Cepstrum Features, page 87

Chapter 1

Introduction

Person identification has become an integral part of our everyday activities. Considering the incessant threats, automation of person identification is unequivocally indispensable [1]. Mechanisms like *token based system* (e.g. passport, smart card) and *knowledge based system* (e.g. secret code, password) are existing for quite long time. These systems have the disadvantage of physical possession of the token or piece of information like password that is used to prove the authentication of an individual. Furthermore, these mechanisms are very prone to spoofing. On the contrary, biometric traits have the unique advantage of being held physically by the user, making it near impossible to spoof [2].

Biometrics is an automated method of authenticating an individual based on physiological and behavioral characteristics. The characteristics are distinct and can distinguish between a *genuine* person and an *imposter*. The physical presence of the subject makes it very difficult to spoof the biometric system. The authentication is performed using various biometric traits like face, fingerprint, iris, ear, etc. The choice of a biological measurement to qualify as a biometric trait is based on the following properties:

- **Distinctiveness or uniqueness:** A biometric modality must have features that allow high levels of discrimination in selecting any particular individual while rejecting everyone else. The larger the number of people to be distinguished, the more important this factor becomes.

- **Stability:** There is a likelihood of changes in a biometric modality over a period of time due to age, accident, or disease. However, a biometric should preserve enough features so that these changes will have a minimal effect on the system's ability to discriminate. Stability may be of less significance where re-enrolment can be simply or easily achieved, or where re-issue over shorter duration is legally required.
- **Scalability:** A biometric should be capable of being processed efficiently, both at acquisition time and when it is searched in a database for identification-based access. Scalability issues may be less of a concern for verification-based access control systems than for large identification systems.
- **Usability:** A major selling feature in the adoption of biometrics is its convenience. If a biometric is difficult or slow to use, it probably won't be adopted. There is also a question of acceptance of the trait by some social/religious sect.
- **Inclusiveness:** An extremely high proportion of the population should be measurable, particularly for large-scale identity systems. A biometric which excludes some users causes additional complexities in managing security. A secondary authentication system is needed if a fraction of the population does not bear the biometric trait.
- **Insensitivity:** Changes in the external environment e.g., lighting, temperature etc. within reasonable boundaries should not cause system failures due to malfunction of the trait.
- **Vulnerability:** It should be difficult to create a fake prosthetic biometric (known as spoofing), or to steal and use a detached one.
- **Privacy:** Ideally the permission of the owner of a biometric should need to be sought before acquisition of the trait. A trait should not be easily captured without a person's notice/permission.

Biometrics is evolving constantly, which has engendered a workable industry holding great promise for the future. This curiosity has attracted many organizations to explore the implementation of complete biometric systems. Different biometric traits have been studied by the scientific community for real time deployment of the technology. The most successfully used automated biometric identifiers include fingerprint, face, palmprint, iris, and signature. Fingerprint identification is one of the most well-established and publicized biometrics. Because of their uniqueness fingerprints have been used for identification for over a century, more recently becoming automated due to advancements in computing capabilities. Fingerprint identification is popular because of the inherent ease in acquisition, the numerous sources (ten fingers) available for collection, and their established use and collections by law enforcement and immigration. There was immense interest from the Federal Bureau of Investigation (FBI) to develop a system to automate its fingerprint identification process, which had quickly become overwhelming and required many man-hours for the manual process. The con of fingerprint biometric is that it is exposed to outside environment; hence susceptible to change in its pattern. Moreover, for children the pattern as well as the size of fingerprint changes very quickly.

Face is another popular biometric modality, which has found usage in current devices like smartphone, tablet, or personal computer to replace password. Human being use the face information as a primary means to recognize humans. Because of its natural appearance, face biometrics is acceptable in ideal situations. The conventional optical imaging devices are used to capture the face; hence data acquisition is economical. Despite of being a very strong biometric trait, the current technologies are not able to handle certain problems till now. There has been little progress in making face recognition invariant with respect to aging effect. Also image acquisition in different illuminations affect badly the accuracy of the recognition system.

Palmprint recognition inherently implements many of the same matching characteristics that have been adopted for fingerprint recognition. Hence it is known to be one of the most well-known and best publicized biometrics. Both palm and

finger biometrics are represented by the information presented in a friction ridge impression. This information combines ridge flow, ridge characteristics, and ridge structure of the raised portion of the epidermis. The data represented by these friction ridge impressions allows a decision that corresponding areas of friction ridge impressions either originated from the same source or not. Because fingerprints and palms have both uniqueness, they have been used for over a century as a trusted form of identification. However, palm recognition has been slower in becoming automated due to some restraints in computing capabilities and live-scan technologies. Also it shares the same cons of fingerprint trait.

The comparison of various biometric traits based on different characteristics is shown in Table 1.1. In contrast to other biometric traits, iris is an established biometric modality [3] due to its high universality, uniqueness, stability over time, performance, and ability to counteract spoof attacks (refer Table 1.1). An iris recognition system operates by mathematical analysis of texture patterns that are imaged at certain distance from the eye [4]. Recently, iris biometric has evolved as a mainstream field of biometric applications adverting to its performance. Such systems are deployed at United Arab Emirates (UAE) linking 27 air, land, and sea-ports of entry [1]. In India, a large-scale project Aadhaar [5] is undertaken to issue unique identification number to everyone across the country using fingerprint, face, and iris. Though in sufficiently matured stage, iris still needs considerable attention by the researchers. The transition of iris from laboratory technology to real time deployment has highlighted some interesting research challenges. For instance, exhaustively searching country-sized iris database, recognition under scenarios when iris data is either noisy or unavailable, and effect of aging on iris [6]. In this thesis, an effort has been made to re-investigate the performance of iris biometric under the aforesaid real-time challenges and identify the measures to mitigate the shortcomings, if any.

Before exploring research issues in iris, it is recommended to consider its anatomical structure in detail. Iris is a thin circular disk in the eye with dark circular

opening in the center known as the pupil as shown in Figure 1.1. The texture pattern in iris comprises two tissues: the front pigmented fibrovascular tissue is known as a stroma and, beneath the stroma, pigmented epithelial cells. The stroma is connected to a sphincter muscle, which constricts the pupil in a circular motion, and a set of dilator muscles, which pulls the iris radially to enlarge the pupil [7]. The constriction and dilation of pupil control the amount of light entering the eye. The flowery pattern surrounding the pupil, commonly referred as *iris*, is unique and used for personnel identification.



Figure 1.1: Illustration of the front pigmented fibrovascular tissue known as a stroma from high quality eye images [8].

1.1 Anatomy of Iris Image

A detail study is required to understand the texture rich pattern of the iris for recognition. The iris is composed of several layers. Heavily pigmented epithelial cells constitute the posterior surface [9]. These cells make it impenetrable by light. There are two cooperative muscles for controlling the pupil, that constitute the anterior surface. Next is the stromal layer, which consists of collagenous connective tissue in arch-like style. There are radially arranged corkscrew like blood vessels coursing through this layer. The most anterior layer is more densely packed, especially with individual pigment cells (called chromatophores). The visual appearance of the iris is due to its multilayered structure. The anterior surface of the iris is found to be divided

Table 1.1: Comparison of different biometric modalities based on their characteristics (H: High, M: Medium, and L: Low) [1].

Modality	Universality	Uniqueness	Permanence	Collectability	Performance	Acceptability	Circumvention
Face	H	L	M	H	L	H	L
Fingerprint	M	H	H	M	H	M	H
Hand Geometry	M	M	M	H	M	M	M
Keystrokes	-	-	L	M	L	M	M
Hand Vein	M	M	M	M	M	M	H
Iris	H	H	H	M	H	L	H
Retinal Scan	H	H	M	L	H	L	H
Signature	L	L	L	H	L	H	L
Voice Print	M	L	L	M	L	H	L
F. Thermogram	H	H	L	H	M	H	H
Odor	H	H	H	L	L	M	L
DNA	H	H	H	L	H	L	L
Gait	M	L	L	H	L	H	M
Ear	M	M	H	M	M	H	H

into two parts: a central pupillary zone and a surrounding ciliary zone. The border of these two areas is termed the collarette. It has a zigzag circumferential ridge like structure resulting as the anterior border layer, which ends near the pupil. The ciliary zone contains many interlacing ridges resulting from stromal support. Contractile lines here can vary with the state of the pupil. Additional meridional striations result from the radiating vasculature. Other assorted variations in appearance owe to crypts (irregular atrophy of the border layer), nevi (small elevations of the border layer), and freckles (local collections of chromatophores). In contrast, the pupillary zone can be relatively flat; it often shows radiating spoke-like processes and a pigment frill where the posterior layers heavily pigmented tissue shows at the pupil boundary. The iris color results from the differential absorption of light impinging on the pigmented cells in the anterior border layer.

When there is little pigmentation in the anterior border layer, light reflects back

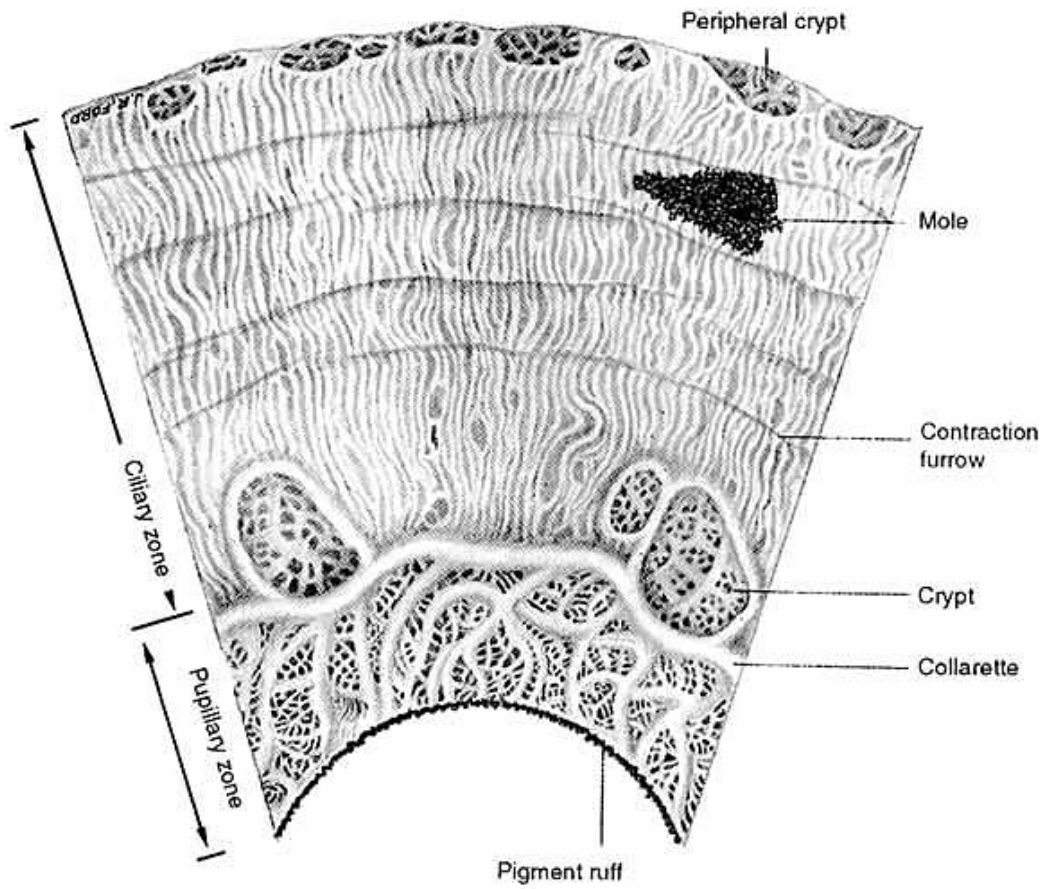


Figure 1.2: Different modes of operation of a generic biometric system.

from the posterior epithelium and is scattered as it passes through the stroma to yield a blue appearance. Progressive levels of anterior pigmentation lead to darker colored iris. Claims that the structure of the iris is unique to an individual and is stable with age come from two main sources. The first source of evidence is clinical observations. During the course of examining large numbers of eyes, ophthalmologists and anatomists have noted that the detailed pattern of an iris, even the left and right iris of a single person, seems to be highly distinctive. Further, in cases with repeated observations, the patterns seem to vary little, at least past childhood. The second source of evidence is developmental biology. There, one finds that while the general structure of the iris is genetically determined, the particulars of its minutiae are critically dependent on circumstances (e.g., the initial conditions in the embryonic precursor to the iris). Therefore, they are highly unlikely to be replicated via the natural course of events. Rarely, the developmental process goes awry, yielding only a rudimentary iris (aniridia) or a marked displacement (corectopia) or shape distortion (coloboma) of the pupil.

Developmental evidence also bears on issues of stability with age. Certain parts of the iris (e.g., the vasculature) are largely in place at birth, whereas others (e.g., the musculature) mature around two years of age. Of particular significance for the purposes of recognition is the fact that pigmentation patterning continues until adolescence. Also, the average pupil size (for an individual) increases slightly until adolescence [1]. Following adolescence, the healthy iris varies little for the rest of a persons life, although slight depigmentation and shrinking of the average pupillary opening are standard with advanced age. Various diseases of the eye can drastically alter the appearance of the iris. It also appears that intensive exposure to certain environmental contaminants (e.g., metals) can alter iris pigmentation. However, these conditions are rare. Claims that the iris changes with more general states of health (iridology) have been discredited. On the whole, these lines of evidence suggest that the iris is highly distinctive and, following childhood, typically stable. Nevertheless, it is important to note that large-scale studies that specifically address

the distinctiveness and stability of the iris, especially as a biometric, have yet to be performed.

1.2 Automated Iris Biometric System

An iris biometric system is typically a pattern recognition system that acquires the iris image of an individual, extracts features (represented in the form of a template), and compares this feature set against the feature set(s) stored in the database. The input biometric template (commonly referred to as *gallery* template) is stored in the database during enrollment. The template which is presented to the biometric system for claiming the identity is known as *probe*. A generic iris biometric system has four major modules:

- a. **Image acquisition module** requires an iris biometric scanner to acquire images. The acquisition setup plays a crucial role on the performance of any biometric system. For instance, iris images acquired loosely (without any restriction on the user) may pose serious challenges.
- b. **Preprocessing module** extracts the *region of interest* from the input iris image. Preprocessing is performed to localize the inner pupil and outer iris boundary. The annular ring between pupil and iris boundary are transformed from Cartesian space to polar space using homogeneous rubber sheet model [4]. This transformation generates the normalized iris image which facilitates the feature extraction process.
- c. **Feature module** extracts significant details from the normalized iris image using mathematical models. The extracted features should be unique and must achieve invariance to transformations between the gallery and probe iris images.
- d. **Matching module** finds the correspondences between the two feature sets using an appropriate matcher. The matcher either validates the identity of an individual by performing one to one comparison or to generate a ranked list of identities

for one to many comparisons [1]. Figure 1.3 illustrates different modules of an automated iris biometric system.

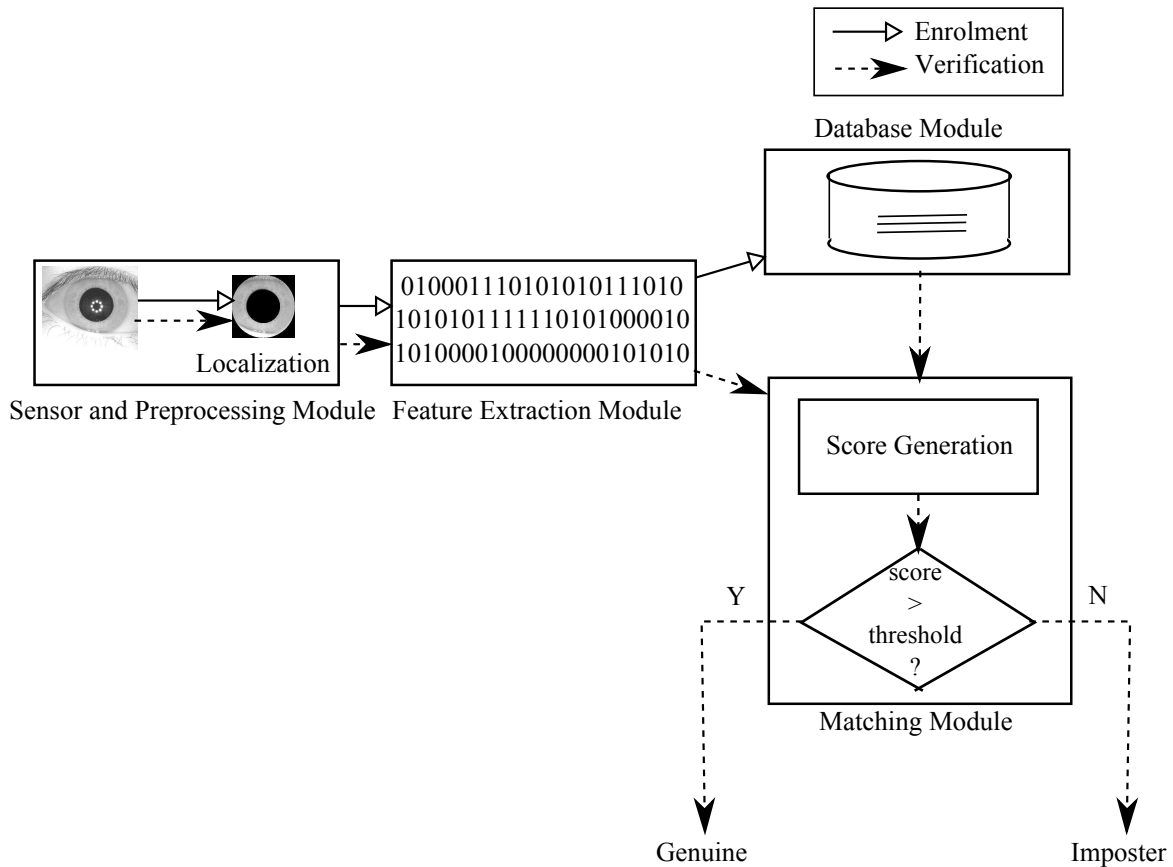


Figure 1.3: Different modules of an automated iris recognition system [10].

Depending upon the application context, a biometric system operates in verification (also known as recognition) or identification modes as shown in Figure 1.4. In verification mode, the system authenticates the identity claimed by an individual by comparing his template with an already stored template in the database. Identification mode, in contrast, finds the identity of the probe template by searching all gallery templates present in the database.

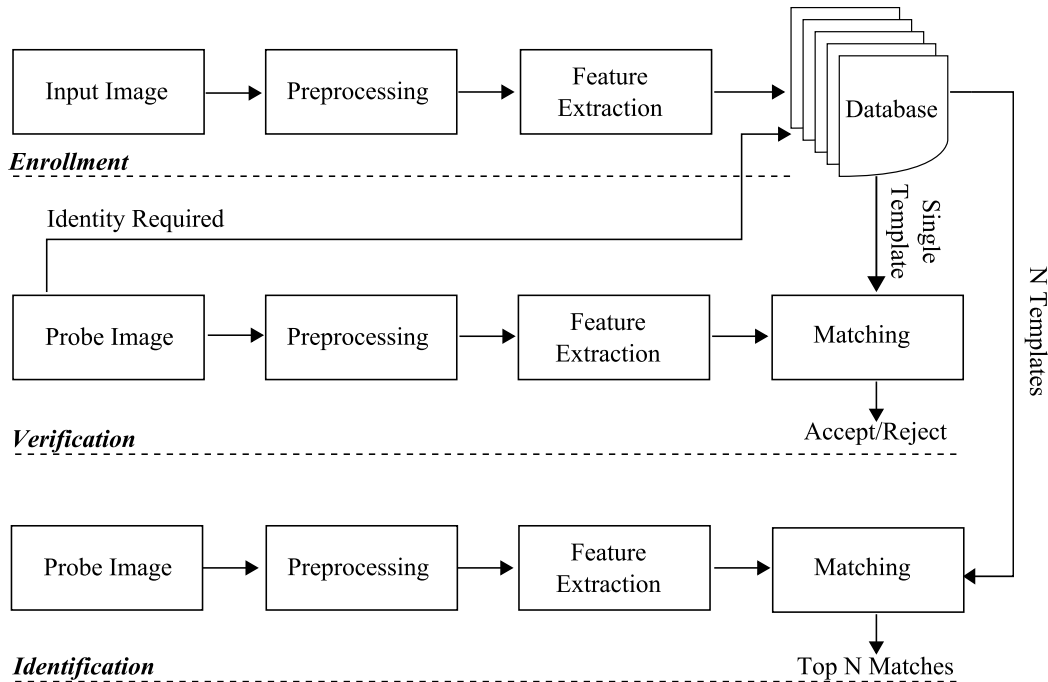


Figure 1.4: Different modes of operation of a generic biometric system.

1.3 Fusion in Biometrics

Biometric system that requires single source of evidence to perform authentication is known as unimodal systems. However, a single biometric trait is not expected to meet all the requirements such as accuracy, cost, availability, etc. There are some challenges which in general, affects the performance of any biometric system:

- The acquired biometric image may change over time or may be affected by noise. For instance, facial features are subject to age over a period of time. Similarly, fingerprint effected by scar or voice effected by cold may pose vulnerabilities to a biometric system.
- The biometric data may be unavailable for a subset of population. The presence of cuts and bruises on the fingerprint brings down the system performance. Similarly, it is difficult to acquire iris images with some pathological problem in the eye.

- Circumvention is easy with a single biometric trait. Some traits such as fingerprint can be spoofed by showing a fake fingerprint structure on a synthetic material.

Multimodal biometric fusion utilises more than one source of evidence for authentication. Fusion is very useful to overcome the limitations inherent to unimodal approaches. Depending upon the *nature of evidence* available, the fusion algorithm can be multi-sensor, multi-algorithm, multi-instance, multi-unit, and multi-modal as shown in Figure 1.5. The *multi-sensor* system utilises more than one sensor to capture single biometric trait of an individual. In *multi-algorithm* system, for a single biometric trait, multiple feature extraction algorithms or multiple matchers are combined. The multiple images of the same biometric trait are acquired from a single biometric sensor in *multi-instance* systems. In *multi-unit* system, multiple units of the same modality are used to perform authentication. For instance, information from left and right iris or fingerprint images can be combined to improve the performance. The multi-unit fusion approaches improve the recognition accuracy without incurring any additional hardware cost. The combination of more than one biometric trait generates a *multi-modal* system. For example, combining iris with the face improves the performance of “on the move” type of recognition systems.

Based on the *level of fusion*, the approaches can be further categorised into sensor level, feature level, match score level, and decision level as shown in Figure 1.6. In *sensor level* fusion, the raw biometric data from multiple sensors (multi-sensor) or multiple instances of a biometric from the same sensor (multi-instance) are fused. *Feature level* fusion involves integrating more than one feature set from different biometric algorithms (multi-algorithm) into a single feature set. In *match score* level fusion, the match scores generated from multiple biometric matchers are combined to generate a consolidated score value. In *decision level* fusion, the final recognition decisions are combined to develop a multimodal biometric system.

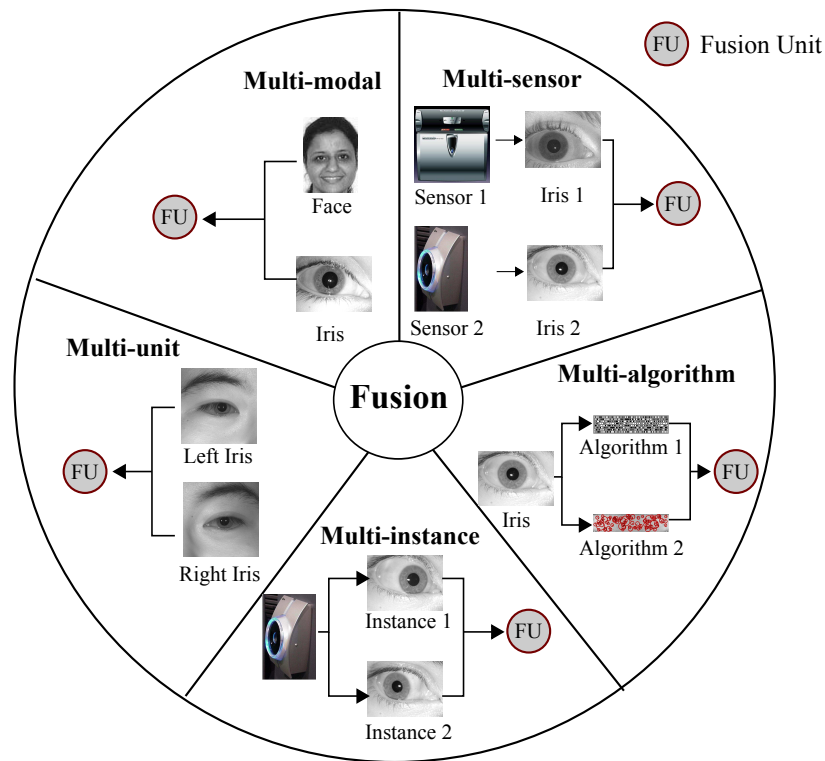


Figure 1.5: Categorisation of fusion approaches depending upon the nature of evidence.

1.4 Iris Biometric Databases

Use of common databases give proper platform to compare two or more methods devised by separate research groups. This section presents the iris biometric databases that are existing and widely used by researchers to validate their respective approaches. Performance of iris recognition systems in unconstrained environments is still a challenging task, which require special attention. Extraction of iris region, occlusion segmentation, large scale detection, and many other issues need further investigation. All these above said issues can be addressed if investigated on carefully designed databases.

Table 1.2 presents the most widely used iris databases that are released for iris research. CASIA, UBIRIS, and IITD are such databases. CASIA IRISv3-Interval (hereafter called CASIAv3 throughout the thesis) database, formed and released by

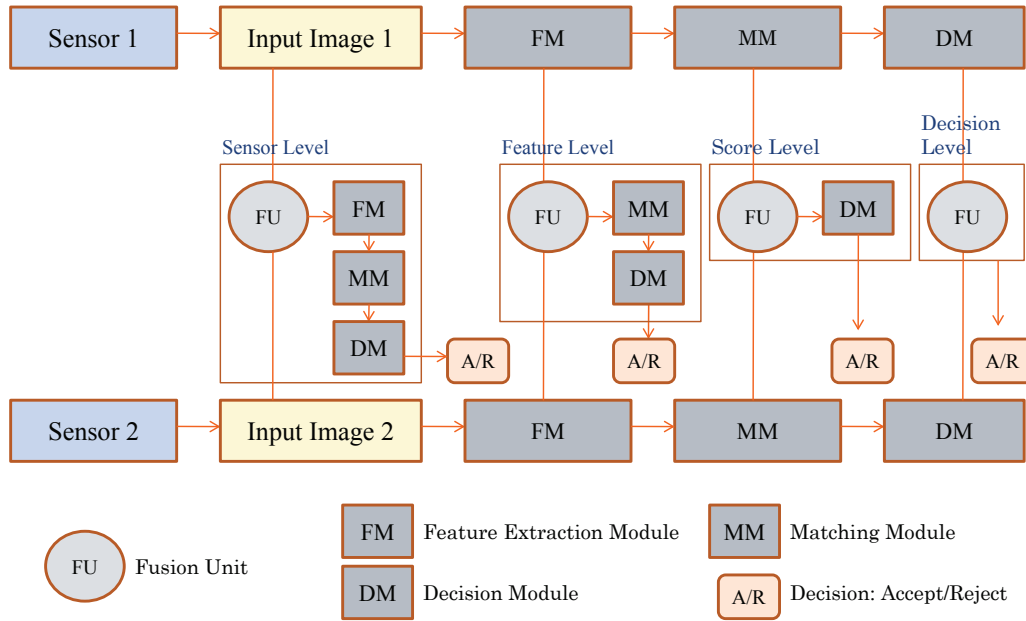


Figure 1.6: Various levels of fusion in multimodal biometric.

Chinese Academy of Sciences, China. It contains images from 249 subjects and each image is having resolution 320×280 . A self-developed close-up iris camera is used to capture the iris images. CASIAv3 dataset contains illumination variance and noises due to specular highlights. The designed camera has circular NIR LED array with suitable luminous flux for iris imaging. Due the designed camera, very clear images are captured and well-suited to study the detailed texture features of iris images.

UBIRISv1 database is consists of 1877 images collected from 241 subjects in two distinct sessions. The main characteristic of this database is to incorporate images with several noise factors, simulating less constrained image acquisition environments. This enables the evaluation of the robustness of iris recognition methods. For the first image capture session, noise factors are minimized, specially those relative to reflections, luminosity and contrast, having installed image capture framework inside a dark room. In the second session, the image acquisition place is changed in order to introduce natural luminosity factor. This includes the appearance of heterogeneous images with respect to reflections, contrast, luminosity and focus problems. Images

collected at this stage simulate the ones captured by a vision system without or with minimal active participation from the subjects, adding several noise problems. These images will be on the recognition stage compared to the ones collected during first session.

The IIT Delhi Iris Database mainly consists of the iris images collected from the students and staff at IIT Delhi, New Delhi, India. This database has been acquired in Biometrics Research Laboratory during Jan - July 2007 using JIRIS, JPC1000, digital CMOS camera. The image acquisition program was written to acquire and save these images in bitmap format and is also freely available on request. The currently available database is from 224 users, all the images are in bitmap format. All the subjects in the database are in the age group 14 - 55 years comprising of 176 males and 48 females. The database of 1120 images is organized into 224 different folders each associated with the integer identification/number. The resolution of these images is 320×240 pixels and all these images were acquired in the indoor environment.

Table 1.2: Detail of some existing iris databases

Database	Research Lab	Version	Acquisition Device	Images	Subjects	Resolution	Color Model
CASIA [11]	IIS Recognition Research Group, Center for Biometrics and Security Research, National Laboratory of Pattern Recognition, Institute of Automation, Chinese Academy of Sciences Beijing, China	TestV1	IrisGuard AD100	10000	1000	640 × 480	Grayscale
		IRISv1	Self-developed	756	108	320 × 280	Grayscale
		IRISv2	OKI IRISPASS-h	1200	60	640 × 480	Grayscale
			CASIA-IrisCamV2	1200	60	640 × 480	Grayscale
		IRISv3-Interval	Close-up iris camera	2639	249	320 × 280	Grayscale
		IRISv3-Lamp	OKI IRISPASS-h	16212	411	640 × 480	Grayscale
		IRISv3-Twins	OKI IRISPASS-h	3183	200	640 × 480	Grayscale
		IRISv4-Interval	Close-up iris camera	2639	249	320 × 280	Grayscale
		IRISv4-Lamp	OKI IRISPASS-h	16212	411	640 × 480	Grayscale
		IRISv4-Twins	OKI IRISPASS-h	3183	200	640 × 480	Grayscale
		IRISv4-Distance	Long range iris camera	2567	142	2352 × 1728	Grayscale
		IRISv4-Thousand	Irisking IKEMB-100	20000	1000	640 × 480	Grayscale
IRISv4-Syn	By image synthesis	10000	1000	640 × 480	Grayscale		
UBIRIS [12]	Soft Computing and Image Analysis (SOCIA) Group, Department of Computer Science, University of Beira Interior, Portugal	v1	Nikon E5700	1877	241	800 × 600	RGB
		v2	Canon EOS 5D	11102	261	400 × 300	sRGB
IITD [13]	Biometrics Research Laboratory, IIT Delhi	v1	JIRIS, JPC1000, digital CMOS camera	1120	224	320 × 240	Grayscale

1.5 Performance Measures

Biometrics seldom compare two templates from the user who are exactly the same. There is the difference between two templates due to scanning conditions, change in characteristics with respect to aging, change in acquisition scenarios, etc. Therefore, feature sets originating from the same individual need not always be the same. When two different biometric templates originating from the same individual are different then it is known as **intra-class** variations. However, variations that occur between templates originating from two different individuals are known as **inter-class** variations [14]. Two biometric templates, when compared to find the intra-class variation, generates the *genuine* scores. The two biometric templates when compared to find inter-class similarity generates *imposter* scores.

1.5.1 Recognition Performance

The error rate equations for system operating in recognition mode are discussed as follows:

- **False Acceptance Rate** (FAR) or False Match Rate (FMR) is defined as percentage of imposters incorrectly matched to the non-matching template.
- **False Rejection Rate** (FRR) or False Non Match Rate ($FNMR$) is the percentage of genuine people incorrectly rejected by the system.
- **Equal Error Rate** (EER) is the point where FAR equals FRR . In general, lower the equal error rate value, higher the accuracy of the biometric system.
- **Genuine Acceptance Rate** (GAR) is the percentage of genuine scores being correctly accepted and is defined as $GAR = 1 - FRR$. A hypothetical score distribution curve is shown in Figure 1.7. This curve graphically demonstrates the performance measures used in recognition mode.
- **Receiver Operating Characteristic** (ROC) curve is a comprehensive way to analyze the performance of a biometric system. It depicts the dependence of

FAR with GAR for change in the value of threshold. The curve can be plotted using linear, logarithmic or semi-logarithmic scale.

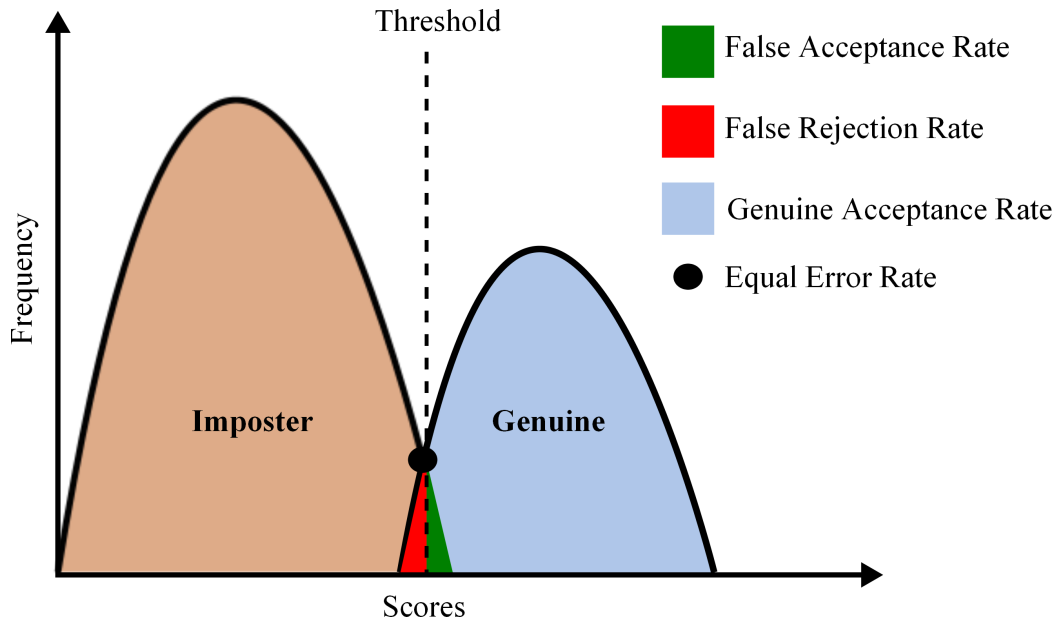


Figure 1.7: A hypothetical curve demonstrating the performance measures used during recognition.

1.5.2 Identification Performance

During identification, the gallery space is partitioned into bins for search time reduction. The error rate equations of systems operating in identification mode [14] can be defined using Cumulative Match Characteristic (CMC) Curve, which is defined below:

Cumulative Match Characteristic (CMC) Curve The rank- k identification indicates the number of correct identities that occur in top k matches. Let R_k denote the number of elements of probe set in top k and N be the total number of images enrolled in the database, then the probability of identification is given by $pi = \frac{R_k}{N}$. Cumulative Match Characteristic curve represents the probability of identification pi at various ranks k .

1.6 Wavelet: A Suitable Candidate for Texture Analysis

A close inspection of an iris image reveals its richness in texture. The texture information is higher at the collarette. Apart from that, it consists of random characteristics like radial furrows, concentric furrows, pigment dots, crypts etc. These attributes have different frequencies, which can be best described by a multiresolution analysis (MRA) technique. The discrete wavelet transform is an MRA technique, which can represent the iris image in different orientation and scaling.

Wavelet transform is a multiresolution technique, which has found successful applications in digital image processing. It is found to offer some advantages over classical block transform techniques such as the discrete cosine transform (DCT). It carries high importance with the problem of designing suitable multiresolution transforms that are adapted to the given image signal, in the sense that they maximize the coding gain at each resolution level. A simple alternating optimization algorithm is derived for solving this problem in the framework of the lattice realization of para-unitary quadrature mirror filters (QMF). The wavelet transform has the following advantages over its counter parts:

- The wavelet transform is a multiresolution description of an image: the decoding can be processed sequentially from a very low resolution, corresponding to a very compact code, to the highest resolution. Schemes based on the Laplacian pyramid also offer this advantage, but the wavelet transform allows furthermore perfect reconstruction.
- The wavelet transform is closer to the human visual system than the DCT transform. Hence, the artifacts introduced by wavelet transform coding with a high compression ratio and adequate perceptual quantization are less annoying than those introduced at the same bit rate by the DCT.
- The wavelet transformation of an image creates a data structure known as the

scale-space representation. In this representation, the high (spatial) frequency signals are precisely located in the pixel domain, while the low-frequency signals are precisely located in the frequency domain. Whereas the DCT has a spatial resolution that is independent of frequency, the spatial resolution of the wavelet transformation increases linearly with frequency. Therefore, sharp edges, which are well localized spatially and have a significant high-frequency content, can be represented more compactly with the wavelet transformation than with the DCT. On the other hand, the overall spectrum of most images is very much of a low-pass type. Now, while the frequency resolution is independent of frequency for the DCT, it is inversely proportional to frequency in the wavelet transformation. This allows the wavelet transformation to separate the dominating low frequency end of the spectrum into increasingly finer subbands. For strongly low-pass signals, the spectra of the subband signals provided by the wavelet transformation will be whiter in the subbands that contribute significantly to the signal power.

The key point of texture analysis is that extracted texture features must represent at the same time some local and some global characteristics of texture [15–17]. Psychovisual studies indicate that human visual system processes visual information in a multiscale way. It has been found that the responses of cells in visual cortex in the brain are similar to the Gabor functions. That is why Gabor filters have been so intensively studied in the context of texture analysis [18]. They offer multiscale and multiorientation processing of textural information. Wavelet filter bank is another multiscale approach to carry out the texture analysis [19,20]. However, Gabor filters have disadvantages over wavelet filter bank:

- Gabor functions do not form an orthogonal basis set, which results in non-compact representation of feature; hence requires more memory during computation.
- There are no efficient algorithms exist for computing the forward and inverse

transformations.

- The time required for extracting feature is computationally quite high, which limits the retrieval speed.

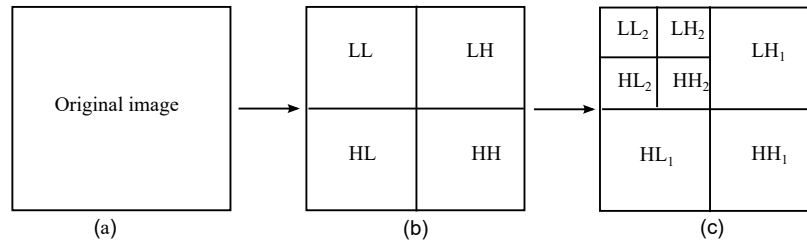


Figure 1.8: Two level decomposition using DWT (a) original image (b) First level decomposition (c) Second level decomposition

In linear phase discrete wavelet transform [21–28] (DWT), the image is actually decomposed i.e., divided into four sub-bands and critically sub-sampled by applying DWT as shown in Fig. 1.8. These subbands labeled LH₁, HL₁ and HH₁ represent the finest scale wavelet coefficients i.e., detail images while the sub-band LL₁ corresponds to coarse level coefficients i.e., approximation image. To obtain the next coarse level of wavelet coefficients, the sub-band LL₁ alone is further decomposed and critically sampled. This results in a two-level wavelet decomposition as shown in Fig. 1.8(b). Similarly, to obtain further decomposition, LL₂ will be used. This process continues until some final scale is reached. The values or transformed coefficients in approximation and detail images (subband images) are the essential features, which are shown here as useful for texture analysis and discrimination. As micro-textures or macro-textures have non-uniform gray level variations, they are statistically characterized by the features in approximation and detail images. In other words, the values in the subband images or their combinations or the derived features from these bands uniquely characterize a texture. The features obtained from these wavelet transformed images are shown to be used for texture classification.

1.7 Research Challenges

Despite of being an established biometric modality, there are open issues associated with iris recognition systems. These issues need to be addressed for making it user friendly and successful in real time implementation. Iris image acquisition is a cumbersome task, which must be done with utmost care. Otherwise, the extraction of region of interest is not done properly. Segmentation failure will lead to reduced accuracy. Feature extraction from such images lay big challenge, that must be done carefully. Wavelet filter banks and Gabor filters have been extensively used extracting features from iris images. Also wavelet filter bank is found to yield superior results than its counterparts. Hence, it is required to study the performance of various wavelet filter bank extensively in non-ideal situations.

1.8 Research Objectives

The aforementioned research challenges are addressed to improve the performance of the iris biometric system in practical scenarios. The research objectives are to:

1. Study the performance of a proven biorthogonal wavelet filter bank named CDF 9/7 [29] for feature extraction. Biorthogonal wavelet filter bank have been extensively used for texture analysis. Hence, a CDF 9/7 is chosen to extract energy feature from non-ideal iris images. The reason behind CDF 9/7 wavelet filter bank is its symmetric and energy preservation property. This is why it has been used in JPEG 2000 [30] standard compression scheme.
2. Improve the frequency selectivity of 9/7 biorthogonal filter bank. Frequency selectivity plays a vital role in feature extraction. It is known that B-Spline family wavelet filter bank can be presented by a half-band polynomial. Hence semidefinite programming technique can be used to optimize the wavelet parameters to increase performance of the recognition system.
3. Develop a structured biorthogonal wavelet filter bank based on triplet half band

filter bank. Since structured design helps in achieving good frequency response, it can help characterize iris texture properly.

4. Develop compact feature representation for iris recognition. It is highly desirable to store compact features in the gallery. It is known that cepstrum [31] components of an image give more weight to the high frequency block and helps in developing a robust feature. In order to achieve the goal, wavelet cepstrum based feature is studied.

1.9 Thesis Organization

This thesis starts with an introduction to biometrics including the research challenges and objectives. It is organized into seven chapters where each chapter portrays the contributions specific to a domain. The layout of this thesis is given below.

Chapter 2: Literature review

The existing literature is explored covering three major domains of iris feature extraction: (a) global feature, (b) local feature, and (c) region based feature representation. A tabular comparison of various approaches are presented along with the reported performance at the end.

Chapter 3: CDF 9/7 for iris feature extraction

This chapter deals with study of CDF 9/7 biorthogonal wavelet filter bank. The normalized images are preprocessed and then CDF 9/7 wavelet filter bank is applied to extract energy features. The performance of the same is then evaluated and compared with some of the contemporary methods.

Chapter 4: Tunable 9/7 filter bank for iris feature extraction

A tunable approach for developing 9/7 filter is studied. This method deals with representation of the half-band polynomial from z -domain to x -domain. The motivation behind this is to increase the frequency selectivity of the filter bank.

Then, semidefinite programming technique is used to optimize the low/high pass filter co-efficients. Then the energy feature is extracted from the normalized iris images.

Chapter 5: Iris feature extraction using THFB

In this chapter, triplet half-band filter bank is studied for energy feature extraction from normalized iris images. To characterize the iris texture, a 10^{th} order half-band polynomial is considered. This filter bank has superior frequency selectivity, time-frequency localization apart from other parameters.

Chapter 6: Wavelet cepstrum features for iris recognition

This chapter presents an experimental investigation of wavelet cepstrum based features. Cepstrum features are well investigated in speech recognition. With this motivation, wavelet cepstrum based method is used to extract energy feature from normalized iris images. The proposed technique is then compared with other techniques.

Chapter 7: Conclusions and future Work

This chapter presents the conclusions derived from the proposed methodologies with more emphasis on achievements and limitations. The scopes for future research are highlighted at the end.

Chapter 2

Literature Review

Iris is known to be one of the most popular biometric trait among all other modalities. Since the iris feature remains stable over a period of time, it is highly reliable. These properties have motivated many researchers to explore the feasibility of using iris as a standard biometric modality. Daugman has proposed the first operational iris recognition system in 1993 [4]. This landmark proposition has established iris as a potential biometric modality with many real-time applications [5]. However, it has many challenges to mitigate to be accepted in real-time applications. Since iris is rich in texture, it has to be characterized properly. It has many attributes, with varied frequency. Hence a multi-resolution analysis can help us achieve the goal. In this thesis, contributions are made to represent feature by studying the application of filter bank in iris biometrics. Basically, the iris features can be global, local, or region based. Since literature in each direction is independent of the other, the state-of-the-art approaches are explored for each category. The existing literature is described covering three major domains of feature extraction in iris biometrics as shown in Figure 2.1. In Section 2.1, *global feature* extraction for iris biometrics is given in brief. Different *region based feature* extraction approaches are discussed in Section 2.2 followed by Section 2.3 that summarizes few well-known *local feature* extraction approaches for iris.

A careful study on automatic iris recognition reveals that numerous works have been reported since the early 2000. Basically, the features suggested so far are clarified

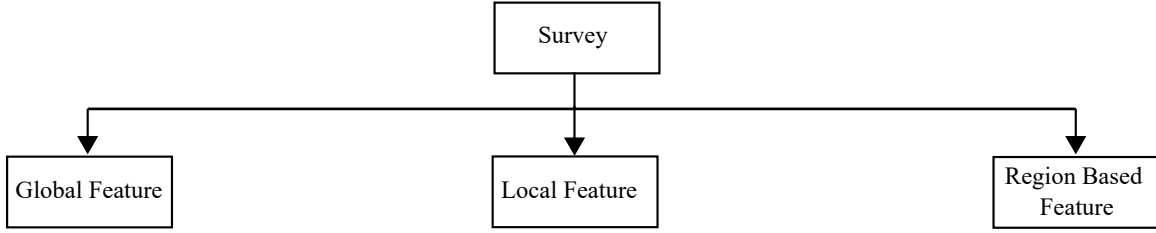


Figure 2.1: Categorization of literature explored in iris biometrics into three domains.

into three different categories: global, local, and region based features. In this section, we have given the review of different features in sequel.

2.1 Global Features

In these schemes, the features are extracted without distinguishing an object from the background. This is particularly suitable under scenarios when the complete image describes the potential features that can be used for identification. Global features are widely considered for iris recognition.

Wildes [32] has developed a iris recognition system, which requires image acquisition in a very constraint environment. He has developed a technique to perform contour fitting in two steps. The first step deals with the conversion of image intensity information into binary edge-map. Second step employs a edge points voting scheme to instantiate particular contour parameter values. A gradient based edge detection is used to recover the edge-map that consists of thresholding the magnitude of the image intensity gradient i.e.

$$|\nabla G(x, y) * I(x, y)|, \text{ where } \nabla \equiv \left(\frac{\partial}{\partial x}, \frac{\partial}{\partial y} \right),$$

while $G(x, y) = \frac{1}{2\pi\sigma^2} e^{-\frac{(x-x_0)^2+(y-y_0)^2}{2\sigma^2}}$ is a two-dimensional Gaussian with center (x_0, y_0) and σ represents the standard deviation that smooths thespatial scale of edges under consideration. After extracting the annular region from the raw iris image, the texture is characterized with the pyramid of Laplacian constructed with four different resolution levels. Normalized correlation is then used for classification purpose.

Nabti et al. [33] have studied a multiscale edge detection approach to localize

the iris region. The same is implemented using wavelet decomposition and gradient method. Then, the popular rubber sheet method is used to normalize the segmented iris region. The iris texture is analyzed using first wavelet maxima components in horizontal and vertical directions using five scales to extract all dominant features. Then for each component special Gabor filter bank is applied with four scales and six orientations to obtain 240 filtered images. The feature vector is created in two different ways, i.e. statistical measure by considering *mean* and *variance* (480 feature elements) and *moment invariant features* (1680 feature elements).

Boles and Boashash [34] have proposed the application of 1-D wavelet transform to compute the zero-crossing representation at different resolution levels of a concentric circle on an iris image. To mitigate the effect of noise at finer levels few low-level resolutions are considered excluding the coarsest level. The disadvantage of this method is that, zero crossing is not a robust feature. It provides much less information along a virtual circle on the iris which affects the recognition accuracy. Lim et al. [35] have studied the application of Haar wavelet for feature extraction using normalized iris image. They have employed the bisection method to determine the center of pupillary boundary and then the radius increased gradually to segment the limbus boundary. Further the segmented iris region is converted from cartesian to polar form to obtain a 450×60 normalized image. They have decomposed the iris image by applying Haar wavelet up to four levels to get the 28×3 sub-images. Finally, feature vector is organized by combining 84 features in the HH sub-image of the high-pass filter of the fourth level decomposition and average value for the three remaining high-pass filter coefficients. The dimension of the resulting feature vector is 87. To reduce space and computational time for manipulating the feature vector, each real value is quantized into binary value by simply converting the positive value into 1 and the negative value into 0. They have experimented the performance of Haar wavelet and proved the superiority of Haar wavelet over Gabor transform. The limitation of this method is that, it loses middle frequency components of the iris, so may not perform well in noisy situations.

Ma et al. [36, 37] have developed a iris recognition system that consists of two phases. The first phase deals with assessment of quality of input image, and then selection of a clear iris image from such a sequence. The second phase deals with the application of spatial filters which can correctly characterize the iris texture to capture the local details of the iris so as to produce discriminating texture features. Then the classification is done by employing a nonparametric statistical approach to study the performance over a sizeable database. Costa and Gonzaga have extended the work of Ma et al. to selectively carry out the quality assessment from a sequence of video. Then from the acquired good quality frames, statistical features are extracted for recognition purpose. The recognition accuracy is very promising with average accuracy of 99.1%. Ma et al. [38] have proposed a three step method to preprocess raw iris image: (i)iris localization and removal of eyelid and eyelashes (ii) normalization of iris region (iii) contrast enhancement to mitigate the problem due to lighting condition. Then a set of 1-D intensity signals are constructed, which are capable of retaining the most sharp variations in the original iris image using wavelet transform. They have used a wavelet function, which is a quadratic spline of a finite support to extract features. Hamming distance is used for classification. The performance of their algorithm is near perfect on CASIA database.

Sun and Tan [39] have developed multilobe differential filters (MLDF) to compute ordinal measures. Ordinal measures help encode qualitative information of visual signal instead of quantitative values. An MLDF operator moves across the whole normalized iris image and each ordinal comparison is encoded as one bit (1 or 0 according to the sign of the filtering result). All of the binary iris codes constitute a composite feature of the input iris image, namely, ordinal code (OC). The dissimilarity between two iris images is determined by the Hamming distance of their features. In order to cope with the possible rotation difference between the two iris images, the input ordinal code is circularly rotated at different starting angles to match the template *ordinal code*. And the minimum Hamming distance of all matching results is the measure describing the dissimilarity between the two iris images. The

disadvantage of the proposed method is that ordinal measures computed from distant image regions lose the locality property and accuracy is affected by nonuniform illuminations.

Vatsa et al. [40] have proposed a *SVM* based approach to select locally enhanced regions from normalized iris images to extract global features using 1-D log polar Gabor transform, and local topological features using Euler numbers. These features are combined together to get good recognition accuracy. Dong et al. [41] have proposed a class-specific weight map based learning method to extract iris features. Velisavljevic [42] has proposed a method to extract iris features using the oriented separable wavelet transforms i.e. *directionlets*. The generated iris code is binary string having fixed length.

Sanchez-Avila and Sanchez-Reillo [43, 44] have discussed two approaches to iris biometric system. First one is based on Gabor filter and for classification Hamming distance is considered. Another approach deals with zero-crossing representation of two different iris representations. They have experimented with different classifiers like Euclidean distance and d_Z . Another translation, scale, and rotation invariant approach is also proposed by the authors. The results obtained are very promising with classification accuracy up to 99.60% and equal error rate 0.12%. Chin et al. [45] have proposed S-Iris code for cancelable iris biometrics. They have used 1-D Log-Gabor filter to extract feature from normalized iris images. Then the feature vector is reduced to produce S-Iris code that provides higher accuracy and reduced complexity. Huang et al. [46] have proposed a rotation invariant iris feature extraction by applying non-separable wavelet and Gaussian Markov random fields (GMRF). The first phase consists of designing eight non-separable wavelet filters to provide information in eight different directions. To achieve rotation invariance to deal with head tilt and eye rotation, GMRF is used to characterize the filtered iris images. Hollingsworth et al. [47] have proposed to improve the overall accuracy of iris code by fusion of Hamming distance and fragile bit distance.

Global feature extraction is also discussed for noisy iris, off-angle iris recognition [2,

48–60].

2.2 Region Based Features

The most notable and commercially accepted work, is reported by Daugman [4], who has proposed 2-D Gabor filter to demodulate phase information of an iris image to create an *iriscode* for the authentication. The disadvantage of Daugman’s method is that, it is very time consuming. In another work, Ma et al. [37] have proposed a bank of spatial filters to extract iris features. They have considered two iris regions in the horizontal direction very close to the pupil from iris image after using quality descriptor for checking suitability for texture analysis. For extracting iris feature, they have proposed Gabor filter modulated with circularly symmetric sinusoidal function.

Miyazawa et al. [61,62] have incorporated a technique of “eyelid masking” to deal with irrelevant eyelid region, and considered only the lower half of the iris region to deal with occlusion. Then, 2-D Fourier Phase Code (FPC) is used for representing iris information. Matching is performed using *phase only correlation*. When two iris images are similar, their POC function gives a distinct sharp peak; otherwise the peak drops significantly. Monroe and Rakshit [63,64] have proposed patch based technique to extract FFT and DCT based features from normalized iris images. Their proposed algorithm is able to produce 100% correct accuracy rate in ideal condition.

Proenca and Alexandre [65] have proposed a method to deal with non-ideal iris feature extraction. The proposed technique deals with dividing the segmented and normalized iris image into six regions. Then 2-D Gabor filters are applied for independent feature extraction and comparison for each region. Rahulkar et al. [66–68] have proposed a region based technique for energy feature extraction using 2-D wavelet derived from a new class of biorthogonal wavelet filter bank.

2.3 Local Features

Local features are those patches of an image that differ from its neighborhood. They are extracted around special points or *keypoints*. The features extracted around each detected keypoint are stored as a *descriptor*. Keypoint descriptors are based on the appearance of an object at particular interest points and are invariant to image scale and rotation. They are also robust to changes in illumination, noise, and minor changes in viewpoint. Local features find correct correspondence between the gallery and probe images irrespective of large variations in transformation, occlusion, and illumination. These features have shown good performance for biometrics recognition. Below we discuss few notable works in local feature extraction from iris images:

Chenhong and Zhaoyang [69] have studied the application of automatic scale selection for local feature extraction from normalized iris images. Their proposed system first filters the given iris image by adopting a bank of Laplacian of Gaussian (LoG) filters with many different scales and computes the normalized response of every filter. The maxima of normalized response over scales for each point are selected together as the optimal filter outputs of the given iris image. The feature vector consists of location and scale information, which is then binary coded for iris feature representation.

SIFT (scale invariant feature transform) is a well known keypoint descriptor for object recognition [70]. SIFT is applied to regions of iris which does not require polar transformation. The idea is to develop a keypoint descriptor that is capable of performing well for iris textures. Mehrotra et al. [71, 72] proposed an iris recognition technique using interest point pairing. The feature set comprises spatial location of each corner point (detected using Harris) and entropy information of window around the corner. The corner points are paired using dual stage approach. At the first stage, the potential corners are obtained by finding Euclidean distance between spatial coordinates. These potential corners are used to find actual corners based on their affinity around a window, which is measured using Mutual Information (MI). The

authors in [73, 74] have developed an iris recognition system by applying Speeded Up Robust Features (SURF) directly on annular iris images. This system performs well for iris because of its capability to distinguish significant texture features from the background. Mehrotra et al. [75] have developed a technique to combine Fourier transform with SIFT. The Fourier based keypoint descriptors are paired using phase-only correlation (POC) . The combination of SIFT with Fourier for feature extraction and matching using phase-only correlation is found to perform better compared to SIFT. Noh [76] et al. have proposed a local feature based iris recognition using discrete wavelet frame (DWF) filter. For classification they have considered Hamming distance.

Du et al. [77] have proposed an iris recognition system by combining Gabor wavelet with SIFT to generate Gabor descriptor. Both phase and magnitude of Gabor wavelet values are used as features. The Gabor feature descriptor is invariant to scale, deformation, rotation, and contrast of two iris images. This approach performs well for frontal and off-angle iris images taken under non-cooperative scenarios. It is assumed that the rich texture pattern of iris undergoes non-linear deformation due to pupil contraction and dilation. Zhang et al. [78] proposed deformable DAISY matcher for robust iris feature matching. The dense DAISY descriptors are extracted from the normalised iris image for low computational cost. The set of keypoints are localised on the feature map to match using deformation tolerant matching strategy. Sun et al. [79] proposed a recognition system using bovine iris images captured from non-cooperative audiences. The pupil and iris circles are localised using active counters and features are extracted using SIFT. After removing keypoints from pupil region, the keypoint descriptor is generated using bag-of-features and then distance of histogram representations is adopted for matching. Local feature based approaches have shown to improve the iris recognition performance.

Yu et al. [80] have proposed a multi-channel Gabor filter based key point extraction technique and Euclidean distance as classifier for iris recognition. Bakshi et al. [10] have proposed a multi-scale local feature extraction technique for periocular

recognition. The proposed feature is capable of extracting high-dimensional subtle features existent in the iris region as well as low-dimensional gross features in the periphery skin region of the iris. The robustness of the developed feature is due to its ability to find coarse-to-fine features in multi-scale and different phases of the same.

Table 2.1: Recognition through iris biometric

Year	Authors	Feature extraction algorithm	Feature matching algorithm	Testing database	Performance results
1993	Daugman [4]	256 byte iris code comprising most significant bits from multi-scale quadrature 2-D Gabor wavelet	Hamming Distance	592 images (480 × 640 8-bit) from 323 subjects captured in 3 years by Ophthalmology Associates of Connecticut	EER : 1 in 131000
1997	Wildes [32]	4 level multiscale Laplacian pyramid	normalized correlation	10 images for each of 60 iris captured from 40 subjects [two sessions, inclusion of twin subjects]	no false positive, and no false negative
1998	Boles and Boashash [34]	1-D Zero Crossing Wavelet transform	two dissimilarity functions	128 × 128 grayscale images captured from single eye of each subject [different illumination and eye-to-camera distance]	Accurate in case of noise free images, partially successful in classifying noisy images
2001	Lim et al. [35]	87 bit feature vector using 2-D Haar Wavelet	Learning Vector Quantization	6000 iris images from 200 subjects of same age group captured in 3 months	Accuracy 99.3%
2003	Ma et al. [37]	vector of length 1,536 using Multichannel spatial filters	Fisher linear discriminant + three distance measure + bootstrap learning method	Constructed CASIA database for this experiment	Accuracy 99.43%
2004	Daugman [3]	2048 bit phase vector by 2-D Wavelet Demodulation	Hamming Distance	eye images from trials in Britain, the USA, Japan, and Korea	EER : 1 in 4 million
2004	Ma et al. [38]	1-D Key local variation using dyadic wavelet transform (quadratic-spline)	Hamming Distance	CASIA	Accuracy 100% with EER 0.07% [Feature extraction + Matching time 250.7ms]
2007	Monro et al. [64]	2,343 bit long iris feature code based on 1-D DCT	product-of-sum approach to Hamming Distance	CASIA, BATH	100% Correct Recognition Rate, worst case theoretical EER: 2.59×10^{-4}

Continued on next page ...

Table 2.1: Continued from previous page ...

Year	Authors	Feature extraction algorithm	Feature matching algorithm	Testing database	Performance results
2007	Proenca and Alexandre [65]	2-D Gabor Filter	Hamming Distance + classification scheme using multiple signatures	a subset of 800 images from 80 subjects chosen from each database : UBIRIS, CASIA, ICE	EER for UBIRIS: 2.38% EER for CASIA: 1.01% EER for ICE: 1.03%
2008	Vatsa et al. [40]	1-D Log polar Gabor transform for global feature, and Euler number for local feature	Hamming Distance + 2v SVM based fusion strategy	ICE, CASIA, UBIRIS	ICE: 0.74% FRR at 0.0001% FAR CASIA: 0.38% FRR at 0.0001% FAR UBIRIS: 7.35% FRR at 0.0001% FAR
2008	Nabti and Bouridane [33]	Wavelet maxima component + Special Gabor filters (Statistical Features) + Moment Invariants	Hamming Distance	CASIA	Correct Recognition Rate: Through statistical features: 99.52% Through moment invariants: 99.60%
2009	Velisavljevic [42]	Variable length (640 - 10240 bits) iris code by oriented separable wavelet transform (directionlets)	Hamming Distance	CASIA-IrisV3-Lamp	Maximum accuracy obtained is 94.7% with EER 4.124%
2009	Sun and Tan [39]	Ordinal Measures (OM) using Gaussian Kernel	Hamming Distance + Bootstrap learning scheme	BATH, CASIAv1, CASIA-IrisV3-Lamp, and ICE2005	EER on BATH: 4.39×10^{-4} EER on CASIA V1: 3.70×10^{-3} EER on CASIA V3: 3.48×10^{-3} EER on ICE2005 Left eyes: 1.06×10^{-2} EER on ICE2005 Right eyes: 5.72×10^{-3}
2010	Abhyankar and Schuckers [81]	Rotation invariant bi-orthogonal wavelet neural network using 5/3 filter	Hamming Distance	CASIA, BATH, Clarkson University Database, MAE, West Virginia University Database	EER 0% for 0° - 42° image rotation, accuracy falls below 40% for images with rotation upto 60°
2010	Chou et al. [54]	Derivative of Gaussian + Laplacian of Gaussian	Classifier ensembles	CASIA-v3-Interval and UBIRIS-v1	EER: for CASIA-v3-Interval : 0.031% for UBIRIS-v1 : 0.258%

Continued on next page ...

Table 2.1: Continued from previous page ...

Year	Authors	Feature extraction algorithm	Feature matching algorithm	Testing database	Performance results
2010	Huang et al. [82]	8 directional filters using symmetric orthogonal matrices + GMRF	Fisher linear discriminant + Polynomial classifier	CASIA-IrisV3-Lamp, UBIRIS, UPOL,	For all tested databases, the FRR is satisfactorily less for slightly high FAR
2011	Dong et al. [41]	256 × 16 bit long iris code from personalized weight map used to assign optimized weights to two Ordinal features (OF): 17-px trilobe OF, and 8-px bilobe OF	Hamming Distance	CASIAIrisV3-Lamp, BATH, and ICE2005 are used, CASIA-Iris-MultiReg is constructed for this experiment	EER for CASIA-IrisV3-Lamp: 7.75×10^{-3}
2013	Raffei et al. [83]	Multiscale representation of local Radon transform	Hamming Distance score combination	UBIRISv2	99.4% Accuracy with d' index 3.33
2013	Rahulkar et al. [67]	52 integer values from 2D non-separable non-redundant hybrid directional wavelet filter bank	k-out-of-n:A (KONA) post classifier	CASIA-Iris-v2, MMU1, UBIRIS	CASIA-Iris-v2:2.10% FRR at 0.1% FAR MMU1:2.02% FRR at 0.1% FAR UBIRIS:5.93% FRR at 0.1% FAR

2.4 Observations

The existing literature has offered new insights into the domain of iris. Some key observations from the existing literature are:

- Existing techniques extensively rely upon global features for implementing iris recognition system. Whereas, hybrid approach i.e. region based features are used successfully with improved performance over their counterparts.
- Since image acquisition is a challenging task, segmentation failure may occur frequently due to head tilt, eye rotation, and other factors.
- Wavelet based features are widely used for iris texture analysis due to their unique advantage.
- The existing wavelet filter bank are yet to be studied to carry out feature extraction in non-ideal environment.
- Since biorthogonal wavelet filter bank are used for iris texture analysis, special attention need to be paid to increase the frequency selectivity.

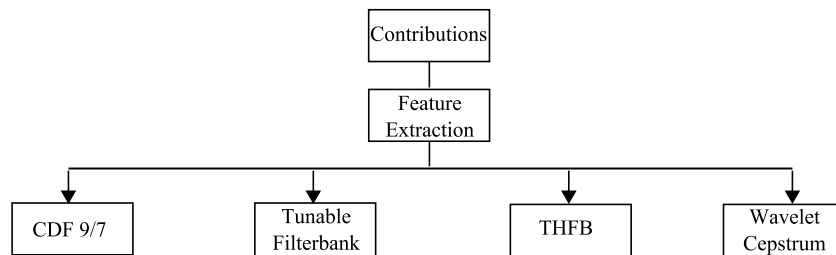


Figure 2.2: Contributions of this thesis.

In this thesis, an endeavour has been made to address the aforementioned issues. The contributions span across applications of different biorthogonal wavelet filter bank in the domain of iris biometrics as shown in Figure 2.2. Region based features are developed taking into consideration segmentation failure. The idea is to mitigate the effect of different unwanted artifacts during recognition. To characterize iris pattern,

frequency selectivity is given importance during the design of biorthogonal wavelet filter bank. The propositions of this thesis are discussed in detail in the subsequent chapters.

Chapter 3

CDF 9/7 for Iris Feature Extraction

Wavelet transforms have been broadly utilized in different image processing applications for more than two decades. For still-image coding [84, 85], in spite of the fact that the difference between a wavelet transform and Discrete Cosine Transform (DCT) is under 1 dB, wavelet transform offers extraordinary preferences over other mainstream transform being utilized as a part of image processing area. It is the multiresolution property of wavelet transform that gives better space-frequency analysis which makes it more suitable for certain image processing applications. Even wavelet transform can be used for removing block like artifacts [86] during image compression. The tree structure of wavelet transform makes wavelet based image compression achieve a high degree of scalability. This is the motivation behind the application of Cohen – Daubechies – Feauveau 9/7 (CDF 9/7) [29, 87] in JPEG2000 image compression scheme over DCT. In texture rich image analysis, biorthogonal filter banks (FB) are favored primarily because of their symmetry properties.

In this chapter, we have investigated the iris feature extraction technique using CDF 9/7 filter bank. Most of the iris recognition systems have been found to give near perfect performance in constraint environment. Unfortunately the accuracy falls drastically when the constraints are relaxed during image acquisition process. These include dilation of pupil, occlusion due to eyelids and eye lashes, and most importantly non-orthogonal view of iris. These factors result in reduced accuracy of the overall

system. In this work, a technique has been proposed to deal with segmentation failure and occlusion. The experimental studies deal with the superiority of CDF 9/7 filter bank over the frequency based techniques.

More accurate the iris texture representation, more reliable is the iris recognition system. A generalized block diagram of iris recognition system is shown in Fig. 3.1. It basically consists of four stages: image acquisition, preprocessing, feature extraction and matching. In the image acquisition stage the raw iris image is acquired using a dedicated camera. The preprocessing stage deals with segmentation and normalization of raw iris image. Then the features are extracted and stored in a database as reference. The normalization process is a cumbersome task, where there may be segmentation failure. This may severely affects the iris recognition accuracy.

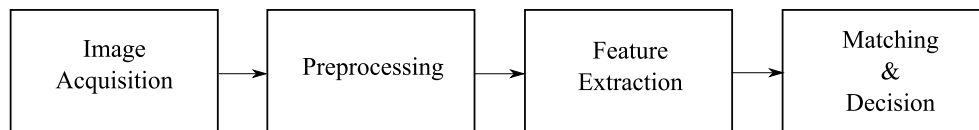


Figure 3.1: Generalized block diagram of iris-recognition system

In this chapter, we have intended to extract iris features using CDF 9/7 filter bank in non-ideal situations. The rest of the paper is organized as follows: Section 3.1 deals with some of the highly regarded works on iris recognition system followed by filter bank and iris texture analysis in Section 3.2. In Section 3.3, comparative study is given; then concluding remark is given in Section 3.4.

3.1 Related Work On Biorthogonal Filter Bank

A thorough literature survey reveals that considerable efforts have been put to devise various types of wavelet filter banks. Attention has been paid mostly in the development of orthogonal filter banks. Still biorthogonal filter banks have been paid importance due to its special characteristics such as *linear phase*, *better frequency selectivity*, and *regularity*. These earlier said properties are very much useful in image

analysis. Below we present some state of the art works in the field of biorthogonal filter bank.

Phoong, Vaidyanathan, and Ansari [88] have proposed a new class of two channel biorthogonal wavelet filter bank. Their proposed technique covers both causal stable *infinite impulse rate* (IIR) filter banks and linear phase finite impulse rate (FIR) filter banks. In their developed filter bank, perfect reconstruction is preserved structurally with low complexity. The analysis and synthesis filter design is based on a single transfer function, which makes the design procedure simple. The analysis low pass filter and synthesis low pass filter are made regular by imposing arbitrary number of zeros at $\omega = \pi$. It is guaranteed that both the low pass filters have same number of zeros. Their proposed method can also be easily mapped from 1D to 2D. This mapping is able to preserve the many of the properties of the 1D system. Frequency selectivity can also be controlled by tuning the control function used for designing the filter bank. Gawande et al. [89] have developed a two-channel one-dimensional wavelet filter bank using a modified generalized lifting structure and hybrid lifting scheme. The first filter bank is designed using general half band polynomial by imposing any number of vanishing moments. The generalized even-step and odd-step lifting structure is derived separately to obtain FIR filter banks. The second approach is based on the combination of individual even-step and odd-step lifting structure called as hybrid lifting structure to improve the frequency response of filters.

The most notable work reported in the literature of biorthogonal wavelets and used extensively in different image processing applications is the popular CDF 9/7 filter bank [29]. It is derived from the Lagrange half band polynomial (LHBP). It is adopted as standard for JPEG 2000 compression scheme as well as for fingerprint compression standard by FBI [90]. CDF 9/7 filter bank has all the desired properties: perfect reconstruction, regularity, near-orthogonality, and frequency selectivity. Since all the filter coefficients are irrational, one major disadvantage of CDF 9/7 filter bank for highly efficient implementation is that the computational complexity of discrete wavelet transform is much higher than that of the biorthogonal spline wavelet filters.

On the other hand, CDF 9/7 performs better than spline wavelet filters in image compression application. Villasenor et al. [91] have discussed about 6/10 filter bank. Their proposed filter bank is also based on LHBP [92]. A different factorization technique is adopted in the designing of the filter bank. The 6/10 filter design can also be inherited from the CDF 9/7 design procedure. More performance issues about MIT 9/7 filter bank, 9/11 filter bank can be found in [91, 93].

From the literature, it is found that the wavelet filter bank has emerged as a formal, and unified tool for different signal and image processing applications. Being a multiresolution technique, it has been applied successfully for extracting features from texture images. Unlike Gabor filter bank, it has low computational cost. Hence, wavelet filter bank is now-a-days preferred, as they produce excellent result on classification and segmentation of such images.

3.2 Proposed Iris Texture Analysis with CDF 9/7 Filter Bank

The two-channel filter bank [21, 94, 95] is shown in Fig. 3.2. The perfect reconstruction (PR) condition for the two-channel FB is given by the following two equations:

$$H_0(Z)G_0(Z) + H_0(-Z)G_0(-Z) = 2 \quad (3.1)$$

$$H_1(z) = z^{-1}G_0(-Z), G_1(z) = zH_0(-Z) \quad (3.2)$$

The product filter $P(z) = H_0(z)G_0(z)$ in (1) belongs to a special class of filters known as half band filter. The analysis scaling and wavelet functions are given by the following dilation equations:

$$\phi(t) = \frac{2}{|H_0(\omega)|_{\omega=0}} \sum_n h_0(n)\phi(2t - n) \quad (3.3)$$

$$\psi(t) = \frac{2}{|G_0(\omega)|_{\omega=0}} \sum_n h_1(n)\phi(2t - n) \quad (3.4)$$

where $h_0(n)$ and $h_1(n)$ are the analysis low-pass filter and high-pass filter coefficients,

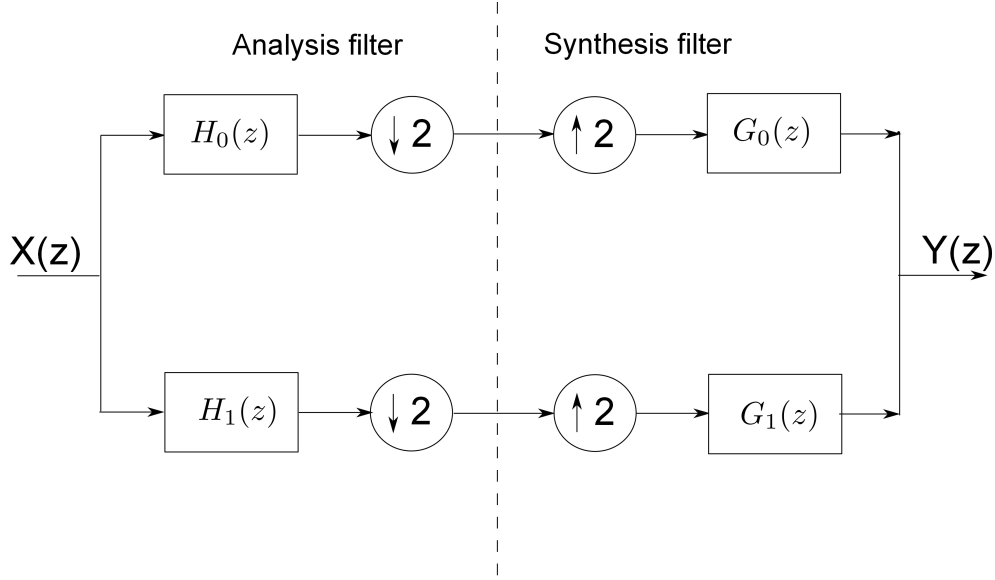


Figure 3.2: Block diagram of two band filter bank

respectively.

CDF 9/7 filter bank is designed upon Lagrange half band polynomial (LHBP). It is given by the following equation:

$$P_K(z) = z^K \left(\frac{1+z^{-1}}{2} \right)^{2K} \times \left\{ \sum_{n=0}^{K-1} \binom{K+n-1}{n} \left(\frac{(2-z-z^{-1})}{4} \right)^n \right\} \quad (3.5)$$

Filter banks designed using LHBP are imposed to have maximum number of zeros at $z = -1$, and thus, it has a maximally flat frequency response at $\omega = \pi$. CDF 9/7 family of filter banks are by far the most widely used (JPEG 2000) and popular biorthogonal filter banks.

A close inspection of the iris image reveals that, it contains non-uniform texture informations. The presence of different artifacts like crypts, radial furrows, concentric furrows, pigment dots, and collarette makes it random. Since all these artifacts have different frequencies, they can be best described by a multiresolution analysis (MRA) like CDF 9/7.

3.2.1 Advantage of CDF 9/7 Filter Bank over FFT

1. **Orthogonality:** In a filter bank, it is highly desired that the analysis and synthesis filters are similar. It is a quantitative measure of how far a biorthogonal filter bank is from orthogonality [96]. In the proposed approach, $|H_0(\frac{\pi}{2}) - G_0(\frac{\pi}{2})|$ is used to measure the orthogonality of the designed filters. Also, it is well known that orthogonality conserves the energy. This property helps in texture classification in the presence of noise. CDF 9/7 filter bank has orthogonality value 0.63.
2. **Time - frequency localization:** Time - frequency localization [97,98] criteria plays a very important role in texture analysis. The spatial and frequency localizations are calculated by using the following equations:

$$\Delta\omega^2 = \frac{\pi^2}{3} + 4 \sum_{n=0}^{L-2} \sum_{m=n+1}^{L-1} \frac{(-1)^{m-n}}{P(m-n)^2} h_m h_n \quad (3.6)$$

$$\text{where, } P = \sum_{n=0}^{L-1} h_n^2$$

$$\Delta t^2 = \frac{1}{P} \sum_{n=0}^{L-1} (n - \bar{t})^2 h_n^2 \quad (3.7)$$

$$\text{where, } \bar{t} = \frac{\sum_n n h_n}{\sum_n h_n}.$$

The time localization Δt^2 of the analysis low pass filter is computed to be 0.56 and frequency localization $\Delta\omega^2$ for the same is 0.57.

3. **Linear phase:** Linear phase is important because it ensures that the entire waveform is shifted by the same time. In non-linear phase system, since the different frequency components are delayed by different amounts, the waveform is distorted. A non-linear wavelet system badly affects the shape of the output signal, which in turn results in decrease of the texture discrimination capability. Since the proposed filter bank is based on a linear half band polynomial, it maintains the linear phase property.

3.2.2 Feature Extraction using CDF 9/7

Image acquisition of same iris image of the same eye may be variable due to pupil dilation, camera-to-eye distance, head tilt, and eye rotation within its socket. Hence, location and segmentation of the pupillary boundary and the limbic boundary is the first stage in iris preprocessing. Both the inner and outer boundaries of the iris are usually regarded as circles. The popular iris segmentation technique developed by Daugman called *integro-differential operator* (IDO) [4] is used and normalized with the help of Daugman's rubber sheet model of the fixed size 60×360 (Fig. 3.4). During segmentation, it is found that at times there are segmentation failures; hence, there are occlusion in the normalized images (Fig. 3.5). Following the approach of Proenca and Alexandre [65], the annular iris is then converted to a strip through mapping the intensities of polar coordinate points to corresponding Cartesian coordinate points as shown in Fig. 3.4(b). Since different regions of the iris have different qualities, the normalized iris this strip is fused with a mask to remove regions with low quality (higher noise). The mask (explained in Fig. 3.3) having the same size as the strip is filled with 1 at every pixel except the 2nd horizontal block when segmented into six equal horizontal regions. To fuse the iris strip with this mask (shown symbolically in Fig. 3.4(c)), a bitwise multiply operation (\otimes) is conducted. As a result, the strip obtained as output is masked by black pixel in the region which contains occlusion due to eyelids. The resultant strip retains the regions useful for recognition and removes noise-prone region (shown in Fig. 3.4(d)). The remaining five equal regions of the iris strip comprise our location of interest. The entire process is described in the block diagram in Fig. 3.7.

Since energy [99] is an important characteristic in identifying texture, the normalized energy is computed from each channel of the CDF 9/7. The wavelet energy in horizontal, vertical and diagonal directions at i^{th} level decomposition is,

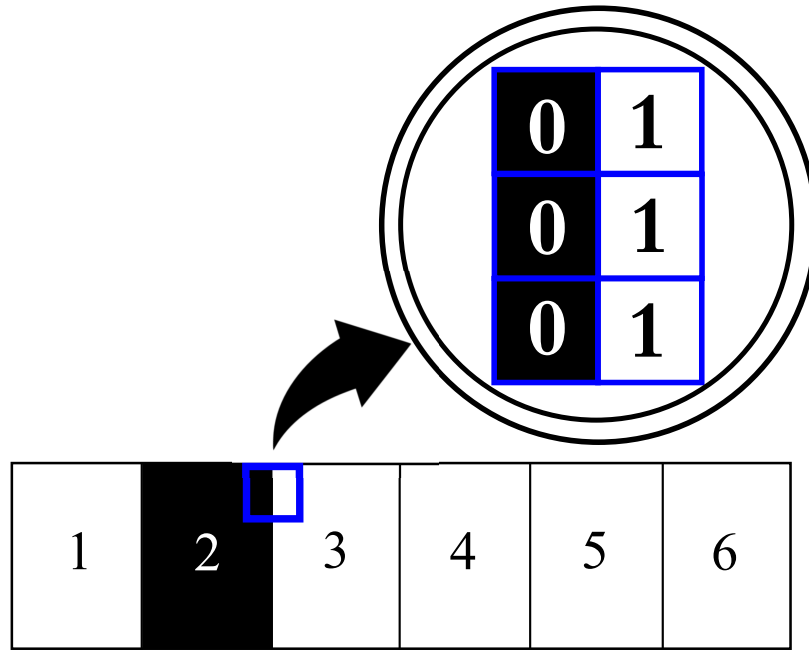


Figure 3.3: Normalized iris image divided into six equal regions

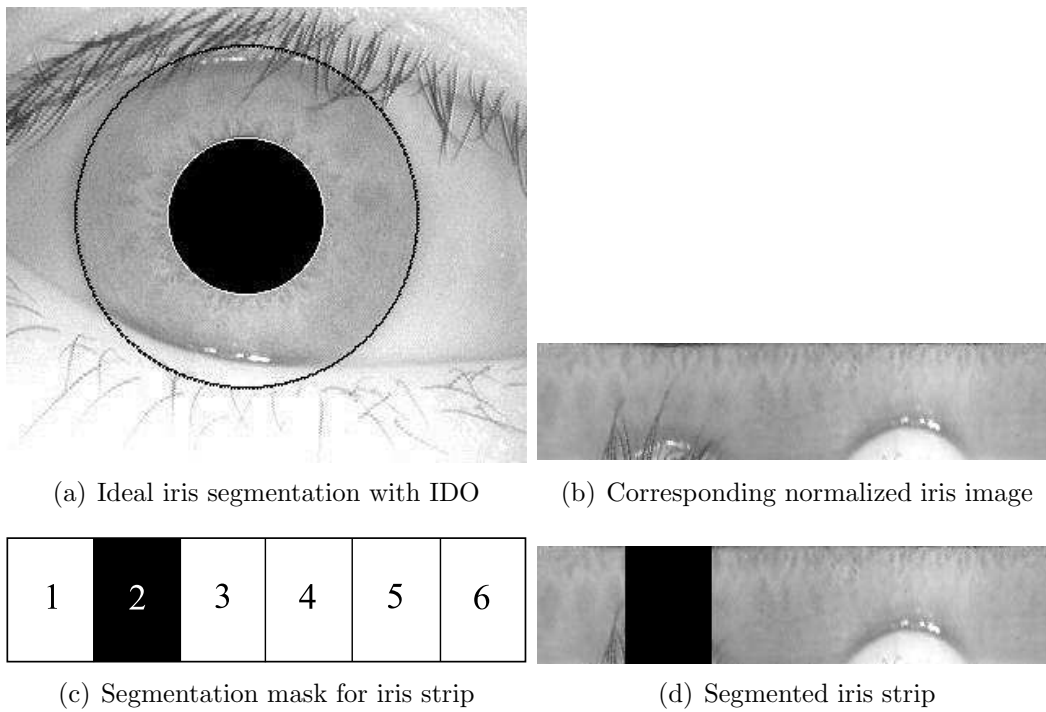


Figure 3.4: Iris localization with IDO

respectively defined as:

$$E_i^h = \frac{1}{M \times N} \sum_{m=1}^M \sum_{n=1}^N H_i(m, n)^2 \quad (3.8)$$

$$E_i^v = \frac{1}{M \times N} \sum_{m=1}^M \sum_{n=1}^N V_i(m, n)^2 \quad (3.9)$$

$$E_i^d = \frac{1}{M \times N} \sum_{m=1}^M \sum_{n=1}^N D_i(m, n)^2 \quad (3.10)$$

These energies represent the strength of the iris image's details in different directions at the i^{th} wavelet decomposition level. The feature vector (FV) is derived by concatenating the features at different scales and orientations as:

$$FV = [E_i^h, E_i^v, E_i^d]_{i=1,2,\dots} \quad (3.11)$$

The total number of subbands for CDF 9/7 is $3 \times i + 1$. The derived FVs of each

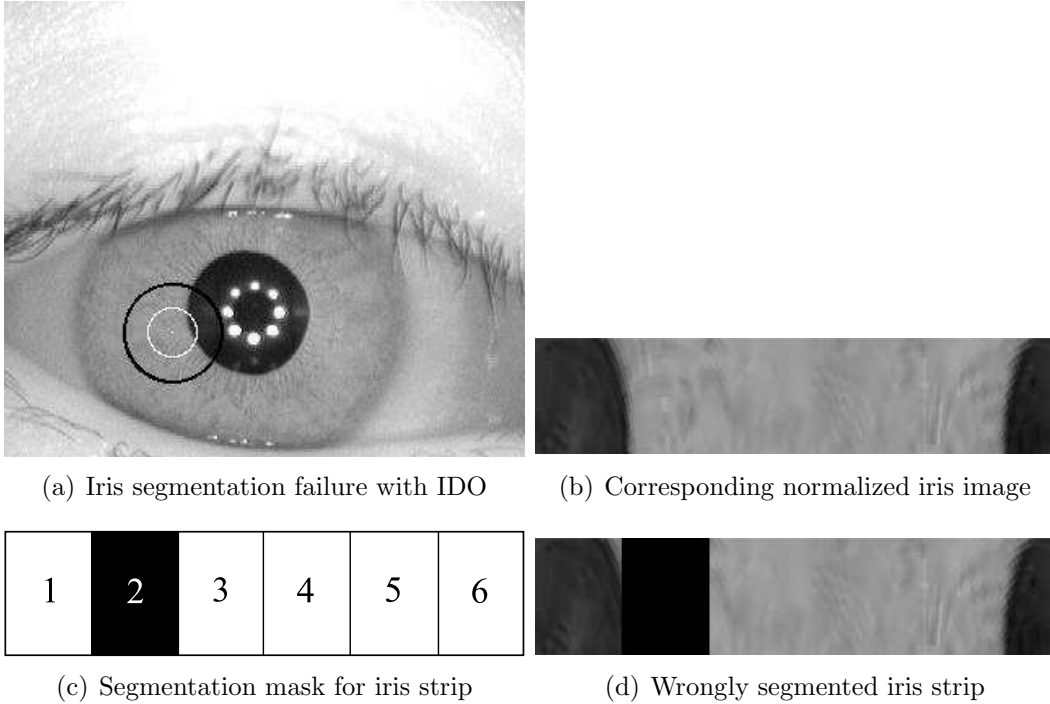


Figure 3.5: Iris localization failure with IDO

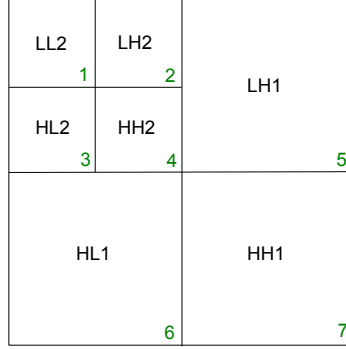


Figure 3.6: Two level decomposition using wavelet

region are stored in the database as reference during enrollment process.

To generate match score, we have considered the Canberra distance (CD) between test iris FV and that of the databases. The use of CD is due to the normalization property of individual feature components before computing the distance between test iris FV and that of the databases. The CD is computed as:

$$CD(X, Y) = \sum_{i=1}^B \frac{|X_i - Y_i|}{|X_i| + |Y_i|} \quad (3.12)$$

where, B is the dimension of FV. X_i is the i^{th} component of test FV and Y_i is i^{th} component of training image FV. When two images are from same subject, CD is expected to have a value close to zero. If matching between two images from two different subjects is performed, the value of CD is expected to be high. A properly chosen threshold can hence classify genuine and imposters.

3.3 Results and Discussion

This section discusses the result obtained on applying CDF 9/7 filter bank for iris recognition. The result obtained ensures the efficacy of the filter bank in extracting region based feature from iris template and yield accuracy. The performance of CDF 9/7 filter bank has been tested with a Near Infrared (NIR) databases CASIAv3 [11], IITD [13] as well as a visual spectrum database UBIRISv1 [12]. The following

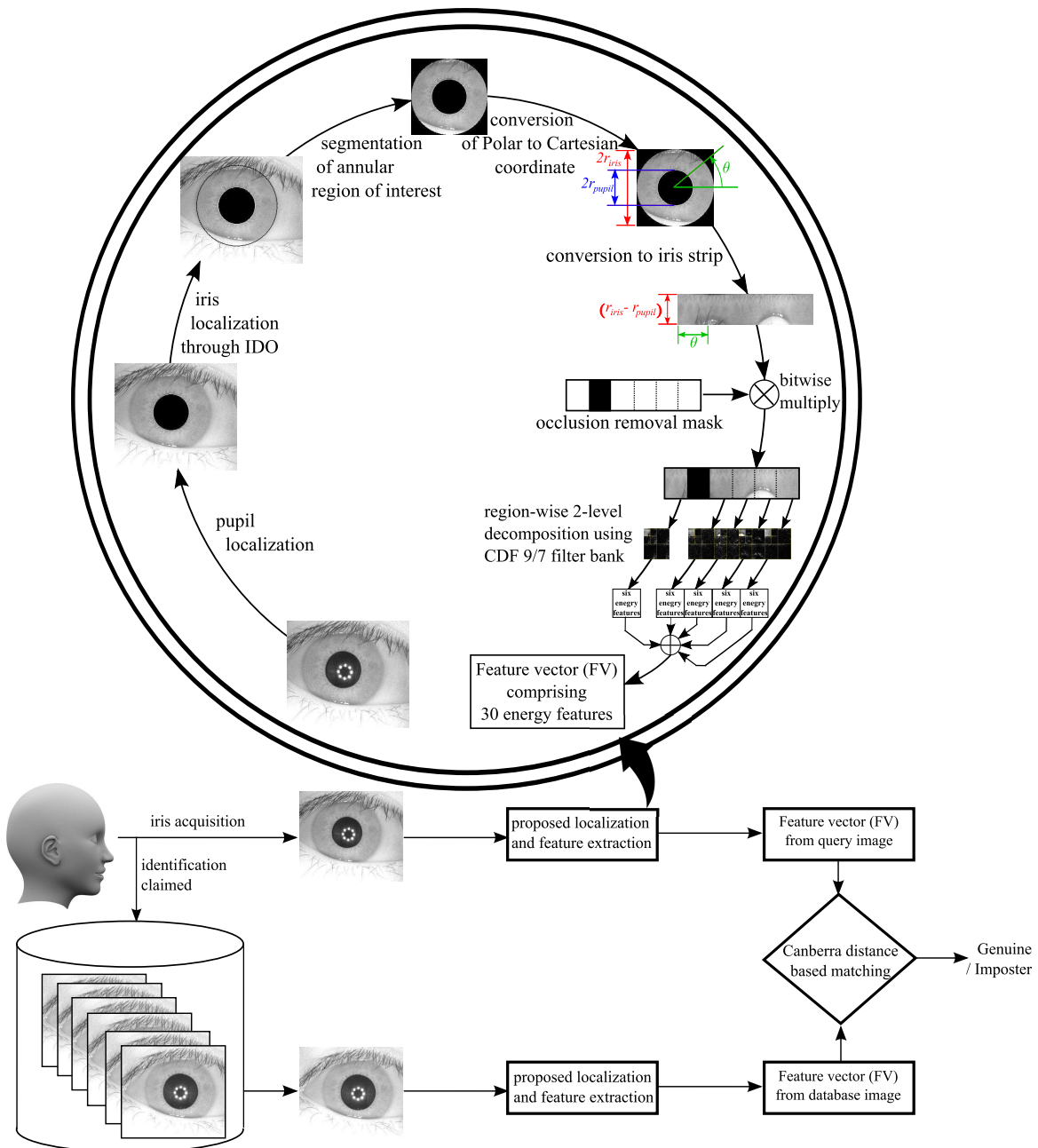
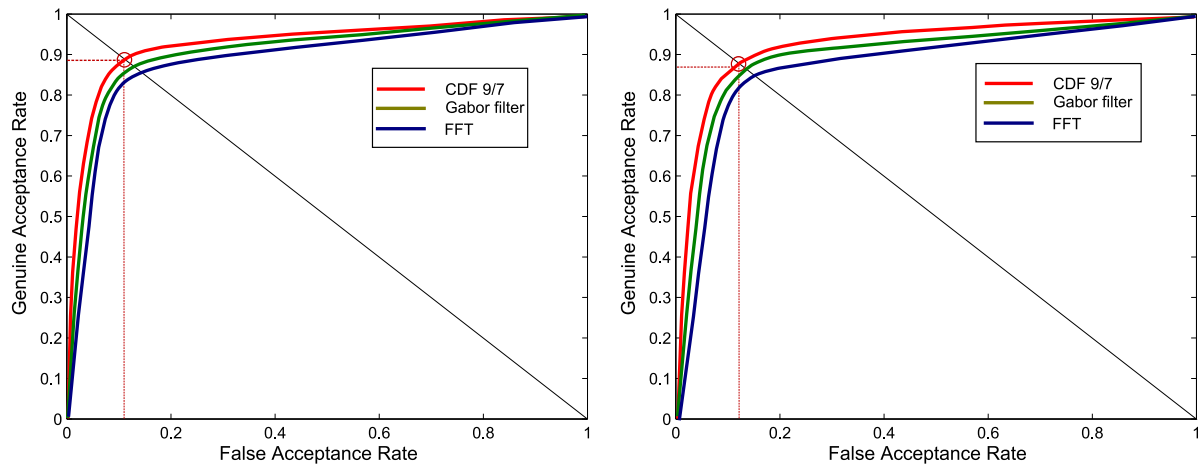


Figure 3.7: Block diagram showing proposed approach for iris recognition system

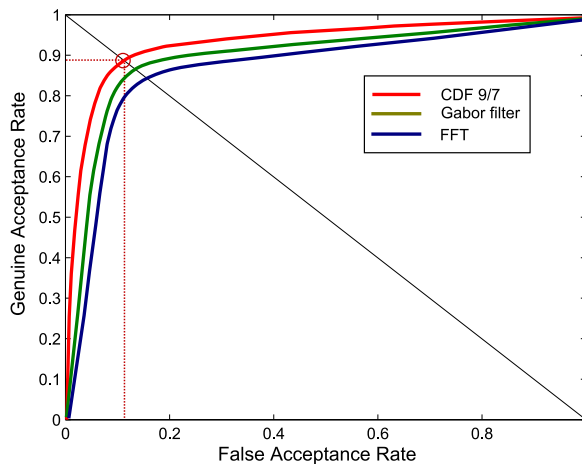
performance measures have been used to evaluate the efficacy of the proposed approach: false acceptance rate (FAR), false rejection rate (FRR), receiver operating characteristic (ROC), area under curve (AUC), and equal error rate (EER).

Table 3.1: Comparative analysis of proposed feature on different databases

Performance →		AUC (%)	FAR (%)	GAR (%)	d' index
Database ↓	Approaches ↓				
CASIA _{v3}	FFT	85.58	15.89	87.05	1.32
	Gabor filter	86.45	14.69	87.60	1.55
	CDF 9/7	88.25	11.53	88.03	1.76
UBIRIS _{v1}	FFT	84.61	16.18	85.40	0.98
	Gabor filter	85.71	14.32	85.95	1.52
	CDF 9/7	86.43	13.53	86.39	1.31
IITD	FFT	83.69	15.24	82.62	1.15
	Gabor filter	84.84	14.26	83.95	1.65
	CDF 9/7	87.31	13.89	88.51	1.71

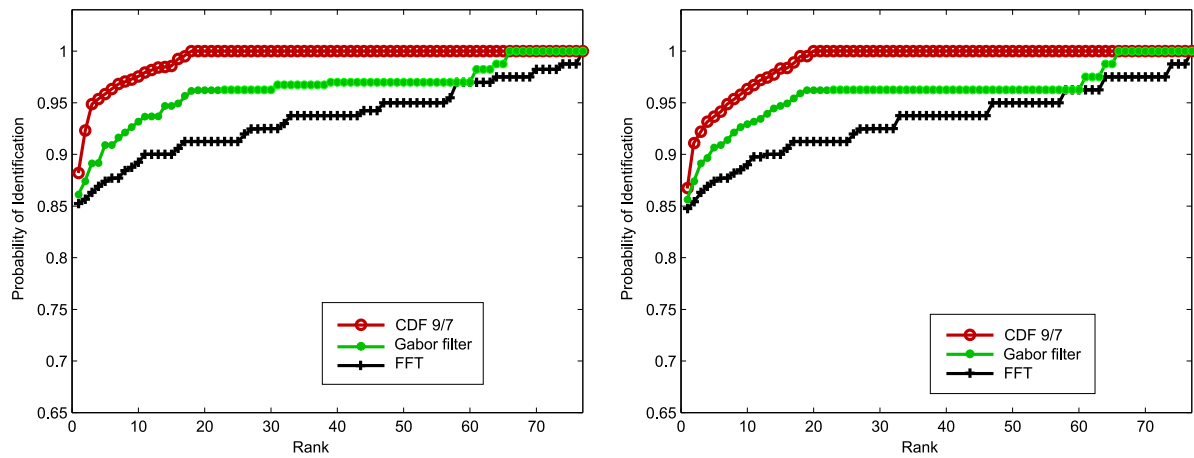


(a) ROC curve of tunable filter bank on CASIAv3 (b) ROC curve of tunable filter bank on UBIRISv1

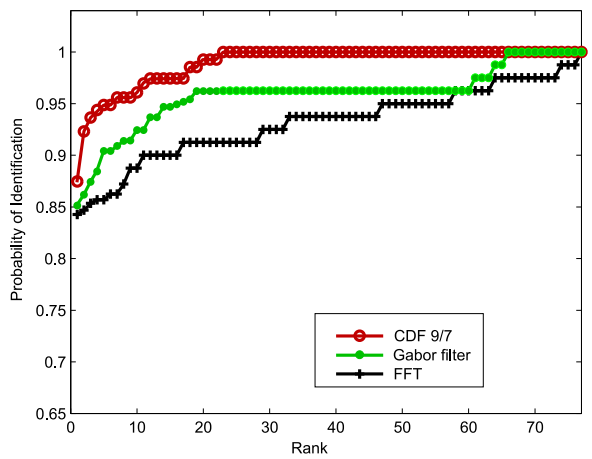


(c) ROC curve of tunable filter bank on IITD

Figure 3.8: Performance of CDF 9/7 filter bank technique on CASIAv3, UBIRISv1, and IITD databases



(a) CMC curve of CDF 9/7 filter bank on CASIAv3 (b) CMC curve of CDF 9/7 filter bank on UBIRISv1



(c) CMC curve of CDF 9/7 filter bank on IITD

Figure 3.9: CMC curves on CDF 9/7 filter bank feature on CASIAv3, IITD, and UBIRISv1 databases

3.3.1 Analysis of Results

During preprocessing of CASIAv3 and UBIRISv1 databases, it is found that IDO results in segmentation failure many a times (refer to Fig. 3.5). The proposed technique is compared with FFT based approach developed by Monro and Zhang [63]. Their technique performs with 100% accuracy in ideal conditions for BATH database [100] as reported in [63,64]. But experimentally it is found that accuracy of their approach falls drastically in non-ideal conditions of CASIAv3 [11] and UBIRISv1 [12]. CDF 9/7 provides satisfactory result in non-ideal scenarios and outperforms FFT based approach (as presented in Table 3.3).

3.4 Summary

In this chapter, performance study of CDF 9/7 filter bank is presented for iris feature extraction in non-ideal conditions. Being a MRA technique, iris texture analysis with CDF 9/7 is found to be superior than some of the existing schemes. A region based technique is considered on the normalized iris to deal with eyelid occlusion and pupillary occlusion. The performance of the same has been validated using standard databases like CASIAv3 and UBIRISv1.

Chapter 4

Tunable Filter Bank for Iris Feature Extraction

In signal processing, multirate system and filter banks have got numerous applications. The off-the-shelf traditional filter banks available are highly regular. They have poor frequency selectivity due to wide transition band. On the contrary, frequency selectivity plays a very vital role in various image processing and pattern recognition applications. In this chapter, two channel half band filter bank is discussed. The design of the proposed filter bank is based on half band polynomial in the variable x . The design procedure deals with deriving filter coefficients in the polynomial domain represented in the variable x with respect to the coefficients of the corresponding function in z -domain. Due to the simple structure of a parametric polynomial in general, we can impose some free parameters to provide a tuning opportunity to optimize and control the wavelet filter characteristics. Perfect reconstruction and desired number of vanishing moments (NVM) are incorporated into the design procedure. The method is systematic, renders a reasonable optimization problem, and it offers wavelet filters ranging from the maximally flat to the sharpest transition band. The proposed filter bank is termed as tunable filter bank (TFB).

4.1 Design Issues in Multirate Filters

Literature on multiresolution analysis reveals about different types of wavelet filter bank. These include ordinary discrete wavelet transform, dual tree complex wavelet transform, and later on extended to directionlet transform, framelets etc. These wavelets several properties i.e. orthogonality, biorthogonality, regularity. Multiresolution analysis allows the decomposition of a signal into its approximation and details. On the theoretical level this is an analysis-synthesis configuration, while the practical view assumes that a signal is represented by its approximation coefficients at some scale and that it is decomposed in terms of its coefficients at a larger scale. As one must compute these coefficients on several different scales, the necessity of a wavelet filter bank is well understood. Two-channel orthogonal filter banks cannot have linear phase except for Haar wavelets. In contrast, biorthogonal filter banks have more degrees of freedom and allow linear phase, an important property that some special filters possess.

In its basic form a low pass filter is regular if it has at least one zero at $z = -1$, the so-called number of vanishing moments (NVM). While regularity is an important task in wavelet-based compression, frequency-selectivity is also another significant factor to be considered with in applications such as denoising, subband coding, classification and recognition. Traditional maximally flat wavelet filters are highly regular but have poor frequency-selectivity. It is known that regularity and frequency-selectivity are in an inverse relationship. The challenge here is to propose a wavelet design method that presents the best frequency-selectivity for the given regularity or degree of flatness. In other words, the problem is defined as how to design wavelet filters with the sharpest transition band for a fixed number of vanishing moments. This work is motivated by the possibility, and the need for improvements of wavelet filters characteristics in two-channel perfect reconstruction filter banks. The necessity stems from the lack of a clear control over the frequency response of the filters in terms of passband/stop band edges, number of vanishing moments, and ripples.

The possibility of such improvements is related to the flexibility and number of free parameters available in the design space, and the recent achievements in semidefinite programming (SDP) and convex optimization techniques in general.

Various approaches have been considered for the design of perfect reconstruction filter banks, e.g. the Remez exchange algorithm, least squares, and eigen filter. Optimization of filter banks is investigated for invariant supervised texture segmentation. Multiscale directional filter bank [101, 102] is discussed extensively to suppress the aliasing effect, as well as to minimize the reduction in frequency resolution where the problem of aliasing in decimated bandpass images on directional decomposition has been addressed. SDP is used successfully to improve the orthogonality error of existing orthogonal filter banks. SDP based framework has been proposed [25] to guarantee the global optimality; it has been shown that an implicit form of regularity constraint imposition is much more appropriate in terms of numerical accuracy.

4.2 Proposed Tunable Filter Bank

As suggested by Patil et al. [94], it is known that a wavelet filter bank can be designed using a half band polynomial. It can be reduced to a product filter $P(z)$, denoted as follows:

$$\begin{aligned}
 P(z) = H_0(z) * G_0(z) = a_0 + a_2 z^{-2} + a_4 z^{-4} + \dots + a_{\frac{K}{2}-2} z^{-\frac{K}{2}+2} + z^{\frac{K}{2}} \\
 + a_{\frac{K}{2}-2} z^{-\frac{K}{2}+2} + \dots + a_0 z^{-K} \quad (4.1)
 \end{aligned}$$

where, K is an even number.

The application of parametric polynomials have been justified in filter design. The objective is to derive the filter coefficients in the polynomial domain (in the variable x) with respect to the coefficients of the corresponding function in z -domain. The approach is as follows:

1. The product filter, $P(z)$ (described using co-efficients \mathbf{a}), is considered to be optimized for its coefficients such that the desired design characteristics are met.
2. A univariate polynomial, $T(x)$ (described using co-efficients \mathbf{b}), is employed. The aim is to express the co-efficients of $T(x)$ in terms of the co-efficients of $P(z)$.
3. Then, $T(x)$ can be represented through semidefinite programming (SDP), to bound the frequency response for a given transition band and ripples.
4. An optimization problem is then defined to determine the co-efficients \mathbf{b} , which in turn help compute co-efficients \mathbf{a} .

Since, (4.1) can be represented using the following equation:

$$P(z) = R(z)(z + 1)^{-2m} \quad (4.2)$$

where, $R(z)$ is the remainder term computed after carrying out polynomial division and m represents number of zeros to be imposed at $z = -1$. The objective is to calculate optimized co-efficients of $R(z)$ for a specified vanishing moments and ripples, which will result in better frequency selectivity.

Let us assume a univariate polynomial $T(x)$ given by the following equation:

$$T(x) = (b_M x^M + b_{M-1} x^{M-1} + \dots + b_1 x + b_0)(x - 1)^m \quad (4.3)$$

$$T(x) = f_N(b)x^N + f_{N-1}(b)x^{N-1} + \dots + f_1(b)x + (-1)^m b_0$$

where $M + m = N$, m is the vanishing moments, $N = K/2$, $\mathbf{f}(\mathbf{b})$ refers to a function of b_i s with $i = 0 \dots, M$ to denote coefficients in the polynomial domain. The filter function given in (4.3), can be transformed into z -domain through change of variables, which is given below: $x = \frac{1}{2}(1 - \cos \omega) = \frac{1}{2}(1 - \frac{1}{2}(z + z^{-1})) = -\frac{1}{4}z(1 - z^{-1})^2$ where $z = e^{j\omega}$. To ensure perfect reconstruction, following half band condition must be

satisfied:

$$T(x) + T(1 - x) = 1 \quad (4.4)$$

Since, the aim is to find the optimized co-efficients of z-domain, we need to relate $\{a_0, a_2, \dots, a_{\frac{K}{2}-1}, a_{\frac{K}{2}}\}$ and $\{b_M, \dots, b_0\}$. The filter kernels for designing $H_0(z)$ and $G_0(z)$ are similar to described by Tay i.e.

$$\Lambda(x) \triangleq T_1(x) \quad (4.5)$$

$$\Omega(x) = T_1(x) + 2T_2(x) - 2T_1(x)T_2(x) \quad (4.6)$$

where $T_1(x)$ and $T_2(x)$ are derived from (4.3) and represented with two different free parameter vectors **b1** and **b2**. The low-pass filters $H_0(z)$ and $G_0(z)$ can be described as follows:

$$H_0(z) = \Lambda \left(\frac{-z(1 - z^{-1})^2}{4} \right) \quad (4.7)$$

$$G_0(z) = \Omega \left(\frac{-z(1 - z^{-1})^2}{4} \right) \quad (4.8)$$

A change of variable in (4.3), results in the following:

$$\begin{bmatrix} f_N(b) \\ f_{N-1}(b) \\ \vdots \\ f_1(b) \end{bmatrix} = \left(\begin{bmatrix} 1 & 0 & \dots & 0 \\ (-1)^1 \binom{k}{1} & 1 & \dots & 0 \\ \vdots & \vdots & \dots & \vdots \\ (-1)^N \binom{k}{N} & (-1)^N \binom{k-2}{N-1} & \dots & 1 \end{bmatrix} \times \begin{bmatrix} -(\frac{1}{4})^N & 0 & \dots & 0 \\ 0 & -(\frac{1}{4})^{N-1} & \dots & 0 \\ \vdots & \vdots & \dots & \vdots \\ 0 & 0 & \dots & -(\frac{1}{4})^0 \end{bmatrix} \right)^{-1} \begin{bmatrix} a_0 \\ 0 \\ a_2 \\ 0 \\ \vdots \\ a_{\frac{k}{2}-1} \\ a_{\frac{k}{2}} \end{bmatrix} \quad (4.9)$$

To illustrate the proposed tunable filter bank [103], we consider a half band polynomial of 14th order as follows:

$$P(z) = a_0 + a_2z^{-2} + a_4z^{-4} + a_6z^{-6} + a_7z^{-7} + a_6z^{-8} + a_4z^{-10} + a_2z^{-12} + a_0z^{-14} \quad (4.10)$$

If we start with a maximally flat filter i.e. for $N = 7$, then we have to set $m = 4$. Hence, the half band polynomial is reduced to:

$$P(z) = R(z)(z + 1)^{-8}$$

where, $R(z)$ is a 6th order remainder polynomial. Since this maximally flat filter can be obtained without any optimization, unfortunately it doesn't have a sharper transition band. Hence, we need to achieve a sharper transition by not imposing maximum number of zeros at $z = -1$. Below, we consider the polynomial in (4.2), for which we impose four zeros at $z = -1$. Hence, for $N = 7$, we have $m = 2$ i.e.

$$P(z) = R(z)(z + 1)^{-4}$$

where, $R(z)$ is a 10th order remainder polynomial. The co-efficient vector in z-domain consists of $\mathbf{a} = \{\mathbf{a}_0, \mathbf{a}_2, \mathbf{a}_4, \mathbf{a}_6, \mathbf{a}_7\}$. If we consider the same in univariate polynomial in the variable x , then we get

$$T(x) = (b_5x^5 + b_4x^4 + b_3x^3 + b_2x^2 + b_1x + b_0)(x - 1)^2 \quad (4.11)$$

where, $\mathbf{b} = \{\mathbf{b}_5, \mathbf{b}_4, \mathbf{b}_3, \mathbf{b}_2, \mathbf{b}_1, \mathbf{b}_0\}$. So we have $\mathbf{f}(\mathbf{b})$ as follows:

$$\begin{bmatrix} b_5 \\ b_4 \\ b_3 \\ b_2 \\ b_1 \\ b_0 \\ -2b_0 \\ b_0 \end{bmatrix} + \begin{bmatrix} 0 \\ -2b_5 \\ -2b_4 + b_5 \\ -2b_3 + b_4 \\ -2b_2 + b_3 \\ -2b_1 + b_2 \\ b_1 \\ 0 \end{bmatrix} = \begin{bmatrix} -16384 & 0 & 0 & 0 & 0 & 0 & 0 & 0 \\ 57344 & 4096 & 0 & 0 & 0 & 0 & 0 & 0 \\ -78848 & -12288 & -1024 & 0 & 0 & 0 & 0 & 0 \\ 53760 & 13824 & 2560 & 256 & 0 & 0 & 0 & 0 \\ -18816 & -7168 & -2240 & -512 & -64 & 0 & 0 & 0 \\ 3136 & 1680 & 800 & 320 & 96 & 16 & 0 & 0 \\ -196 & -144 & -100 & -64 & -36 & -16 & -4 & 0 \\ 2 & 2 & 2 & 2 & 2 & 2 & 2 & 1 \end{bmatrix} \times \begin{bmatrix} a_0 \\ 0 \\ a_2 \\ 0 \\ a_4 \\ 0 \\ a_6 \\ a_7 \end{bmatrix} \quad (4.12)$$

From (4.12), we have $b_4 = -3b_3 - 6b_2$, $b_5 = 2b_3 + 4b_2$ and therefore, $b_5 = -16384a_0$, $b_4 = -24576a_0$, $b_3 = -13312a_0 - 1024a_2$, $b_2 = 2560a_0 + 512a_2$, $b_1 = 2$, and $b_0 = 1$.

Since we are considering the design of biorthogonal filter bank, non-negativity condition for the frequency response of the product filter can be relaxed. Since in the design principle, we have considered a polynomial that consists of odd degree, a sum of square (4.13) is applied bound conditions on $T(x)$. This is as follows:

$$p(x) = (x - \alpha)s_\mu(x) + (\beta - x)s_\eta(x) \quad (4.13)$$

where, $p(x)$ is a non-negative univariate polynomial of degree $2k + 1$ on domain $\mathcal{D} = \{x|x \in [\alpha, \beta], \alpha, \beta \in \mathcal{R}\}$, $s_\mu(x)$ and $s_\eta(x)$ are the sum of squares having degree $\leq 2k$. The passband and stopband edges x_{c_p} and x_{c_s} of the filter kernel $\Lambda(x)$ are satisfied, if the following inequalities are hold good:

$$1 - \delta \leq \Lambda(x) \leq 1 + \delta, \quad x \in [0, x_{c_p}] \quad (4.14)$$

$$\Lambda(x) - 1 + \delta = (x - 0)s_{\mu_1}(x) + (x_{c_p} - x)s_{\eta_1}(x) \quad (4.15)$$

$$1 + \delta - \Lambda(x) = (x - 0)s_{\mu_2}(x) + (x_{c_p} - x)s_{\eta_2}(x) \quad (4.16)$$

$$0.5 \leq \Lambda(x) \leq 1 - \delta, \quad x \in (x_{c_p}, 0.5) \quad (4.17)$$

$$\Lambda(x) - 0.5 = (x - x_{c_p})s_{\mu_3}(x) + (0.5 - x)s_{\eta_3}(x) \quad (4.18)$$

$$1 - \delta - \Lambda(x) = (x - x_{c_p})s_{\mu_4}(x) + (0.5 - x)s_{\eta_4}(x) \quad (4.19)$$

where δ represents ripple, s_μ, s_η are polynomials having degree $\leq 2k$. Similarly for filter kernel $\Omega(x)$, we can have the following inequalities:

$$1 - \delta \leq \Omega(x) \leq 1 + \delta, \quad x \in [0, x_{c_p}] \quad (4.20)$$

$$\Omega(x) - 1 + \delta = (x - 0)s_{\mu_1}(x) + (x_{c_p} - x)s_{\eta_1}(x) \quad (4.21)$$

$$1 + \delta - \Omega(x) = (x - 0)s_{\mu_2}(x) + (x_{c_p} - x)s_{\eta_2}(x) \quad (4.22)$$

$$1 + \delta \leq \Omega(x) \leq \delta_{max}, \quad x \in [x_{c_p}, 0.5] \quad (4.23)$$

$$\Omega(x) - 1 - \delta = (x - x_{c_p})s_{\mu_3}(x) + (0.5 - x)s_{\eta_3}(x) \quad (4.24)$$

$$\delta_{max} - \Omega(x) = (x - x_{c_p})s_{\mu_4}(x) + (0.5 - x)s_{\eta_4}(x) \quad (4.25)$$

$$\delta \leq \Omega(x) \leq 1, \quad x \in (0.5, x_{c_s}] \quad (4.26)$$

$$\Omega(x) - \delta = (x - 0.5)s_{\mu_5}(x) + (x_{c_s} - x)s_{\eta_5}(x) \quad (4.27)$$

$$1 - \Omega(x) = (x - 0.5)s_{\mu_6}(x) + (x_{c_s} - x)s_{\eta_6}(x) \quad (4.28)$$

$$-\delta \leq \Omega(x) \leq \delta, \quad x \in (x_{c_s}, 1] \quad (4.29)$$

$$\Omega(x) + \delta = (x - x_{c_s})s_{\mu_7}(x) + (1 - x)s_{\eta_7}(x) \quad (4.30)$$

$$\delta - \Omega(x) = (x - x_{c_s})s_{\mu_8}(x) + (1 - x)s_{\eta_8}(x) \quad (4.31)$$

where, δ_{max} refers to the amount of overshoot for the corresponding maximally flat filter bank. In the proposed filter bank, a tunable approach is adopted to maintain the overshoot to be less than the corresponding maximally flat filter design. In the design procedure, the co-efficient vector \mathbf{b}_1 is extracted from $T_1(x)$. Similarly, after

optimization of $\Omega(x)$, the co-efficient vector \mathbf{b}_2 is obtained. The filter kernels $\Lambda(x)$ and $\Omega(x)$ are then computed by substituting $T_1(x)$ and $T_2(x)$ in (4.5), and (4.6) respectively.

To design a tunable filter bank, various combinations can be considered. In our design, we have considered $N = 7$, $m = 2$, and $\delta = 0.02$, and the filter co-efficients to implement $H_0(z)$ and $G_0(z)$ is given below:

Table 4.1: Co-efficient vector \mathbf{a} of z -domain

\mathbf{a}	\mathbf{a}_1	\mathbf{a}_2
a_0	-0.0109558471679687	-0.0044677734375000
a_2	0.0414515014648589	0.0246503906250143
a_4	-0.0898694213864434	-0.0783945312497395
a_6	0.3093737670909270	0.3082119140635260
a_7	0.5	0.5

Table 4.2: Co-efficient vector \mathbf{b} of x -domain

\mathbf{b}	\mathbf{b}_1	\mathbf{b}_2
b_5	179.50060	73.20000
b_4	-269.25090	-109.80000
b_3	103.39790	34.23300
b_2	-6.82380	1.18350
b_1	2.00000	2.00000
b_0	1.00000	1.00000

4.2.1 Iris Feature Extraction using Tunable Filter Bank

Application of wavelet filter bank for different image processing applications is a standard practice. Due to its desired properties like time - frequency localization, it can be effectively used for applications like pattern classification, feature extraction, image compression etc. In this chapter, we have illustrated the performance of proposed filter bank for extraction of iris features.

Before feature extraction process can take place, the original raw iris image must be properly segmented in order to extract iris features from an eye image. The

preprocessing involves localization and normalization of the iris image. In our work, we have chosen the popular technique called Daugman's integro-differential operator (IDO) to localize the iris region followed by normalization with the help of Daugman's rubber sheet model. Iris segmentation begins with precisely locating its inner and outer boundaries (pupil and limbus). Since the iris has a circular geometry, the task can be accomplished by IDO for a raw input image $I(x, y)$ that search over the image domain for the maximum in the blurred partial derivative, with respect to increasing radius r , of the normalized contour integral of $I(x, y)$ along a circular arc ds of radius r and center coordinates (x_0, y_0) . It is given by the following equation:

$$R_{iris} \leftarrow \max \left| G_{\sigma}(r) * \frac{\partial}{\partial r} \oint_{(r, x_0, y_0)} \frac{I(x, y)}{2\pi r} ds \right| \quad (4.32)$$

where $*$ denotes convolution and $G_{\sigma}(r)$ is a smoothing function such as a Gaussian of scale σ .

At the beginning σ is set for a coarse scale of analysis so that only the circular transition from iris to sclera is detected. Then after this strong circular boundary is more precisely estimated, a second search begins within the confined central interior of the located iris for the fainter pupillary boundary, using a finer convolution scale and a smaller search range defining the paths (x_0, y_0) of contour integration. Frequent image acquisition of same iris image of the same eye may be variable due to pupil dilation, camera-to-eye distance, head tilt, and eye rotation within its socket. During segmentation, it is found that at times there are segmentation failures; hence, there are occlusion in the normalized images (Fig. 3.5).

To deal with occlusion, we have modified the technique proposed by Proenca and Alexandre [65] and applied it on normalized iris images. Since different regions of the iris have different qualities and local iris image regions with better quality have better classification capability, the normalized iris image is divided into multiple regions. The entire iris image is divided into six equal regions, which contains highly discriminating features. Then five regions are selected (except region 2) so as to

minimize some effect of occlusions during iris recognition. Wavelet derived from tunable filter bank is applied on each of these five regions to extract energy feature from each. Two-dimensional DWT decomposition allows us to analyze an image simultaneously at different resolution levels and orientations. Different functions for energy can be used to extract features from each subband for classification. The energy of each subband provides a measure of the image characteristics in it. The energy distribution has important discriminatory properties for images and as such can be used as a feature for texture classification. The wavelet energy in horizontal, vertical and diagonal directions at i^{th} level decomposition is, respectively defined as:

$$E_i^h = \frac{1}{M \times N} \sum_{m=1}^M \sum_{n=1}^N H_i(m, n)^2 \quad (4.33)$$

$$E_i^v = \frac{1}{M \times N} \sum_{m=1}^M \sum_{n=1}^N V_i(m, n)^2 \quad (4.34)$$

$$E_i^d = \frac{1}{M \times N} \sum_{m=1}^M \sum_{n=1}^N D_i(m, n)^2 \quad (4.35)$$

These energies represent the strength of the iris image's details in different directions at the i^{th} wavelet decomposition level. The feature vector (FV) is derived by concatenating the features at different scales and orientations as:

$$FV = [E_i^h, E_i^v, E_i^d]_{i=1,2,\dots}, \quad (4.36)$$

The total number of subbands for the proposed filter bank is $3 \times i + 1$. The derived FVs of each region are stored in the database as reference during enrollment process.

For classification purpose, we have considered the Canberra distance (CD) between test iris FV and that of the databases. The use of CD is due to the normalization property of individual feature components before computing the distance between test iris FV and that of the databases. The CD is computed as:

$$CD(X, Y) = \sum_{i=1}^B \frac{|X_i - Y_i|}{|X_i| + |Y_i|} \quad (4.37)$$

where, B is the dimension of FV. X_i is the i^{th} component of test FV and Y_i is i^{th} component of training image FV.

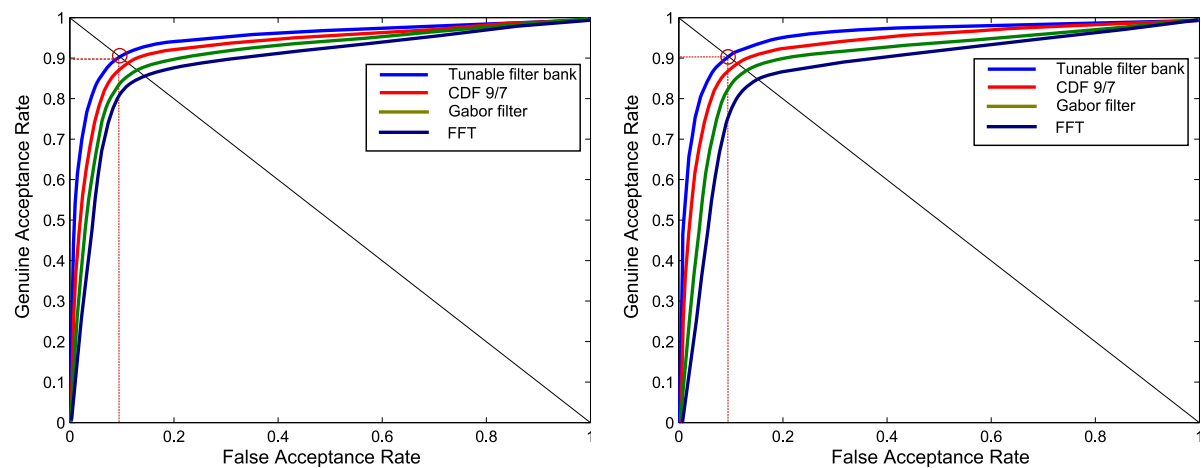
4.3 Results and Discussion

The proposed technique is tested on publicly available CASIAv3, UBIRISv1, and IITD databases. The details about the databases can be found in Section 1.4. The following metrics are employed to evaluate the performance of the proposed biometric system: false acceptance rate (FAR), false rejection rate (FRR), receiver operating characteristic (ROC), area under curve (AUC), and equal error rate (EER).

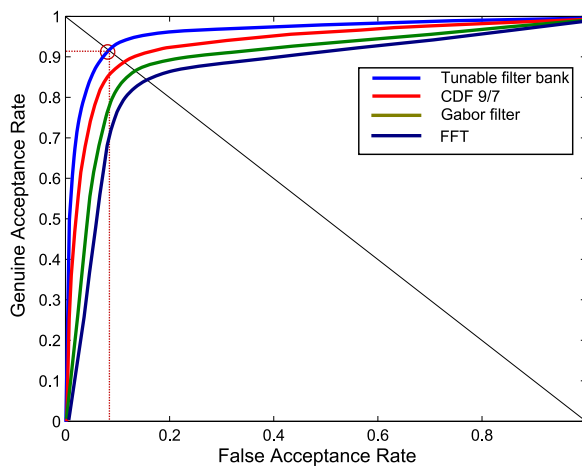
During preprocessing, it is found that IDO results in segmentation failure many times(Fig. 3.5). In our experiment, selected images were considered, mostly occluded ones from both the databases. It is found that segmentation failure seriously affects the recognition accuracy. The proposed technique is compared with FFT based approach developed by Monro and Zhang [63]. Their proposed technique, gives 100% result in ideal conditions as reported; but experimentally it is noted that accuracy of the same falls drastically in non-ideal conditions. Still tunable filter bank provides satisfactory results (as shown in Table 4.3, Fig. 4.1, and Fig. 4.2).

Table 4.3: Comparative analysis of proposed feature on different databases

Performance →		AUC (%)	FAR (%)	GAR (%)	d' index
Database ↓	Approaches ↓				
CASIAv3	FFT	85.58	15.89	87.05	1.32
	Gabor filter	86.45	14.69	87.60	1.55
	CDF 9/7	88.25	11.53	88.03	1.76
	Proposed TFB	91.65	8.45	91.75	1.98
UBIRISv1	FFT	84.61	16.18	85.40	0.98
	Gabor filter	85.71	14.32	85.95	1.52
	CDF 9/7	86.43	13.53	86.39	1.31
	Proposed TFB	90.51	9.15	90.17	1.76
IITD	FFT	83.69	15.24	82.62	1.15
	Gabor filter	84.84	14.26	83.95	1.65
	CDF 9/7	87.31	13.89	88.51	1.71
	Proposed TFB	89.72	10.54	89.98	1.79

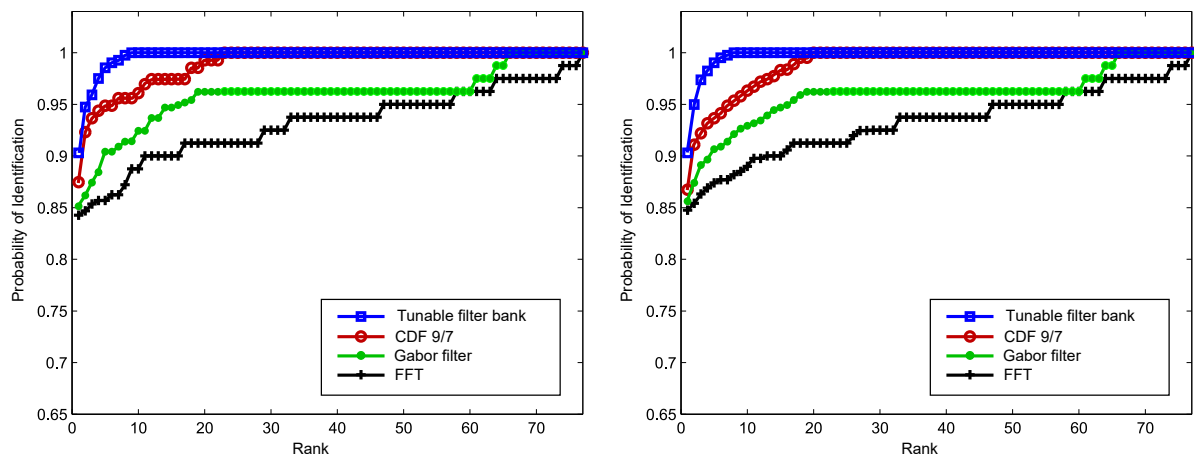


(a) ROC curve of tunable filter bank on IITD (b) ROC curve of tunable filter bank on UBIRISv1

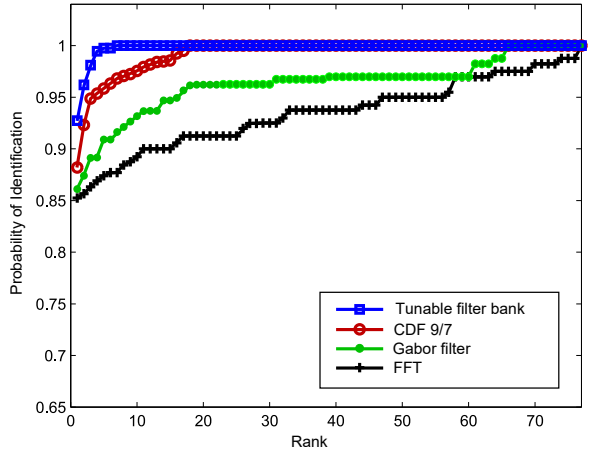


(c) ROC curve of tunable filter bank on CASIAv3

Figure 4.1: Performance of tunable filter bank technique on CASIAv3, UBIRISv1, and IITD databases



(a) CMC curve of tunable filter bank on IITD (b) CMC curve of tunable filter bank on UBIRISv1



(c) CMC curve of tunable filter bank on CASIAv3

Figure 4.2: CMC curves on tunable filter bank feature for IITD, UBIRISv1, and CASIAv3 databases

4.4 Summary

In this work, we have suggested a tunable filter bank for multi-resolution analysis to any 2-D signal. The proposed filter bank is derived from a univariate polynomial in the x -domain of order 14. Since the designed filter bank is obtained by not imposing maximum number of zeros, it is found have improved frequency selectivity. As a result, the filter bank has the ability to capture the texture details present in the 2-D signal. To validate, the proposed tunable filter bank has been applied to extract texture features from iris templates. Initially, the original iris template is subdivided into six different equispaced sub-templates. Two level decomposition has been made to each one except the second sub-template to alleviate the noise due to eyelids, eyelashes, and segmentation faults. Energy features are extracted from each decompositions. Simulation has been carried out on three different databases CASIV3, UBIRISv1, and IITD and performance measures like FAR, GAR, and AUC are compared with energy features derived from Fourier transform, Gabor transform, and CDF 9/7 filter bank respectively. It is observed that, the proposed energy feature outperforms others existing techniques.

Chapter 5

Iris Feature Extraction Using THFB

In this chapter, an approach for the construction of two-channel biorthogonal filter banks is presented. This approach helps overcome constraints that are encountered in an otherwise effective set of techniques described, while retaining the advantages of a simple design and feature-rich structure. The filter bank discussed is based on triplet half band filter bank (THFB) [67,68,104,105], which is used for iris feature extraction. The existing biorthogonal filter banks lead to perfect-reconstruction filter-bank structures for causal stable infinite-duration impulse response (IIR) filter banks and linear-phase finite-duration impulse response (FIR) filter banks with good frequency selectivity. However, one encounters certain restrictions on the filter responses obtained from that structure. For example, in linear-phase FIR filter banks, the magnitude response at the frequency $\omega = \frac{\pi}{2}$ is required to be 0.5 for the analysis low pass filter and 1.0 in the synthesis low pass filter or vice versa. This precludes effective control of the passband response of the synthesis low pass filter (as that of the high pass analysis filter), a situation that is undesirable in some applications where lossy coding is used.

The design of the THFB is based on the use of a triplet of half band filters which are combined in a convenient form of a transfer function with adjustable parameters that provide the necessary flexibility in obtaining the desired response. Note that in [88], the filter banks are derived from a pair of half band filters. In the new

method, the addition of just one extra half band filter and related parameters allow the circumvention of the constraints mentioned above. It is important to note that it is not an increase in filter order that provides the improvement, but the flexibility in choosing the frequency response that allows one to overcome the magnitude constraints discussed above. Design procedures are described for the construction of the filter banks by casting the approximation problem in a form that easily lends itself to Remez exchange algorithm.

5.1 Related Work on THFB

Ansari, Kim, and Dedovic [104] were the first to introduce about THFB. Their proposed filter bank is designed using three kernels which has structural PR, feature-rich structure, and a simple design. In their work, two methods are proposed to design two-channel 1-D biorthogonal FBs based on the triplet of half band filters. The first method is based on Lagrange half band filters which results in maximal flatness filters (due to maximum regularity) with slow frequency roll-off. The second method employs the Remez algorithm, where equiripple filters with user-defined cutoff frequencies are obtained. It has sharp frequency roll-off but does not have the regularity condition. The shape parameter is used to achieve a global shaping of the frequency response with greater flexibility. However, regularity order related to the number of zeros at is not specified.

Tay [106, 107] has discussed about a new class of even-length wavelet filters, called the even-triplet half band filter bank (ETHFB). The filters are constructed from the parametric Bernstein polynomial and have the advantage that perfect reconstruction and vanishing moments are structurally imposed. Two versions of the ETHFB were derived and their use in the design of Hilbert pairs was presented. The matching technique of design was utilized whereby the ETHFB was designed to match the frequency response of a given odd-length filter bank. A simple least squares formulation for the determination of the parameters of the ETHFB was presented.

The ETHFB is more versatile than the even-length Bernstein filter bank and is able to match a wider variety of odd-length filter banks. This can be attributed mainly to the shape parameter which can be used to great effect for global shaping of the frequency response of the ETHFB.

Eslami and Radha [108] have proposed structural multidimensional multichannel filter banks using a three-step lifting scheme. Their developed filter bank is claimed to have desirable numbers of vanishing moments for the analysis and synthesis banks. This results in better regularity and better frequency selectivity. Rahulkar et al. [105] have developed THFB with the help of half band polynomials (HBP). They have described the three kernels with the help of HBP. Then by not imposing maximum zeros, they derived different order of wavelets from the THFB. Their proposed method has better frequency selectivity w.r.t CDF 9/7.

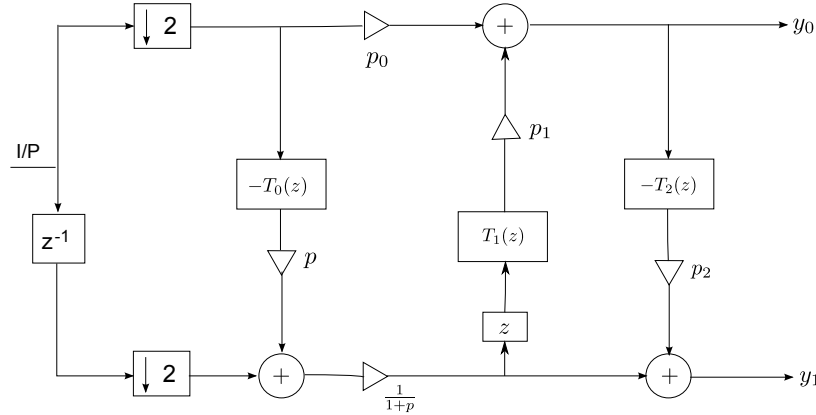


Figure 5.1: Analysis filters of THFB

5.2 Proposed Filter Bank

It is known that a wavelet filter bank can be designed using a half band polynomial [94]. It can be denoted with a product filter $P(z)$, described as,

$$P(z) = H_0(z) * G_0(z) \quad (5.1)$$

The THFB has three half band filters each for analysis and synthesis low pass filters given by:

$$H_0(z) = \frac{1+p}{2} + \frac{T_1(z)}{2} - \frac{pT_0(z)T_1(z)}{2} \quad (5.2)$$

$$G_0(z) = \frac{1+pT_0(z)}{1+p} + \frac{1-p}{1+p}T_2(z) \times \left[\frac{1+p}{2} - \frac{T_1(z)(1+pT_0(z))}{2} \right] \quad (5.3)$$

where $T_0(z)$, $T_1(z)$, and $T_2(z)$ are the half band filters (Fig. 5.1), which approximate as 1 in the passband and 0 in the stopband. The analysis and synthesis high pass filters are obtained using (3.1). The parameter (degree of freedom) provides the flexibility in order to choose the magnitude at $\omega = \frac{\pi}{2}$.

While designing a HBP, it is ensured that, it should have independent parameters, which can have direct control over the frequency response of the low pass filter of the analysis and synthesis filter banks. The low pass filters are computed using the following steps:

Step 1 Consider a generalized half band polynomial $P(z)$ i.e.

$$P(z) = a_0 + a_2z^{-2} + a_4z^{-4} + \dots + a_{\frac{K}{2}-2}z^{-\frac{K}{2}-2} + z^{\frac{K}{2}} + a_{\frac{K}{2}-2}z^{-\frac{K}{2}+2} + \dots + a_0z^{-K} \quad (5.4)$$

The objective is to design a_i of $P(z)$.

Step 2 Impose M^{th} order flatness at $\omega = \pi$

$$\frac{d^i}{d\omega^i}P(\omega)|_{(\omega = \pi)} = 0, \quad i = 0, 1, \dots, L$$

Since, $M < ((\frac{K}{2})+1)$, the desired degree of freedom is obtained by not imposing maximum number of zeros.

Step 3 Obtain M constraints on the co-efficients a_i of $P(z)$ by imposing M^{th} order flatness constraints. Then the polynomial is expressed in terms of independent

Step 4 The product filter $P(z)$ is then factorized to compute the analysis and synthesis low pass filters.

The proposed THFB consists of a product filter $P(z)$ of order K expressed with the co-efficients a_i . This polynomial is used to devise the three half band polynomials by imposing the zeros at $z = -1$. It is ensured that, these three polynomials are expressed with the help of single co-efficients a_0 . The required class of three kernels given in Eq. 5.2 and Eq. 5.3 is obtained by the following equations:

$$T_0(z) = P_1(z) - 1 \quad (5.5)$$

$$T_1(z) = P_2(z) - 1 \quad (5.6)$$

$$T_2(z) = P_3(z) - 1 \quad (5.7)$$

These three designed kernels are then used in the three-step ladder structure proposed in [104] to obtain a new class of analysis and synthesis low pass filters $H_0(z)$ and $G_0(z)$, respectively. Due to the use of THFB and general half band polynomial, the frequency response of both the proposed filters (analysis/synthesis) are simultaneously improved (by avoiding the decision of factorization). Perfect reconstruction and regularity constraints are structurally imposed and near-orthogonality and linear phase properties are achieved. The three polynomials P_i are designed from a single polynomial by imposing zeros at $z = -1$ i.e.

$$P_i(z) = (1 + z^{-1})^{N_i} \times R_i \quad (5.8)$$

where, $i = 1, 2, 3$ and R_i represents the remainder polynomial for each kernel. The remainder polynomial is of the form:

$$R_i = a_0 + a_1 z^{-1} + a_2 z^{-2} + \dots + a_0 z^{-(K-N_i)}$$

The challenge lies with the remainder polynomial is to reconstruct all the co-efficients of R_i with a_0 . This will help in providing only one degree of freedom for the three kernels, which in turn give flexible frequency response.

In our proposed THFB, we have considered an half band polynomial of 10^{th} order is considered as follows:

$$p(z) = a_0 + a_2z^{-2} + a_4z^{-4} + z^{-5} + a_4z^{-6} + a_2z^{-8} + a_0z^{-10}$$

With the help of the synthetic-division method, three polynomials $P_1(z)$, $P_2(z)$, and $P_3(z)$ are obtained by extracting zeros at $z = -1$. It is found that all the polynomials are expressed in a_0 . The computation is as follows:

$$\begin{aligned} P_1(z) &= \\ &a_0 + (-3a_0 - \frac{1}{16})z^{-2} + (2a_0 + \frac{9}{16})z^{-4} + z^{-5} + (2a_0 + \frac{9}{16})z^{-6} + (-3a_0 - \frac{1}{16})z^{-8} + a_0z^{-10} \\ P_2(z) &= (1 + z^{-1})^2(a_0 - 2a_0z^{-1} - \frac{1}{16}z^{-2} + (2a_0 + \frac{1}{8})z^{-3} + (\frac{3}{8} - 2a_0)z^{-4} + (2a_0 + \\ &\frac{1}{8})z^{-5} - \frac{1}{16}z^{-6} - 2a_0z^{-7} + a_0z^{-8}) \\ P_3(z) &= (1 + z^{-1})^3(a_0 - 3a_0z^{-1} + (3a_0 - \frac{1}{16})z^{-2} + (-a_0 + \frac{3}{16})z^{-3} + (-a_0 + \frac{3}{16})z^{-4} + \\ &(3a_0 - \frac{1}{16})z^{-5} - 3a_0z^{-6} + a_0z^{-7}) \end{aligned}$$

The optimized value of a_0 is found to be 0.69675×10^{-3} , using the MATLAB routine *fminunc*. Now the three kernels can be obtained using (5.5), (5.6), and (5.7). The shaping parameter p is set 0.414213 so that desired frequency response can be obtained. The lengths of filters $H_0(z)$ and $G_0(z)$ are 21 and 31, respectively.

5.2.1 Iris Feature Extraction using THFB

Application of wavelet filter bank for different image processing applications is a standard practice. Due to its desired properties like time - frequency localization, it can be effectively used for applications like pattern classification, feature extraction, image compression etc. In this paper, we have illustrated the performance of the proposed filter bank for extraction of iris features.

Before feature extraction process can take place, the original raw iris image must be properly segmented in order to extract iris features from an eye image. The preprocessing involves localization and normalization of the iris image. In our

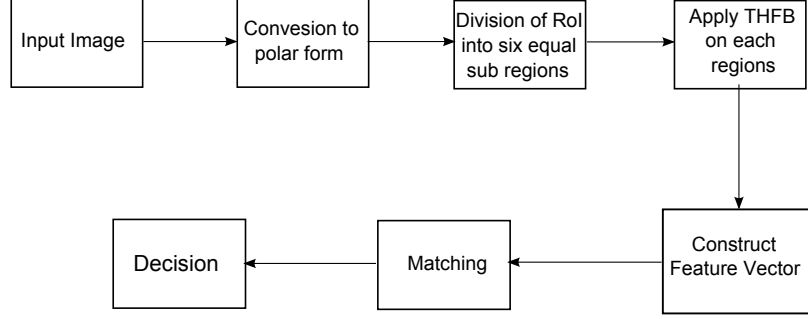


Figure 5.2: Proposed approach

work, we have chosen the popular technique called Daugman's integro-differential operator (IDO) [4] to localize the iris region followed by normalization with the help of Daugman's rubber sheet model. Iris segmentation begins with precisely locating its inner and outer boundaries (pupil and limbus). Since the iris has a circular geometry, the task can be accomplished by IDO for a raw input image $I(x, y)$ that search over the image domain for the maximum in the blurred partial derivative, with respect to increasing radius r , of the normalized contour integral of $I(x, y)$ along a circular arc ds of radius r and center coordinates (x_0, y_0) . It is given by the following equation:

$$\max_{(r, x_0, y_0)} \left| G_\sigma(r) * \frac{\partial}{\partial r} \oint_{(r, x_0, y_0)} \frac{I(x, y)}{2\pi r} ds \right| \quad (5.9)$$

where $*$ denotes convolution and $G_\sigma(r)$ is a smoothing function such as a Gaussian of scale σ .

At the beginning σ is set for a coarse scale of analysis so that only the circular transition from iris to sclera is detected. Then after this strong circular boundary is more precisely estimated, a second search begins within the confined central interior of the located iris for the fainter pupillary boundary, using a finer convolution scale and a smaller search range defining the paths (x_0, y_0) of contour integration. Frequent image acquisition of same iris image of the same eye may be variable due to pupil dilation, camera-to-eye distance, head tilt, and eye rotation within its socket. During segmentation, it is found that at times there are segmentation failures; hence, there are occlusion in the normalized images (Fig. 5.3).

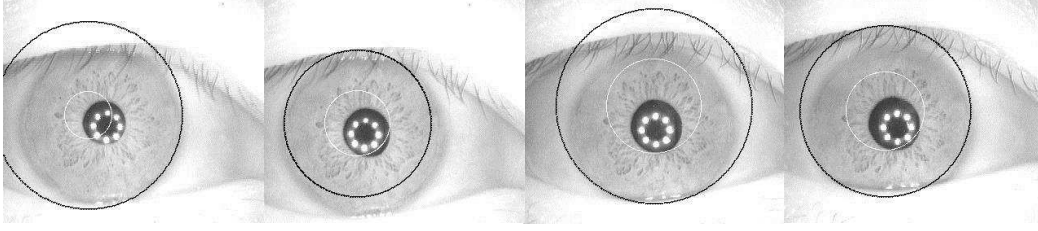


Figure 5.3: Iris segmentation failure with IDO

To deal with occlusion, we have modified the technique proposed by Proenca and Alexandre [65] and applied it on normalized iris images. Since different regions of the iris have different qualities and local iris image regions with better quality have better classification capability, the normalized iris image is divided into multiple regions (explained in 3.3). In the present case, the entire iris image is divided into six equal regions, which contains highly discriminating features. As described in Chapter 3, five regions are selected (except region 2) so as to minimize some effect of occlusions during iris recognition. The normalized iris this strip is fused with a mask to remove regions with low quality (higher noise). The mask having the same size as the strip is filled with 1 at every pixel except the 2nd horizontal block when segmented into six equal horizontal regions. Wavelet derived from THFB is applied on each of these five regions to extract energy feature from each. Two-dimensional DWT decomposition allows us to analyze an image simultaneously at different resolution levels and orientations. Different functions for energy can be used to extract features from each subband for classification. The energy of each subband provides a measure of the image characteristics in that subband. The energy distribution has important discriminatory properties for images and as such can be used as a feature for texture classification. The wavelet energy in horizontal, vertical and diagonal directions at i^{th} level decomposition is, respectively defined as:

$$E_i^h = \frac{1}{M \times N} \sum_{m=1}^M \sum_{n=1}^N H_i(m, n)^2 \quad (5.10)$$

$$E_i^v = \frac{1}{M \times N} \sum_{m=1}^M \sum_{n=1}^N V_i(m, n)^2 \quad (5.11)$$

$$E_i^d = \frac{1}{M \times N} \sum_{m=1}^M \sum_{n=1}^N D_i(m, n)^2 \quad (5.12)$$

These energies represent the strength of the iris image details in different directions at the i^{th} wavelet decomposition level. The feature vector (FV) is derived by concatenating the features at different scales and orientations as:

$$FV = [E_i^h, E_i^v, E_i^d]_{i=1,2,\dots} \quad (5.13)$$

The total number of subbands for THFB is $3 \times i + 1$. The derived FVs of each region are stored in the database as reference during enrollment process.

For classification purpose, we have considered the Canberra distance (CD) between test iris FV and that of the databases. The use of CD is due to the normalization property of individual feature components before computing the distance between test iris FV and that of the databases. The CD is computed as:

$$CD(X, Y) = \sum_{i=1}^B \frac{|X_i - Y_i|}{|X_i| + |Y_i|} \quad (5.14)$$

where, B is the dimension of FV. X_i is the i^{th} component of test FV and Y_i is i^{th} component of training image FV.

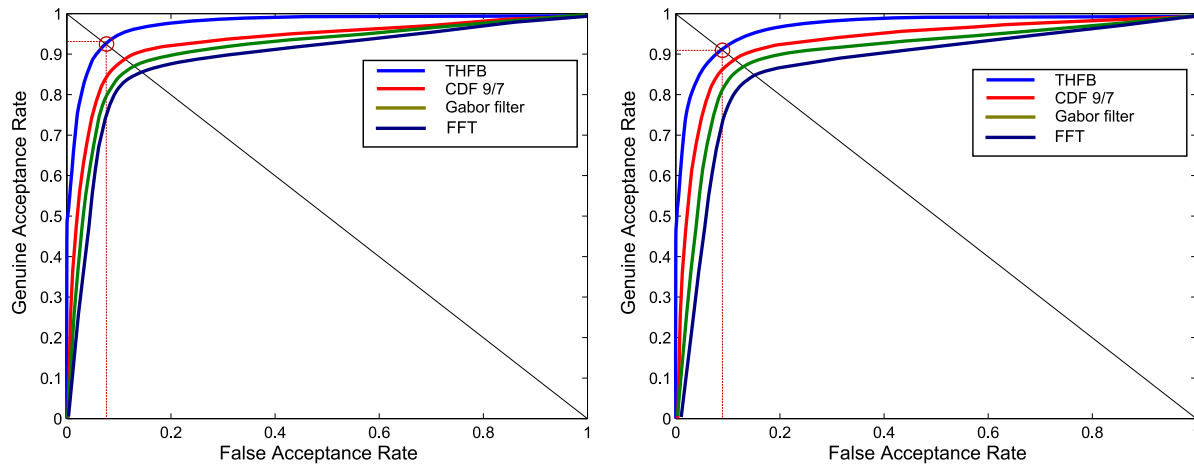
5.3 Results and Discussion

The proposed feature is validated on publicly available CASIAv3 [11], UBIRISv1 [12], and IITD [13] databases to demonstrate its accuracy on subtle features available in NIR images. The following metrics are employed to evaluate the performance of the proposed biometric system: false acceptance rate (FAR), false rejection rate (FRR), receiver operating characteristic (ROC), area under curve (AUC), and equal error rate (EER).

During preprocessing, it is observed that IDO results in segmentation failure on many iris images in all the three databases (Fig. 3.5). To validate the suggested feature on non-ideal iris segmentation, we have selected the iris images mostly the occluded ones. The proposed feature is simulated and compared using the other three features shown in Table 5.3. The features are extracted using FFT, Gabor filter, and CDF 9/7 filter bank respectively. The performance parameters like FAR, GAR, Area Under Curve (AUC) are listed in Table 5.3. It can be observed that the proposed feature based on THFB shows a superior performance as compared to its competent counterparts.

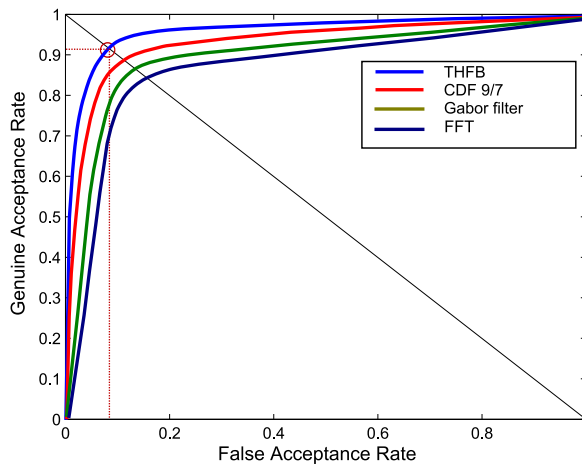
Table 5.1: Comparative analysis of proposed feature on different databases

Performance →		AUC (%)	FAR (%)	GAR (%)	d' index
Database ↓	Approaches ↓				
CASIAv3	FFT	85.58	15.89	87.05	1.32
	Gabor filter	86.45	14.69	87.60	1.55
	CDF 9/7	88.25	11.53	88.03	1.76
	Proposed THFB	94.12	6.02	94.26	2.03
UBIRISv1	FFT	84.61	16.18	85.40	0.98
	Gabor filter	85.71	14.32	85.95	1.52
	CDF 9/7	86.43	13.53	86.39	1.31
	Proposed THFB	92.51	6.26	91.28	1.87
IITD	FFT	83.69	15.24	82.62	1.15
	Gabor filter	84.84	14.26	83.95	1.65
	CDF 9/7	87.31	13.89	88.51	1.71
	Proposed THFB	92.80	6.02	91.62	2.06



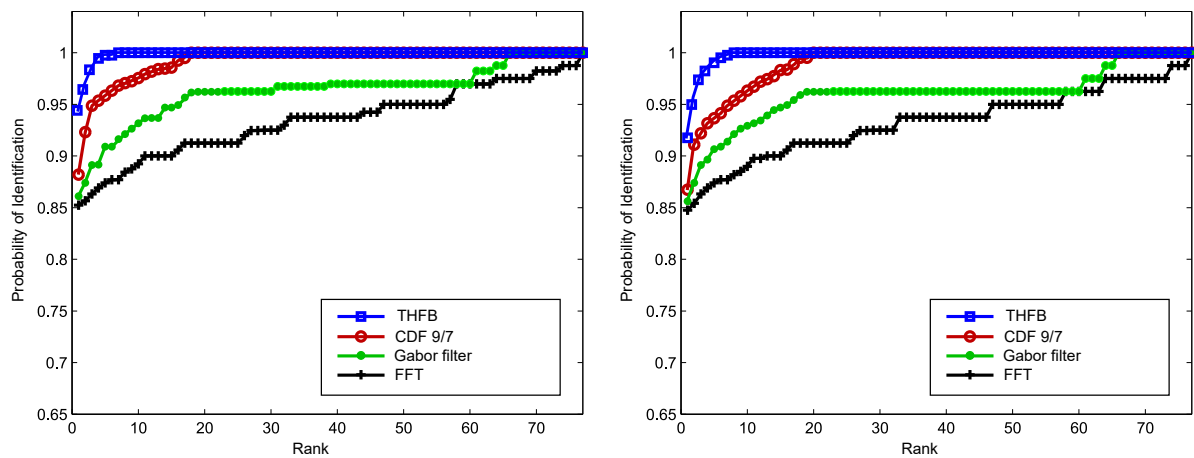
(a) ROC curve of THFB on CASIAv3.

(b) ROC curve of THFB on UBIRISv1.



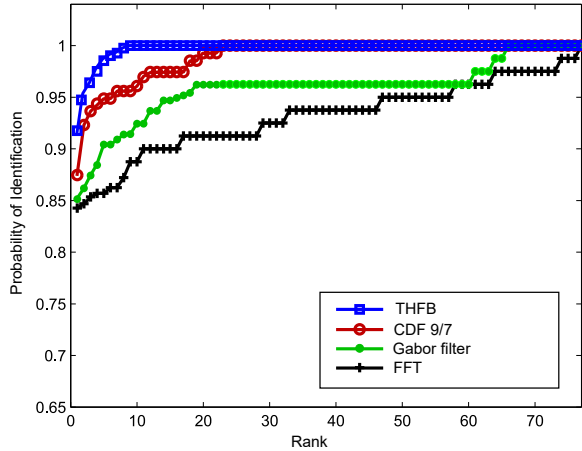
(c) ROC curve of THFB on IITD.

Figure 5.4: Performance of THFB on CASIAv3, UBIRISv1, and IITD databases



(a) CMC curve of THFB on CASIAv3.

(b) CMC curve of THFB on UBIRISv1.



(c) CMC curve of THFB on IITD.

Figure 5.5: CMC curves on THFB based features for CASIAv3, UBIRISv1, and IITD databases

5.3.1 Advantage of the Proposed Approach

1. **Orthogonality:** In a filter bank, it is highly desired that the analysis and synthesis filters are similar. It is a quantitative measure of how far a biorthogonal filter bank is from orthogonality [109]. In the proposed approach, $|H_0(\frac{\pi}{2}) - G_0(\frac{\pi}{2})|$ is used to measure the orthogonality of the designed filters. Also, it is well known that orthogonality conserves the energy. This property helps in texture classification in the presence of noise. The developed filter bank has orthogonality value 0.0018.
2. **Time - frequency localization:** Time - frequency localization criteria plays a very important role in texture analysis. The spatial and frequency localizations are calculated by using the following equations:

$$\Delta\omega^2 = \frac{\pi^2}{3} + 4 \sum_{n=0}^{L-2} \sum_{m=n+1}^{L-1} \frac{(-1)^{m-n}}{P(m-n)^2} h_m h_n \quad (5.15)$$

where, $P = \sum_{n=0}^{L-1} h_n^2$

$$\Delta t^2 = \frac{1}{P} \sum_{n=0}^{L-1} (n - \bar{t})^2 h_n^2 \quad (5.16)$$

where, $\bar{t} = \frac{\sum_n n h_n}{\sum_n h_n}$. The time localization Δt^2 of the analysis low pass filter is computed to be 0.92 and frequency localization $\Delta\omega^2$ for the same is 0.46.

3. **Frequency selectivity:** The error of energy between the designed filter and ideal filter is a method to determine frequency selectivity. This is how the energy at the ripples is minimized. The following objective function is used to determine the value a_0 :

$$E = \int_0^{\frac{\pi}{2}} |1 - H_0(\omega)|^2 d\omega + \int_{\frac{\pi}{2}}^{\pi} |H_0(\omega)|^2 d\omega \quad (5.17)$$

In the proposed THFB, the error in energy is found to be 58.46.

4. **Linear phase:** Linear phase is important because it ensures that the entire waveform is shifted by the same time. In non-linear phase system, since the

different frequency components are delayed by different amounts, the waveform is distorted. A non-linear wavelet system badly affects the shape of the output signal, which in turn results in decrease of the texture discrimination capability. Since the proposed filter bank is based on a linear half band polynomial, it maintains the linear phase property.

5.4 Summary

This chapter suggests a novel triplet half band filter bank (THFB) for multi-resolution analysis (THFB) to any 2-D signal. The proposed THFB is based on three half band polynomials of order ten. The proposed filter bank is found have improved frequency selectivity. As a result, the THFB has the ability to capture the texture details present in the 2-D signal. To validate, the proposed THFB has been applied to extract texture features from iris templates. Initially, the original iris template is subdivided into six different equispaced sub-templates. Two level decomposition has been made to each one except the second sub-template to alleviate the noise due to eyelids, eyelashes, and segmentation faults. Energy features are extracted from each decompositions. Simulation has been carried out on three different databases CASIv3, UBIRISv1, and IITD and performance measures like FAR, GAR, and AUC are compared with energy features derived from Fourier transform, Gabor transform, and CDF 9/7 filter bank respectively. It is observed that, the proposed energy feature outperforms others existing techniques.

Chapter 6

Wavelet Cepstrum Feature for Iris Recognition

Mel-cepstral analysis is one of the most widely used feature extraction technique in speech processing applications including sound recognition and speaker identification. Two-dimensional (2D) cepstrum is also used in image registration and filtering applications. To the best of our knowledge 2D mel-cepstrum which is a variant of 2D cepstrum is rarely studied in image feature extraction and classification problems [110]. The goal of this contribution is to study the wavelet 2D mel-cepstrum feature and show that it is a viable image representation tool. 2D cepstrum is a quefrency domain method. As a result it is a computationally efficient method. It is also independent of pixel amplitude variations and translational shifts. 2D mel-cepstrum which is based on logarithmic decomposition of frequency domain also has the same shift and amplitude invariance properties as 2D cepstrum.

In this chapter, the wavelet based 2D mel-cepstrum feature extraction method is applied to the iris recognition problem. It should be pointed out that our aim is to illustrate the advantages of the 2D mel-cepstrum for iris recognition using a compact feature set. In 2D mel-cepstrum, the logarithmic division of the 2D wavelet detail coefficients provides the dimensionality reduction. This is also an intuitively valid representation as most natural images are low-pass in nature. Unlike the Fourier or DCT domain features, high frequency DFT and DCT coefficients are not discarded in an ad-hoc manner. They are simply combined in bins in a logarithmic manner during

mel-cepstrum computation.

The 2D cepstrum ($\hat{y}(p, q)$) of a 2D image $y(n_1, n_2)$ is defined as:

$$\hat{y}(p, q) = IDFT(\log(|Y(u, v)|^2)) \quad (6.1)$$

where (p, q) represents quefrency coordinates of 2D cepstrum $\hat{y}(p, q)$, $IDFT$ represents the inverse discrete fourier transform, $Y(u, v)$ 2D Discrete Fourier transform (DTFT) of the image $y(n_1, n_2)$.

In 2D mel-cepstrum the DFT domain data is divided into non-uniform bins in a logarithmic manner. The energy of each bin is computed as follows:

$$|G(m, n)|^2 = \sum_{k,l \in B(m,n)} |Y(k, l)|^2 \quad (6.2)$$

$B(m, n)$ is the (m, n) th cell of the logarithmic grid. Cell or bin sizes are smaller at low frequencies compared to high-frequencies. This approach is similar to the mel-cepstrum computation in speech processing. Similar to speech signals most natural images including face images are low-pass in nature. Therefore, there is more signal energy at low-frequencies compared to high frequencies. Logarithmic division of the DFT grid emphasizes high frequencies. After this step 2D mel cepstral coefficients $\hat{y}(p, q)$ are computed using inverse DFT as follows:

$$\hat{y}(p, q) = IDFT(\log(|G(m, n)|^2)) \quad (6.3)$$

Detailed steps of the 2D mel-cepstrum based feature extraction scheme is summarized below:

1. First 2D DFT of iris images ($M \times N$) are calculated.
2. The non-uniform DTFT grid is applied to the resultant DFT matrix and energy $|G(m, n)|^2$ of each cell is computed. Each cell of the grid is also weighted with a coefficient. The new data size is $X \times Y$ where $X \leq M$ and $Y \leq N$.
3. Logarithm of cell energies $|G(m, n)|^2$ are computed.

4. 2D IDFT of the $X \times Y$ data is computed to get mel-cepstrum sequence.

Unfortunately, time-frequency localization property is not achieved by FFT. Hence, we are motivated to study the *wavelet mel-cepstrum* feature (WCF) representation for iris texture.

6.1 Proposed WCF for Iris Recognition

In the literature, various successful applications of cepstrum based features are found [31]. Mostly, it is applied widely in speech processing techniques. Apart from that, it has been used to achieve recognition in face biometrics with high accuracy. A unique representation, known as mel-frequency cepstrum (MFC), is adopted for speech processing. To convert a spectrum of f Hz into m mel, the following equation is used:

$$m = 1127.01048 * \ln \left(1 + \frac{f}{700} \right) \quad (6.4)$$

The mel-frequency cepstrum coefficients (MFCC) , which constitute the MFC, are computed by following the process below:

- Two level wavelet decomposition is performed on the iris image.
- The power spectrum obtained from the detail coefficients is mapped onto the mel scale.
- The logs of the powers at each of the mel frequencies are taken.
- Discrete cosine transform of the mel log powers is computed, which is known as MFCC.

It can be described by the following equation:

$$MFCC = DCT(MT(WT(I))) \quad (6.5)$$

where DCT represents discrete cosine transform, MT represents mel-scale representation of wavelet detail co-efficients, WT represents wavelet transform, and I

is the input iris image.

Before feature extraction process can take place, the original raw iris image must be properly segmented in order to extract iris features from an eye image. The preprocessing involves localization and normalization of the iris image. In our work, we have chosen the popular technique called Daugman's integro-differential operator (IDO) [4] to localize the iris region followed by normalization with the help of Daugman's rubber sheet model. Iris segmentation begins with precisely locating its inner and outer boundaries (pupil and limbus). Since the iris has a circular geometry, the task can be accomplished by IDO for a raw input image $I(x, y)$ that search over the image domain for the maximum in the blurred partial derivative, with respect to increasing radius r , of the normalized contour integral of $I(x, y)$ along a circular arc ds of radius r and center coordinates (x_0, y_0) . It is given by the following equation:

$$\max_{(r, x_0, y_0)} \left| G_\sigma(r) * \frac{\partial}{\partial r} \oint_{(r, x_0, y_0)} \frac{I(x, y)}{2\pi r} ds \right| \quad (6.6)$$

where $*$ denotes convolution and $G_\sigma(r)$ is a smoothing function such as a Gaussian of scale σ .

At the beginning σ is set for a coarse scale of analysis so that only the circular transition from iris to sclera is detected. Then after this strong circular boundary is more precisely estimated, a second search begins within the confined central interior of the located iris for the fainter pupillary boundary, using a finer convolution scale and a smaller search range defining the paths (x_0, y_0) of contour integration. Frequent image acquisition of same iris image of the same eye may be variable due to pupil dilation, camera-to-eye distance, head tilt, and eye rotation within its socket. During segmentation, it is found that at times there are segmentation failures; hence, there are occlusion in the normalized images (Fig. 3.5).

Once the iris images are normalized, wavelet based MFCCs are calculated from the detailed co-efficients. Then the energy of the MFCCs at different orientations (0° , 45° , 90°) from the two level detail co-efficients are computed followed by classification

using Canberra distance.

$$E^h = \frac{1}{M \times N} \sum_{m=1}^M \sum_{n=1}^N H_i(m, n)^2 \quad (6.7)$$

$$E^v = \frac{1}{M \times N} \sum_{m=1}^M \sum_{n=1}^N V_i(m, n)^2 \quad (6.8)$$

$$E^d = \frac{1}{M \times N} \sum_{m=1}^M \sum_{n=1}^N D_i(m, n)^2 \quad (6.9)$$

6.2 Results and Discussion

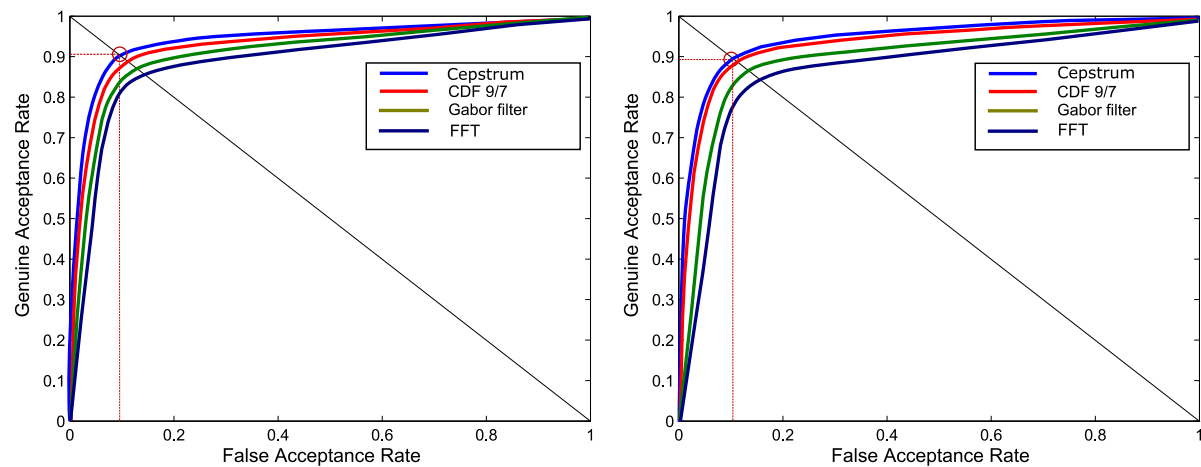
The proposed feature is validated on publicly available CASIAv3 [11], UBIRISv1 [12], and IITD [13] databases to demonstrate its accuracy on subtle features available in NIR images. The details about the databases can be found in Section 1.4. The following performance measures have been used to evaluate the efficacy of the proposed approach: false acceptance rate (FAR), false rejection rate (FRR), receiver operating characteristic (ROC), area under curve (AUC), and equal error rate (EER).

Table 6.1: Computational cost of different iris recognition algorithms (with respect to time)

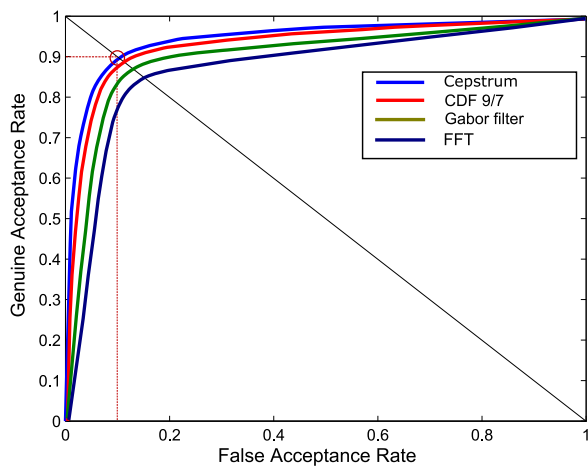
Methods ↓	Feature vector size	Feature extraction time/template (ms)	Feature matching time/template (ms)
FFT	8 × 12	29.40	6.22
Gabor filter	1 × 2048	229.70	27.45
Proposed CDF 9/7 based feature	1 × 30	24.09	5.27
Proposed tunable filter bank	1 × 30	24.25	5.39
Proposed THFB	1 × 30	25.32	5.48
Proposed wavelet based cepstrum	1 × 6	20.06	3.62

Table 6.2: Comparative analysis of proposed feature on different databases

Performance →		AUC (%)	FAR (%)	GAR (%)	d' index
Database ↓	Approaches ↓				
CASIAv3	FFT	85.58	15.89	87.05	1.32
	Gabor filter	86.45	14.69	87.60	1.55
	CDF 9/7	88.25	11.53	88.03	1.76
	Wavelet based cepstrum	89.93	10.45	90.32	1.95
UBIRISv1	FFT	84.61	16.18	85.40	0.98
	Gabor filter	85.71	14.32	85.95	1.52
	CDF 9/7	86.43	13.53	86.39	1.31
	Wavelet based cepstrum	88.97	11.18	89.12	1.46
IITD	FFT	83.69	15.24	82.62	1.15
	Gabor filter	84.84	14.26	83.95	1.65
	CDF 9/7	87.31	13.89	88.51	1.71
	Wavelet based cepstrum	89.86	10.76	89.88	2.01

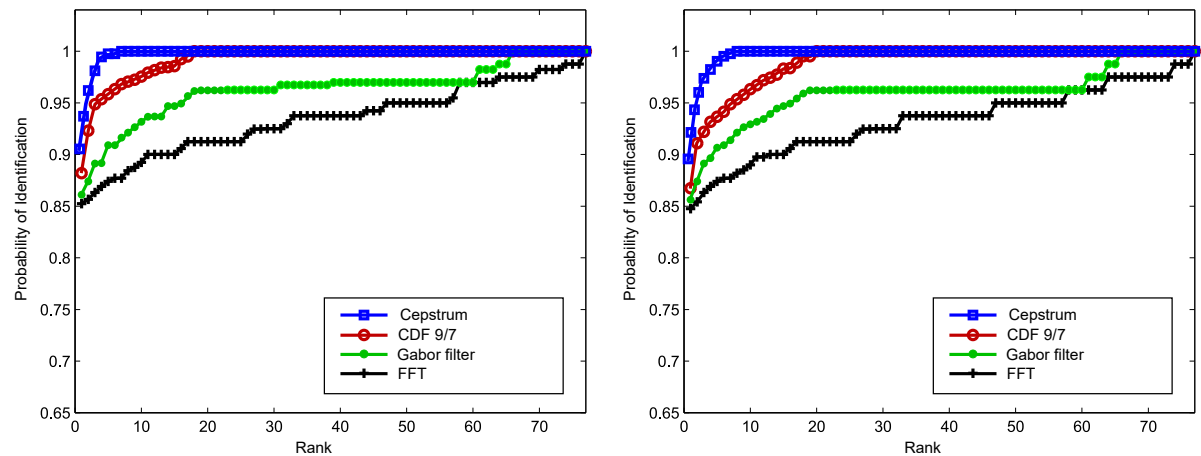


(a) ROC curve of wavelet cepstrum feature on CASIAv3 (b) ROC curve of wavelet cepstrum on UBIRISv1

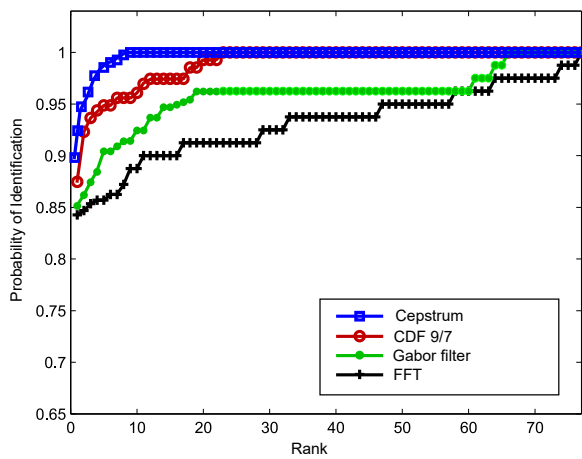


(c) ROC curve of wavelet cepstrum on IITD

Figure 6.1: Performance of wavelet cepstrum on CASIAv3, UBIRISv1, and IITD databases



(a) ROC curve of wavelet cepstrum feature on CASIAv3 (b) ROC curve of wavelet cepstrum on UBIRISv1



(c) ROC curve of wavelet cepstrum on IITD

Figure 6.2: CMC curve on wavelet cepstrum for CASIAv3, UBIRISv1, and IITD databases

6.2.1 Advantage of Wavelet Cepstrum Feature

From the experimental study, the following advantages of wavelet cepstrum features are noted:

- In wavelet cepstrum, non-uniform weights are assigned to the bins. So it is possible to emphasize the high frequency components of the iris image. These are informative and comprehensive to represent the iris texture.
- Since the frequency components are grouped together after wavelet decomposition in mel-scale representation, the resultant dimension is smaller than the original one. Hence, wavelet cepstrum can be used for dimensionality reduction, while preserving the image structure.
- Since decorrelated features are obtained in wavelet MFCC, so the redundant information is discarded. The advantage is that, the features produced are statically independent and hence, comprise an orthogonal space.
- Another advantage of 2D wavelet cepstral feature is that, small change in the features corresponds to small change in perceptual quality. This is very important while carrying out recognition in noisy surroundings.

6.3 Summary

Feature extraction plays a vital role in iris recognition. In this chapter, the application of wavelet mel-cepstrum is suggested for iris feature extraction. The MFCCs have been successfully used to characterize the iris texture. To validate the efficacy of the proposed method, simulation has been carried out on standard databases. It is found that, wavelet based cepstrum feature performs at par with CDF 9/7 filter bank and outperforms other techniques. Since it is desired to store compact feature in the gallery, wavelet cepstrum based technique can be applied, with substantially reduces response time with a trade-off of slightly decreased accuracy Table 6.1. These recorded results summarily conclude the suitability of iris feature extraction with multirate filters.

Chapter 7

Conclusions

In this thesis, different multi-resolution analysis based wavelet filter banks have been studied to improve the performance of iris biometric system under practical scenarios. The proposals deal with the study of CDF 9/7 filter bank, tunable filter bank, THFB followed by wavelet cepstrum feature. The experiments are performed on publicly available CASIAV3, UBIRISv1, and IITD iris databases.

In Chapter 3 the performance of CDF 9/7 filter bank is studied thoroughly for feature extraction from normalized iris images, which include images encountering segmentation failure. Before feature can be extracted, the raw iris images are preprocessed. First, the limbic and pupillary boundaries are segmented. The ROI is then converted to polar form. To deal with occlusion, the normalized iris image is divided into six equal size templates, out of which the second template is discarded since most of the time this region contains occlusion, and unwanted artifacts. Then two level decomposition is applied on the rest five regions, and the feature vector is constructed by extracting the energy feature.

From Chapter 3, it is inferred that CDF 9/7 performs better than frequency based technique like FFT and Gabor filter. Still there is scope for improvement in performance of the used filter bank. Therefore in Chapter 4, the inverse relationship between regularity and frequency selectivity is exploited. Decrease in regularity, in turn increases the frequency selectivity. This trade-off is achieved through SDP. The entire process requires the half band polynomial in z -domain to be represented in the

polynomial domain in variable x . Then using SDP the frequency response is tuned for a given transition band and ripples. The experimental results validate the superiority of tunable filter bank over CDF 9/7.

With the demand for various applications of multirate systems, development of biorthogonal filter banks have been investigated thoroughly. This evolution has brought forward a new class of biorthogonal filter bank known as triplet half band filter bank (THFB). In Chapter 5, design of 10^{th} order THFB is discussed for iris feature extraction. Here three half band filter are combined with adjustable parameters provide the necessary flexibility in obtaining the desired response. The developed filter bank is then used to extract iris feature extraction.

Chapter 6 discusses about another feature extraction technique known as wavelet cepstrum. The proposed technique has been successfully used to characterize the iris texture. To validate the efficacy of the proposed method, simulation has been carried out on standard databases. The performance of wavelet cepstrum feature is compared with some existing techniques. It is found that, wavelet based cepstrum features perform at par with CDF 9/7 filter bank and out performs other techniques.

Scope for Future Work

The applications of wavelet filter banks described in this thesis unwraps some interesting research directions. It is known that overshoot is one of the limitations in the design of half band pair filter bank. Hence, various optimization techniques can be explored to optimize the performance of LeGall 5/3 wavelet filter bank. Also, the design of THFB, which is computationally expensive, can be made simpler by applying this approach.

The contributions in this thesis establish recognition using optimal template by applying wavelet filter bank from iris region. The test is made on CASIAv3, UBIRISv1, and IITD databases. However, there are still many challenges that need to be overcome. One major challenge is the very constraint acquisition environment



Figure 7.1: Failure in image acquisition due to non-cooperative user

with stop-and-stare mechanism. Moreover, performance of iris biometrics is very much dependent on noise free image acquisition in near infrared (NIR) environment. The disadvantage is that NIR illuminated acquisition technique prevents suitable capture of iris in out door environment. Acquisition in visible spectrum allows for capture at longer distances using dedicated camera, where eye region can be detected and captured. However, such practical situations may result with insufficient acquisition of high quality iris region not being captured. This is due to occlusion e.g. blinking, closed eyes, (Fig. 7.1) or other noise factors. In such conditions, we may be able to capture region around the eye, called the periocular region. Hence, wavelet filter banks can be studied to carry out recognition by extracting features from periocular region.

Bibliography

- [1] A. K. Jain, P. Flynn, and A. A. Ross, *Handbook of biometrics*. Springer Science & Business Media, 2007.
- [2] J. K. Pillai, V. M. Patel, R. Chellappa, and N. K. Ratha, “Secure and robust iris recognition using random projections and sparse representations,” *IEEE Transactions on Pattern Analysis and Machine Intelligence*, vol. 33, no. 9, pp. 1877 – 1893, 2011.
- [3] J. Daugman, “The importance of being random: statistical principles of iris recognition,” *Pattern Recognition*, vol. 36, no. 2, pp. 279 – 291, 2003.
- [4] J. G. Daugman, “High confidence visual recognition of persons by a test of statistical independence,” *IEEE Transactions on Pattern Analysis and Machine Intelligence*, vol. 15, no. 11, pp. 1148 – 1161, 1993.
- [5] “Unique Identification Authority of India.” Available: <http://uidai.gov.in/>.
- [6] M. J. Burge and K. W. Bowyer, *Handbook of Iris Recognition*. Springer Publishing Company, 2013.
- [7] “Iris Anatomy.” Available: [http://www.princeton.edu/~achaney/tmve/wiki100k/docs/Iris_\(anatomy\).html](http://www.princeton.edu/~achaney/tmve/wiki100k/docs/Iris_(anatomy).html).
- [8] “Eye Images.” Available: <http://www.behance.net/gallery/Your-beautiful-eyes/428809>.

- [9] “Iris anatomy.” <http://www.oculist.net/downaton502/prof/ebook/duanes/pages/v7/v7c001.html>.
- [10] S. Bakshi, P. K. Sa, and B. Majhi, “A novel phase-intensive local pattern for periocular recognition under visible spectrum,” *Biocybernetics and Biomedical Engineering*, 2013. doi:10.1016/j.bbe.2014.05.003.
- [11] “CASIA Database.” <http://www.cbsr.ia.ac.cn/english/IrisDatabase.asp>.
- [12] “UBIRIS Database.” http://iris.di.ubi.pt/index_arquivos/Page374.html.
- [13] “IITD Database.” http://www4.comp.polyu.edu.hk/~csajaykr/IITD/Database_Iris.htm.
- [14] J. L. Wayman, “Error rate equations for the general biometric system,” *IEEE Robotics and Automation Magazine*, vol. 6, no. 1, pp. 35 – 48, 1999.
- [15] M. Popović, “Texture analysis using 2D wavelet transform: theory and applications,” in *4th International Conference on Telecommunications in Modern Satellite, Cable and Broadcasting Services, 1999*, vol. 1, pp. 149 – 158, IEEE, 1999.
- [16] M. Unser, “Texture classification and segmentation using wavelet frames,” *IEEE Transactions on Image Processing*, vol. 4, no. 11, pp. 1549 – 1560, 1995.
- [17] S. Arivazhagan and L. Ganesan, “Texture classification using wavelet transform,” *Pattern Recognition Letters*, vol. 24, no. 9, pp. 1513 – 1521, 2003.
- [18] O. Pichler, A. Teuner, and B. J. Hosticka, “A comparison of texture feature extraction using adaptive gabor filtering, pyramidal and tree structured wavelet transforms,” *Pattern Recognition*, vol. 29, pp. 733 – 742, August 1996. DOI:10.1016/0031-3203(95)00127-1.

- [19] A. Mojsilovic, M. V. Popovic, and D. M. Rackov, "On the selection of an optimal wavelet basis for texture characterization," *IEEE Transactions on Image Processing*, vol. 9, pp. 2043 – 2050, December 2000. DOI:1057-7149(00)10077-6.
- [20] T. Randen and J. H. Husoy, "Filtering for texture classification: a comparative study," *IEEE Transactions on Pattern Analysis and Machine Intelligence*, vol. 21, no. 4, pp. 291 – 310, 1999.
- [21] M. Vetterli, "A theory of multirate filter banks," *IEEE Transactions on Acoustics, Speech and Signal Processing*, vol. 35, pp. 356 – 372, March 1987. DOI:10.1109/TASSP.1987.1165137.
- [22] P. P. Vaidyanathan, *Multirate systems and filterbanks*. Pearson Education India, 1993.
- [23] D. L. Fugal, *Conceptual wavelets in digital signal processing: an in-depth, practical approach for the non-mathematician*. Space & Signals Technical Pub., 2009.
- [24] S. G. Mallat, "A theory for multiresolution signal decomposition: the wavelet representation," *IEEE Transactions on Pattern Analysis and Machine Intelligence*, vol. 11, pp. 674 – 693, July 1989. DOI:10.1109/34.192463.
- [25] G. Strang and T. Nguyen, *Wavelets and filter banks*. SIAM, 1996.
- [26] P. P. Vaidyanathan and T. Q. Nguyen, "A 'trick' for the design of FIR half-band filters," *IEEE Transactions on Circuits and Systems*, vol. 34, pp. 297 – 300, March 1987. DOI:10.1109/TCS.1987.1086124.
- [27] P. Zahradnik, M. Vlcek, and R. Unbehauen, "Almost equiripple FIR half-band filters," *IEEE Transactions on Circuits and Systems Circuits and Systems - I: Fundamental Theory and Applications*, vol. 46, pp. 744 – 748, June 1999. DOI:10.1109/81.768831.

- [28] A. K. Naik and R. S. Holambe, "Design of low-complexity high-performance wavelet filters for image analysis," *IEEE Transactions on Circuits and Systems Image Processing*, vol. 22, pp. 1848 – 1858, May 2013. DOI:10.1109/TIP.2013.2237917.
- [29] A. Cohen, I. Daubechies, and J. C. Feauveau, "Biorthogonal bases of compactly supported wavelets," *Communications on Pure and Applied Mathematics*, vol. 45, no. 5, pp. 485 – 560, 1992.
- [30] M. Unser and T. Blu, "Mathematical properties of the JPEG2000 wavelet filters," *IEEE Transactions on Image Processing*, vol. 12, pp. 1080 – 1090, September 2003. DOI:10.1109/TIP.2003.812329.
- [31] M. Narwaria, W. Lin, and A. E. Cetin, "Scalable image quality assessment with 2D mel-cepstrum and machine learning approach," *Pattern Recognition*, vol. 45, no. 1, pp. 299 – 313, 2012.
- [32] R. P. Wildes, "Iris recognition: an emerging biometric technology," *Proceedings of the IEEE*, vol. 85, no. 9, pp. 1348 – 1363, 1997.
- [33] M. Nabti and A. Bouridane, "An effective and fast iris recognition system based on a combined multiscale feature extraction technique," *Pattern Recognition*, vol. 41, no. 3, pp. 868 – 879, 2008.
- [34] W. W. Boles and B. Boashash, "A human identification technique using images of the iris and wavelet transform," *IEEE transactions on signal processing*, vol. 46, no. 4, pp. 1185 – 1188, 1998.
- [35] S. Lim, K. Lee, O. Byeon, and T. Kim, "Efficient iris recognition through improvement of feature vector and classifier," *ETRI journal*, vol. 23, no. 2, pp. 61 – 70, 2001.

- [36] L. Ma, Y. Wang, and T. Tan, "Iris recognition using circular symmetric filters," in *16th International Conference on Pattern Recognition, 2002*, vol. 2, pp. 414 – 417, IEEE, 2002.
- [37] L. Ma, T. Tan, Y. Wang, and D. Zhang, "Personal identification based on iris texture analysis," *IEEE Transactions on Pattern Analysis and Machine Intelligence*, vol. 25, no. 12, pp. 1519 – 1533, 2003.
- [38] L. Ma, T. Tan, Y. Wang, and D. Zhang, "Efficient iris recognition by characterizing key local variations," *IEEE Transactions on Image Processing*, vol. 13, no. 6, pp. 739 – 750, 2004.
- [39] Z. Sun and T. Tan, "Ordinal measures for iris recognition," *IEEE Transactions on Pattern Analysis and Machine Intelligence*, vol. 31, no. 12, pp. 2211 – 2226, 2009.
- [40] M. Vatsa, R. Singh, and A. Noore, "Improving iris recognition performance using segmentation, quality enhancement, match score fusion, and indexing," *IEEE Transactions on Systems, Man, and Cybernetics, Part B: Cybernetics*, vol. 38, no. 4, pp. 1021 – 1035, 2008.
- [41] W. Dong, Z. Sun, and T. Tan, "Iris matching based on personalized weight map," *IEEE Transactions on Pattern Analysis and Machine Intelligence*, vol. 33, no. 9, pp. 1744 – 1757, 2011. DOI: 10.1109/TPAMI.2010.227.
- [42] V. Velisavljević, "Low-complexity iris coding and recognition based on directionlets," *IEEE Transactions on Information Forensics and Security*, vol. 4, no. 3, pp. 410 – 417, 2009.
- [43] C. Sanchez-Avila and R. Sanchez-Reillo, "Two different approaches for iris recognition using gabor filters and multiscale zero-crossing representation," *Pattern Recognition*, vol. 38, no. 2, pp. 231 – 240, 2005.

- [44] C. Sanchez-Avila, R. Sanchez-Reillo, and D. de Martin-Roche, “Iris-based biometric recognition using dyadic wavelet transform,” *IEEE Aerospace and Electronic Systems Magazine*, vol. 17, no. 10, pp. 3 – 6, 2002.
- [45] C. S. Chin, A. T. B. Jin, and D. N. C. Ling, “High security iris verification system based on random secret integration,” *Computer Vision and Image Understanding*, vol. 102, no. 2, pp. 169 – 177, 2006.
- [46] J. Huang, X. You, Y. Yuan, F. Yang, and L. Lin, “Rotation invariant iris feature extraction using Gaussian Markov random fields with non-separable wavelet,” *Neurocomputing*, vol. 73, no. 4, pp. 883 – 894, 2010.
- [47] K. P. Hollingsworth, K. W. Bowyer, and P. J. Flynn, “Improved iris recognition through fusion of Hamming distance and fragile bit distance,” *IEEE Transactions on Pattern Analysis and Machine Intelligence*, vol. 33, no. 12, pp. 2465 – 2476, 2011.
- [48] K. Roy, P. Bhattacharya, and C. Y. Suen, “Iris recognition using shape-guided approach and game theory,” *Pattern Analysis and Applications*, vol. 14, no. 4, pp. 329 – 348, 2011.
- [49] R. Szewczyk, K. Grabowski, M. Napieralska, W. Sankowski, M. Zubert, and A. Napieralski, “A reliable iris recognition algorithm based on reverse biorthogonal wavelet transform,” *Pattern Recognition Letters*, vol. 33, no. 8, pp. 1019 – 1026, 2012.
- [50] P. Li and H. Ma, “Iris recognition in non-ideal imaging conditions,” *Pattern Recognition Letters*, vol. 33, no. 8, pp. 1012 – 1018, 2012.
- [51] Q. Wang, X. Zhang, M. Li, X. Dong, Q. Zhou, and Y. Yin, “Adaboost and multi-orientation 2-D gabor-based noisy iris recognition,” *Pattern Recognition Letters*, vol. 33, no. 8, pp. 978 – 983, 2012.

- [52] G. Santos and E. Hoyle, “A fusion approach to unconstrained iris recognition,” *Pattern Recognition Letters*, vol. 33, no. 8, pp. 984 – 990, 2012.
- [53] K. Y. Shin, G. P. Nam, D. S. Jeong, D. H. Cho, B. J. Kang, K. R. Park, and J. Kim, “New iris recognition method for noisy iris images,” *Pattern Recognition Letters*, vol. 33, no. 8, pp. 991 – 999, 2012.
- [54] C. Chou, S. Shih, W. Chen, V. W. Cheng, and D. Chen, “Non-orthogonal view iris recognition system,” *IEEE Transactions on Circuits and Systems for Video Technology*, vol. 20, no. 3, pp. 417 – 430, 2010.
- [55] J. Thornton, M. Savvides, and B. V. K. V. Kumar, “A Bayesian approach to deformed pattern matching of iris images,” *IEEE Transactions on Pattern Analysis and Machine Intelligence*, vol. 29, pp. 596 – 606, April 2007. DOI:10.1109/TPAMI.2007.1006.
- [56] M. D. Marsico, M. Nappi, and D. Riccio, “Noisy iris recognition integrated scheme,” *Pattern Recognition Letters*, vol. 33, no. 8, pp. 1006 – 1011, 2012.
- [57] J. R. Matey, R. Broussard, and L. Kennell, “Iris image segmentation and sub-optimal images,” *Image and Vision Computing*, vol. 28, no. 2, pp. 215 – 222, 2010.
- [58] K. Nguyen, C. Fookes, S. Sridharan, and S. Denman, “Quality-driven super-resolution for less constrained iris recognition at a distance and on the move,” *IEEE Transactions on Information Forensics and Security*, vol. 6, no. 4, pp. 1248 – 1258, 2011.
- [59] P. Li, X. Liu, and N. Zhao, “Weighted co-occurrence phase histogram for iris recognition,” *Pattern Recognition Letters*, vol. 33, no. 8, pp. 1000 – 1005, 2012.
- [60] C. Tan and A. Kumar, “Unified framework for automated iris segmentation using distantly acquired face images,” *IEEE Transactions on Image Processing*, vol. 21, no. 9, pp. 4068 – 4079, 2012.

- [61] K. Miyazawa, K. Ito, T. Aoki, K. Kobayashi, and H. Nakajima, “A phase-based iris recognition algorithm,” in *Advances in Biometrics*, pp. 356 – 365, Springer, 2005.
- [62] K. Miyazawa, K. Ito, T. Aoki, K. Kobayashi, and H. Nakajima, “An effective approach for iris recognition using phase-based image matching,” *IEEE Transactions on Pattern Analysis and Machine Intelligence*, vol. 30, no. 10, pp. 1741 – 1756, 2008.
- [63] D. M. Monro and D. Zhang, “An effective human iris code with low complexity,” in *IEEE International Conference on Image Processing, 2005*, vol. 3, pp. 277 – 280, IEEE, 2005.
- [64] D. M. Monro, S. Rakshit, and D. Zhang, “DCT-based iris recognition,” *IEEE Transactions on Pattern Analysis and Machine Intelligence*, vol. 29, no. 4, pp. 586 – 595, 2007.
- [65] H. Proenca and L. A. Alexandre, “Toward noncooperative iris recognition: a classification approach using multiple signatures,” *IEEE Transactions on Pattern Analysis and Machine Intelligence*, vol. 29, pp. 607 – 612, April 2007. DOI:10.1109/TPAMI.2007.1016.
- [66] A. D. Rahulkar and R. S. Holambe, “Partial iris feature extraction and recognition based on a new combined directional and rotated directional wavelet filter banks,” *Neurocomputing*, vol. 81, pp. 12 – 23, 2012.
- [67] A. D. Rahulkar and L. M. Waghmare and Raghunath S. Holambe, “A new approach to the design of hybrid finer directional wavelet filter bank for iris feature extraction and classification using k-out-of-n:a post-classifier,” *Pattern Analysis and Applications*, vol. 17, no. 3, pp. 529 – 547, 2013. DOI:10.1007/s10044-013-0334-x.

- [68] A. D. Rahulkar and R. S. Holambe, “Half-iris feature extraction and recognition using a new class of biorthogonal triplet half-band filter bank and flexible k-out-of-n:a post-classifier,” *IEEE Transactions on Information Forensics and Security*, vol. 7, pp. 230 – 240, February 2012. DOI:10.1109/TIFS.2011.2166069.
- [69] C. Lu and Z. Lu, “Local feature extraction for iris recognition with automatic scale selection,” *Image and Vision Computing*, vol. 26, no. 7, pp. 935 – 940, 2008.
- [70] D. G. Lowe, “Distinctive image features from scale-invariant keypoints,” *International Journal of Computer Vision*, vol. 60, no. 2, pp. 91 – 110, 2004.
- [71] H. Mehrotra, G. S. Badrinath, B. Majhi, and P. Gupta, “An efficient dual stage approach for iris feature extraction using interest point pairing,” in *IEEE Workshop on Computational Intelligence in Biometrics: Theory, Algorithms, and Applications*, pp. 59 – 62, 2009.
- [72] H. Mehrotra, B. Majhi, and P. Gupta, “Robust iris indexing scheme using geometric hashing of sift keypoints,” *Journal of Network and Computer Applications*, vol. 33, no. 3, pp. 300 – 313, 2010.
- [73] H. Mehrotra, G. S. Badrinath, B. Majhi, and P. Gupta, “An efficient iris recognition using local feature descriptor,” in *IEEE International Conference on Image Processing*, pp. 1957 – 1960, 2009.
- [74] H. Mehrotra, “Iris identification using keypoint descriptors and geometric hashing,” Master’s thesis, National Institute of Technology Rourkela, 2010.
- [75] H. Mehrotra, B. Majhi, and P. K. Sa, “Unconstrained iris recognition using f-sift,” in *8th International Conference on Information, Communications and Signal Processing (ICICS)*, pp. 1 – 5, IEEE, 2011.

- [76] N. Seung-In, K. Bae, Y. Park, and J. Kim, “A novel method to extract features for iris recognition system,” in *Audio-and Video-Based Biometric Person Authentication*, pp. 862 – 868, Springer, 2003.
- [77] Y. Du, C. Belcher, and Z. Zhou, “Scale invariant Gabor descriptor-based noncooperative iris recognition,” *EURASIP Journal on Advances in Signal Processing*, vol. 2010, no. 1, p. 936512, 2010.
- [78] M. Zhang, Z. Sun, and T. Tan, “Deformable DAISY matcher for robust iris recognition,” in *IEEE International Conference on Image Processing*, pp. 3189 – 3192, 2011.
- [79] S. Sun, S. Yang, and L. Zhao, “Noncooperative bovine iris recognition via SIFT,” *Neurocomputing*, vol. 120, pp. 310 – 317, 2013.
- [80] L. Yu, D. Zhang, and K. Wang, “The relative distance of key point based iris recognition,” *Pattern Recognition*, vol. 40, no. 2, pp. 423 – 430, 2007.
- [81] A. Abhyankar and S. Schuckers, “A novel biorthogonal wavelet network system for off-angle iris recognition,” *Pattern Recognition*, vol. 43, no. 3, pp. 987–1007, 2010. DOI: 10.1016/j.patcog.2009.08.008.
- [82] J. Huang, X. You, Y. Y. Tang, L. Du, and Y. Yuan, “A novel iris segmentation using radial-suppression edge detection,” *Signal Processing*, vol. 89, no. 12, pp. 2630 – 2643, 2009.
- [83] A. Raffei, H. Asmuni, R. Hassan, and R. Othman, “Feature extraction for different distances of visible reflection iris using multiscale sparse representation of local Radon transform,” *Pattern Recognition*, vol. 46, pp. 2622–2633, 2013. DOI: 10.1016/j.patcog.2013.03.009.
- [84] D. Wei, J. Tian, J. R. O. Wells, and C. S. Burrus, “A new class of biorthogonal wavelet systems for image transform coding,” *IEEE Transactions on Image Processing*, vol. 7, pp. 1000 – 1013, July 1998. DOI:10.1109/83.701157.

-
- [85] H. H. Kha, H. D. Tuan, and T. Q. Nguyen, "Optimal design of FIR triplet halfband filterbank and application in image coding," *IEEE Transactions on Image Processing*, vol. 20, pp. 586 – 591, February 2011. DOI:10.1109/TIP.2010.2059450.
- [86] J. Lian and Y. Wang, "Energy preserving QMF for image processing," *IEEE Transactions on Image Processing*, vol. 23, pp. 3166 – 3178, July 2014. DOI:10.1109/TIP.2014.2326772.
- [87] K. A. Kotteri and A. E. Bell, "Multiplierless filter bank design: Structures that improve both hardware and image compression performance," *IEEE Transactions on Circuits and Systems for Video Technology*, vol. 16, pp. 776 – 780, June 2006. DOI:10.1109/TCSVT.2006.876360.
- [88] S. M. Phoong, C. W. Kim, and P. P. Vaidyanathan, "A new class of two-channel biorthogonal filter banks and wavelet bases," *IEEE Transactions on Signal Processing*, vol. 43, pp. 649 – 665, March 1995. DOI:10.1109/78.370620.
- [89] J. P. Gawande, A. D. Rahulkar, and R. S. Holambe, "Design of new class of regular biorthogonal wavelet filter banks using generalized and hybrid lifting structures," *Signal, Image and Video Processing*, pp. 1 – 9, September 2015. DOI:10.1007/s11760-015-0814-0.
- [90] "Integrated Automated Fingerprint Identification System." Available: http://www.fbi.gov/about-us/cjis/fingerprints_biometrics/iafis/iafis.
- [91] D. B. H. Tay, "Rationalizing the coefficients of popular biorthogonal wavelet filters," *IEEE Transactions on Circuits and Systems for Video Technology*, vol. 10, pp. 998 – 1005, September 2000. DOI:1051-8215(00)07564-9.
- [92] R. Ansari, C. Guillemot, and J. F. Kaiser, "Wavelet construction using lagrange halfband filters," *IEEE Transactions on Circuits and Systems*, vol. 38, no. 9, pp. 1116 – 1118, 1991.

- [93] C. Jiazhong, G. Weixue, J. Zengwei, X. Tao, L. Hefei, C. Changnian, and W. Xian, "A new design method of 9-7 biorthogonal filter banks based on odd harmonic function," *Circuits, Systems, and Signal Processing*, vol. 31, pp. 1245 – 1255, November 2011. DOI:10.1007/s00034-011-9372-z.
- [94] B. D. Patil, P. G. Patwardhan, and V. M. Gadre, "On the design of FIR wavelet filter banks using factorization of a halfband polynomial," *IEEE Signal Processing Letters*, vol. 15, pp. 485 – 488, 2008. DOI:10.1109/LSP.2008.922295.
- [95] A. N. Willson and H. J. Orchard, "A design method for half-band FIR filters," *IEEE Transactions on Circuits and Systems I: Fundamentals Theory and Applications*, vol. 45, pp. 95 – 101, January 1999. DOI:10.1109/81.739257.
- [96] F. Moreau de Saint-Martin, A. Cohen, and P. Siohan, "A measure of near-orthogonality of PR biorthogonal filter banks," in *International Conference on Acoustics, Speech, and Signal Processing, 1995*, vol. 2, pp. 1480 – 1483, May 1995.
- [97] D. B. H. Tay, "Balanced spatial and frequency localised 2-D nonseparable wavelet filters," in *The 2001 IEEE International Symposium on Circuits and Systems*, vol. 2, pp. 489 – 492, May 2001.
- [98] D. M. Monro and B. G. Sherlock, "Space-frequency balance in biorthogonal wavelets," in *International Conference on Image Processing, 1997*, vol. 1, pp. 624 – 627, IEEE, 1997.
- [99] X. Wu, K. Wang, and Z., "Wavelet energy feature extraction and matching for palmprint recognition," *Journal of Computer Science and Technology*, vol. 20, no. 3, pp. 411 – 418, 2005.
- [100] "BATH University Database." Available: <http://www.bath.ac.uk/elec-eng/research/sipg/irisweb>.

- [101] S. H. Low and Y. C. Li, "A new approach to synthesize sharp 2D half-band filters," *IEEE Transactions on Circuits and Systems - II: Analog and Digital Signal Processing*, vol. 46, pp. 1104 – 1110, August 1999. DOI: 10.1109/82.782061.
- [102] R. H. Bamberger and M. J. T. Smith, "A filter bank for the directional decomposition of images: theory and design," *IEEE Transactions on Signal Processing*, vol. 40, pp. 882 – 893, April 1992. DOI:10.1109/78.127960.
- [103] A. Baradarani, Q. M. J. Wu, M. Ahmadi, and P. Mendapara, "Tunable halfband-pair wavelet filterbanks and application to multifocus image fusion," *Pattern Recognition*, vol. 45, no. 2, pp. 657 – 671, 2012.
- [104] R. Ansari, C. W. Kim, and M. Dedovic, "Structure and design of two-channel filter banks derived from a triplet of halfband filters," *IEEE Transactions on Circuits and Systems - II: Analog and Digital Signal Processing*, vol. 46, pp. 1487 – 1496, December 1999. DOI:1057-7130(99)09870-5.
- [105] A. D. Rahulkar, B. D. Patil, and Raghunath S. Holambe, "A new approach to the design of biorthogonal triplet half-band filter banks using generalized half-band polynomials," *Signal, Image and Video Processing*, vol. 8, no. 8, pp. 1451 – 1457, 2014. DOI:10.1007/s11760-012-0378-1.
- [106] D. B. H. Tay, "ETHFB: A new class of even-length biorthogonal wavelet filters for hilbert pair design," *IEEE Transactions on Circuits and Systems - I*, vol. 55, pp. 1580 – 1588, July 2008. DOI:10.1109/TCSI.2008.916706.
- [107] D. B. H. Tay and M. Palaniswami, "A novel approach to the design of the class of triplet halfband filterbanks," *IEEE Transactions on Circuits and Systems - II: Express Briefs*, vol. 51, pp. 378 – 383, July 2004. DOI:10.1109/TCSII.2004.831430.

-
- [108] R. Eslami and H. Radha, "Design of regular wavelets using a three-step lifting scheme," *IEEE Transactions on Signal Processing*, vol. 58, no. 4, pp. 2088 – 2101, 2010.
- [109] F. M. Saint-Martin, P. Siohan, and A. Cohen, "Biorthogonal filterbanks and energy preservation property in image compression," *IEEE Transactions on Circuits and Systems Image Processing*, vol. 8, pp. 168 – 178, February 1999. DOI:10.1109/83.743852.
- [110] S. Çakir *et al.*, "Image feature extraction using 2d mel-cepstrum," in *20th International Conference on Pattern Recognition (ICPR)*, pp. 674 – 677, IEEE, 2010.
- [111] R. M. da Costa and A. Gonzaga, "Dynamic features for iris recognition," *IEEE Transactions on Systems, Man, and Cybernetics - Part B: Cybernetics*, vol. 42, pp. 1072 – 1082, August 2012. DOI:10.1109/TSMCB.2012.2186125.
- [112] Z. Sun, Y. Wang, T. Tan, and J. Cui, "Improving iris recognition accuracy via cascaded classifiers," *IEEE Transactions on Systems, Man, and Cybernetics - Part C: Applications and Reviews*, vol. 35, pp. 435 – 441, August 2005. DOI:10.1109/TSMCC.2005.848169.
- [113] G. Xu, Z. Zhang, and Y. Ma, "An image segmentation based method for iris feature extraction," *The Journal of China universities of posts and telecommunications*, vol. 15, no. 1, pp. 96 – 117, 2008.
- [114] J. D. M. Jr. and J. Mayer, "Image feature extraction for application of biometric identification of iris – a morphological approach," in *16th Brazilian Symposium on Computer Graphics and Image Processing, 2003*, pp. 391 – 398, IEEE, 2003.
- [115] A. S. Narote, S. P. Narote, L. M. Waghmare, and M. B. Kokare, "Robust iris feature extraction using dual tree complex wavelet transform," in *IEEE*

- International Conference on Signal Processing and Communications, 2007*, pp. 975 – 978, IEEE, 2007.
- [116] F. Jan, I. Usman, and S. Agha, “Reliable iris localization using hough transform, histogram-bisection, and eccentricity,” *Signal Processing*, vol. 93, no. 1, pp. 230 – 241, 2013.
- [117] T. Marciniak, A. Dabrowski, A. Chmielewska, and A. A. Krzykowska, “Selection of parameters in iris recognition system,” *Multimedia Tools and Applications*, vol. 68, no. 1, pp. 193 – 208, 2014.
- [118] W. Chen and S. Yuan, “A novel personal biometric authentication technique using human iris based on fractal dimension features,” in *Acoustics, Speech, and Signal Processing, 2003. Proceedings.(ICASSP’03). 2003 IEEE International Conference on*, vol. 3, pp. 201 – 204, IEEE, 2003.
- [119] D. M. Rankin, B. W. Scotney, P. J. Morrow, and B. K. Pierscioneck, “Iris recognition – the need to recognise the iris as a dynamic biological system: Response to daugman and downing,” *Pattern Recognition*, vol. 46, no. 2, pp. 611 – 612, 2013.
- [120] Y. Li and M. Savvides, “An automatic iris occlusion estimation method based on high-dimensional density estimation,” *IEEE Transactions on Pattern Analysis and Machine Intelligence*, vol. 35, no. 4, pp. 784 – 796, 2013.

Dissemination

Journals

Published

1. **S. S. Barpanda**, B. Majhi, and P. K. Sa, “Region based feature extraction from non-cooperative iris images using triplet half-band filter bank,” *Optics & Laser Technology*, vol. 72, 2015, DOI:10.1016/j.optlastec.2015.03.003.
2. **S. S. Barpanda**, B. Majhi, and P. K. Sa, “Region based feature extraction from non-cooperative iris images using CDF 9/7 filter bank,” *Innovations in System and Software Engineering*, vol. 11, no. 3, 2015, DOI:10.1007/s11334-015-0251-9.

Soubhagya Sankar Barpanda

Department of Computer Science and Engineering,

National Institute of Technology Rourkela,

Rourkela – 769 008, Odisha, India.

+91 94381 31345

soubhagya1984@gmail.com

Qualification

- PhD (CSE) (*Continuing*)
National Institute of Technology Rourkela
- M.Tech. (Research) (CSE)
National Institute of Technology Rourkela, [9.5 CGPA]
- B. Tech
Biju Patnaik University of Technology Rourkela, [First Division]

Publications

- Journals: 03
- Conferences: 02

Permanent Address

Nandapara,

Sambalpur 768 001, Odisha.

Date of Birth

24th June 1984

Index

- Biometrics
 - Modes of Operation, 9
- Biortogonal Wavelet Filter Bank, 41
- CASIAv3 Dataset, 14
- CDF 9/7, 39
- Cepstrum, 85
- Frequency Selectivity, 55
- Half Band Polynomial, 56
- IITD Dataset, 14
- Integro-Differential Operator, 45
- Iris Biometric Databases, 13
- Iris Recognition, 9
- Iris Segmentation, 45
- Mel-Cepstrum, 86
- Mel-Frequency Cepstrum Coefficients, 87
- Multimodal, 11
- Multiresolution Analysis, 55
- Performance Measures
 - Identification, 18
 - Recognition, 17
- Quefreny, 86
- Regularity, 54
- Semidefinite Programming, 56
- Texture Analysis, 20
- Triplet Half Band Filter Bank, 70
- UBIRISv1 Dataset, 14
- Unimodal, 10
- Wavelet Transform, 19